Modelling glioblastoma migration with patient-derived cells, human iPSC-derived cortical neural spheroid, and high-content imaging

Tsang, Victoria

Awarding institution:
King's College London

Modelling glioblastoma migration with patient-derived cells, human iPSC-derived cortical neural spheroid, and high-content imaging

Victoria Tsang

Student number: 1891696

Supervisors: Dr Davide Danovi and Dr Ivo Lieberam

Centre for Gene Therapy and Regenerative Medicine

28th Floor Tower Wing, Guy's Hospital

Great Maze Pond, London SE1 9RT

February 2023

ACKNOWLEDGEMENTS

First, I would like to thank my supervisor Dr Davide Danovi for allowing me to be part of his group and for pushing me to be a more independent researcher. I am incredibly grateful for your inspiring enthusiasm and for your continued encouragement toward me and the project. I would also like to thank my second supervisor Dr Ivo Lieberam for letting me join his group mid-PhD. Thank you for your constant support, knowledge, and insights.

I have to thank Dr Claire Wells and my thesis committee, Prof Karen Liu, Dr Maddy Parsons, and Dr Ciro Chiappini for their expertise and guidance. Thank you to my examiners Prof Ivana Barbaric and Prof Kathreena Kurian for their knowledge and input on my thesis and for taking the time for my VIVA. I am grateful to the Stem Cell Hotel Team, Dr Lazaros Fotopoulos, Thomas Williams, and Erika Wiseman, for all the management and assistance in the imaging facilities. Special thanks to Tom for all your expertise and help in developing my imaging pipelines.

I am thankful to Dr Bronwyn Irving, Dr Léa R'Bibo, and Federica Riccio for their immense help in establishing my tissue culture. This work would not have been possible without them. Special thanks to all the HipSci TC culture members: James Williams, Abigail Isaacson, Dr Alice Vickers, Haneen Alsehli, Dr Jean-François Darrigrand, Dr Tung-Jui Trieu for the companionship in the long TC hours, the sharing of advice, ideas, music…

I feel lucky for my friends, Dr Clarisse Ganier, Dr Jean-François Darrigrand, Dr Tung-Jui Trieu. From fun lunches to scientific advice, thank you for all the amount of support and the time we spent together. To my friend Haneen Alsehli in the Danovi Group, I am so glad we got to embark on this journey together, and thank you for your listening ear.

Being a member of the CSCRM/CGTRM has been a privilege. The whole PhD experience was made better by all the amazing and wholesome people. Thank you to all the management and technical staff who keep the place running. Thank you to Jessica Sells and Dr Ella-Louise Hubber for all the public engagement opportunities where I got to

meet and felt inspired by young minds in science. Thank you to Dr Fay Minty for welcoming me to the CTRM program and for all your help. I am grateful to have been part of the Wellcome Trust cohorts in 2018 and 2019 and for the great friends I have made.

I feel lucky for my school/university friends who made this journey more special and my years in London such a fun experience. I am so excited to be celebrating more milestones together.

I am forever grateful for my parents, Laura, and Flo. Thank you for always believing in me and being here, despite the distance. Special thanks to the rest of my family Mehdi, Kevin, and Brandon! I will not be where I am without all of you. To my little nieces and nephew: Naya, Neji, and Yuna, merci pour les meilleurs calins et tout votre amour.

COVID Impact Statement

The COVID-19 pandemic and restrictions disrupted my PhD research in several ways.

• The laboratory was closed for 4 months during the first national lockdown in 2020. This was shortly after I had started my PhD, meaning I could not perform experiments nor get the training planned.

• The second national lockdown restricted our access to the laboratory and we were constrained to work certain shifts. This limited me in data production and I had to prioritize certain experiments over others. We also had to keep our distance from our coworkers so I was not able to get the training needed in stem cell culture and on certain imaging devices such as the Operetta CLS until the restrictions were lifted.

• The live-imaging Phasefocus Livecyte and the Operetta CLS HCI devices were out of operation for about 6 months. This prevented me from doing more live imaging assays as I had planned earlier in my PhD aims.

Table of Abbreviations

AC-like	Astrocyte-like
Akt/PKB	Protein Kinase B
BDNF	Brain-Derived Neurotrophic Factor
BSA	Bovine serum albumin
BT	BioTracker
BV	Brilliant Violet
CDC42	Cell division control protein 42 homolog
CDK4	Cyclin-dependent kinase 4
CFP	Cyan fluorescent protein
CXCL12	C-X-C Motif Chemokine Ligand 12
CysLT1	Cysteinyl leukotriene receptor 1
ECM	Extracellular matrix
EGFR	Epidermal growth factor receptor
EMT	Epithelial-mesenchymal transition
Eph	Ephrin
EphB1	Ephrin Receptor B1
ERBB2	Erb-B2 Receptor Tyrosine Kinase 2
FAK	Focal Adhesion Kinase
FGFR	Fibroblast Growth Factor Receptor
GBM	Glioblastoma Multiforme
GCGR	Glioma Cellular Genetics Resource
GLUT3	Glucose transporter 3
HCI	High-content imaging
HIF-2α	Hypoxia-inducible factor-2α
HILPDA	Hypoxia Inducible Lipid Droplet Associated
HiPSC	Human induced pluripotent stem cells
ICD-O-3	International Classification of Diseases–Oncology, version 3
IDH1	Isocitrate dehydrogenase 1
IL-10	Interleukin-10
JAK2/STAT3	Janus kinase 2/signal transducer and activator of transcription 3
L1CAM	L1 cell adhesion molecule
LGG	Lower grade glioma
MEM NEAA	MEM Non-essential Amino Acids
MES-like	Mesenchymal-like
MET	Mesenchymal epithelial transition factor receptor

MGMT	O6-methylguanine-DNA methyl transferase
MMP	Matrix metalloproteinases
NF1	Neurofibromin 1
NF-κB	Nuclear factor kappa-light-chain-enhancer of activated B cells
NIR	Near Infra-Red
NPC-like	Neural progenitor cell-like
NS17	GCGR.NS17ST_A
NT-3	Neurotrophin-3
OLIG2	Oligodendrocyte transcription factor 2
OPC-like	Oligodendrocyte progenitor cell-like
PBS	Phosphate-buffered saline
PDGFR	Platelet-derived growth factor receptors
PD-L1	Programmed death-ligand 1
PIK3R1	Phosphoinositide-3-Kinase Regulatory Subunit 1
PKCδ	Protein Kinase C delta
PLO	Poly-L-ornithine
PTEN	Phosphatase and tensin homolog
PTN	Pleiotrophin
RAC-1	Ras-related C3 botulinum toxin substrate 1
ROCK	Rho Associated Coiled-Coil Containing Protein Kinase
ROI	Region of Interest
RT	Room temperature
SD	Standard deviation
shh	Sonic Hedgehog
SOX	Sry-type HMG
TCGA	The Cancer Genome Atlas
TERT	Telomerase reverse transcriptase
TGF-β	Transforming growth factor-beta
TLR4	Focal adhesion complexes
TLR4	Toll-like receptor 4
TMZ	Temozolomide
TP53	Tumour Protein P53
TRADD	Tumour necrosis factor receptor type 1-associated DEATH domain
TUBB/Tuj 1	Beta-tubulin
WHO	World Health Organization

LAY SUMMARY

Glioblastoma Multiforme (GBM) is the most common and aggressive type of brain cancer. Despite current advances, this form of cancer is incurable. It is known for its ability to invade and spread within the brain in a process called glioblastoma migration. GBM cells can migrate through normal brain tissue using the nerve fibres (axons) making them difficult to completely remove with surgery. Since only one-quarter of GBM patients survive longer than one year, further research is needed to develop new treatments and target those migrating cancer cells.

This project aims to develop a cell model mimicking the internal conditions of the brain to study the GBM cells migration on axons. To develop axons, we direct human stem cells into cortical neurons that are then aggregated in a spheroid. We are using different patient-derived GBM cells to represent the disease and a non-cancer neural line as a control. We demonstrated a higher infiltration with the patient-derived GBM cells than the non-cancer control and found several drugs which can inhibit the migration of the cancer cells.

By modelling the GBM internal conditions, we have facilitated the study of GBM migration on axons. This project will bridge the gap between cell and patient drug testing, reducing the use of animal models as well as potentially offering new treatments.

ABSTRACT

Background: Glioblastoma multiforme (GBM) is the most common and aggressive brain tumour in adults. Despite current advances, the existing standard of treatment is ineffective, and the survival prognosis remains just over a year following diagnosis. Migrating tumour cells have been implicated in the therapeutic resistance of GBM. They disperse by using structures such as white matter tracts and inevitably cause the recurrence of the tumour. Bulk tumour sequencing has indicated inter- and intra-tumour heterogeneity which includes the proneural, classical, and mesenchymal subtypes. These classifications with distinct molecular signature correlate with patient prognoses, and as such, this disease will benefit from personalised therapeutic approaches. Valuable cell models able to capture the invasiveness of GBM are critically needed to develop innovative therapies targeting migrating GBM cells. This project aims to develop an *in vitro* model mimicking the GBM microenvironment and investigate the GBM cells migration on axons.

Methods: We established an *in vitro* model mimicking the GBM microenvironment by co-culturing patient-derived GBM cells and human-induced pluripotent stem cell-derived cortical neural spheroids with radiating axons. Patient-derived GBM1 and GBM20, established as described in Wurdak et al. in 2010 and Polson et al. in 2018, maintained their stem cell-like characteristics as well as the molecular signature of the primary tumour of a classical/proneural subtype and a secondary mesenchymal subtype they are respectively derived from. Using HCI, we developed a robust pipeline to quantify the GBM cell infiltration of the neural spheroid in endpoint assays. Images were acquired on the Operetta CLS High-Content Imaging (HCI) system and analysed using the built-in Harmony Imaging and Analysis Software. We also performed live-imaging assays using the label-free HCI system called Phasefocus Livecyte, in which we studied the directionality, displacement, and speed of the GBM cells engaged on axons.

Results: Our data indicated that GBM cells changed morphology when cultured on axons. The live assays demonstrated that patient-derived GBM1 and GBM20 cells as well

as non-cancer neural stem cell NS17 line migrated towards the neural spheroid. However, the endpoint assays showed a significant increase in infiltration of the neural spheroid with the GBM1 and GBM20 cells compared to NS17 cells. Finally, we used this model to screen for several inhibitors to pathways involved in the migration of GBM cells and found promising targets, PF 573228 (FAK inhibitor) and Motixafortide (CXCL12 inhibitor), which significantly decreased GBM20 and GBM1 infiltration of the neural spheroid respectively.

Conclusion: By modelling the GBM microenvironment with the ability of GBM cells to infiltrate the neural spheroid and to screen for compounds affecting cell migration, we have facilitated the investigation of GBM migration on axons ex vivo. The deliverable of this project is expected to bridge the gap between *in vitro* and *in vivo* drug screening, reducing the use of animal models, study time, and costs as well as potentially offer innovative precision-medicine therapies.

TABLE OF CONTENTS

LIST OF FIGURES

LIST OF TABLES

1. INTRODUCTION

1.1. Glioblastoma

1.1.1. Grade IV glioma

Gliomas are the most common form of primary brain tumours in adults (Ostrom *et al.*, 2018). They account for 81% of adult brain tumours and present a worldwide incidence rate of 5 per 100,000 people (Holland, 2000; Claes, Idema and Wesseling, 2007; Ostrom *et al.*, 2014). Previously, it was recommended for gliomas to be categorised in four stages based on their histological features and malignant behaviour according to the International Classification of Diseases–Oncology, version 3 (ICD-O-3) and World Health Organization (WHO) grade, (Ostrom *et al.*, 2014; Ceccarelli *et al.*, 2016; 'World Health Organization Classification of Tumours of the Central Nervous System', 2021; Louis *et al.*, 2021). However, the identification of biomarkers on prognosis has allowed a more effective grading combined with histological features. The WHO CNS5 classified Gliomas, Glioneuronal Tumours, and Neuronal Tumours into six families: (1) Adult-type diffuse gliomas; (2) Paediatric-type diffuse low-grade gliomas; (3) Paediatric-type diffuse high-grade gliomas; (4) Circumscribed astrocytic gliomas; (5) Glioneuronal and neuronal tumours; and (6) Ependymomas (Figure 1.1) ('World Health Organization Classification of Tumours of the Central Nervous System', 2021; Louis *et al.*, 2021). The Adult-type diffuse gliomas are divided into three subcategories which include Astrocytoma, IDH-mutant; Oligodendroglioma, IDH-mutant and 1p/19q-codeleted; and Glioblastoma, IDH-wildtype. The CNS WHO grade 4 includes astrocytoma, IDH-mutant and glioblastoma (GBM), and IDH-wildtype.

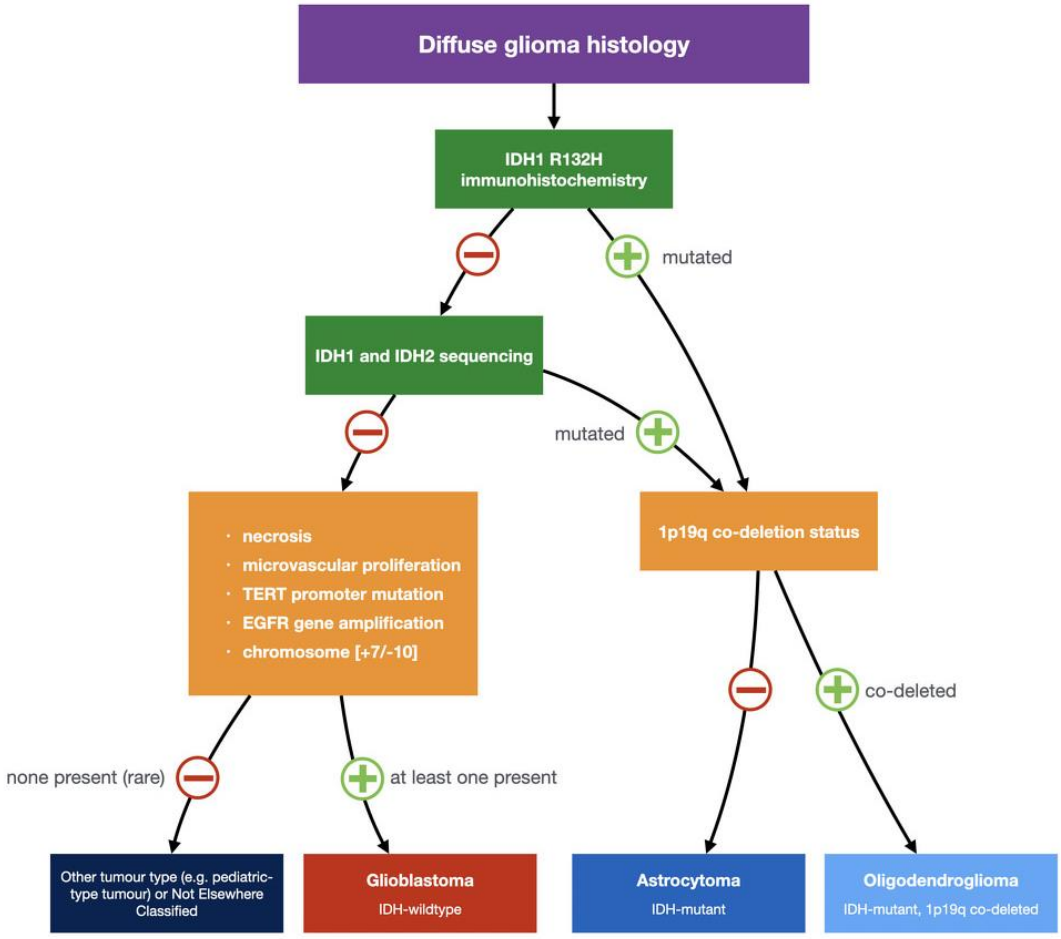

Figure 1.1 A simplified diagram of the classification of adult-type diffuse gliomas. Diagram based on the CNS WHO 5th edition (Gaillard, 2021; Louis *et al.*, 2021)

1.1.2. Epidemiology

The most aggressive form of gliomas, GBM, is a rare tumour which represents 47.7% of all adults gliomas and affects less than 10 per 100,000 people globally (Ostrom *et al.*, 2014, 2018; Ceccarelli *et al.*, 2016; 'World Health Organization Classification of Tumours of the Central Nervous System', 2021; Louis *et al.*, 2021). The incidence of GBM increases with age with the median age of diagnosis at 65 years and the highest rates in individuals at 75-84 years (Ostrom *et al.*, 2013, 2018). As the world population is ageing rapidly, the incidence of GBM is expected to steadily increase in the coming years. GBM is relatively rare in children comprising 3-15% of primary tumours in the central nervous system (Das and Kumar, 2017). The most common paediatric gliomas are pilocytic astrocytomas or

diffuse midline gliomas (Mackay et al., 2017; Schwartzentruber et al., 2012; Capper et al., 2018).

The incidence of GBM is higher in men compared to women (Carrano *et al.*, 2021). It has been reported that Caucasians have a higher incidence compared to black and Asian populations and that the Western world has a higher incidence of gliomas than less developed countries (Ohgaki and Kleihues, 2005; Thakkar *et al.*, 2014). However, this may be a reflection of the socio-economic differences such as limited access to healthcare and underreporting of gliomas cases rather than a significant difference in genetic susceptibility.

1.1.3. Diagnosis and Prognosis

The clinical presentation of GBM largely depends on the nervous system deterioration in the affected brain area. The signs and symptoms vary and range from obvious defects of function such as loss of vision and alteration of language to more subtle problems such as mood disorders, fatigue, and progressive headaches (Alexander and Cloughesy, 2017). In 25% of patients diagnosed with GBM, seizures can occur and can be controlled with anticonvulsants. The current median survival time from diagnosis is 14–16 months with only a 5.6% five-year survival rate despite the current advances and treatment strategies (Stupp *et al.*, 2009; Ostrom *et al.*, 2018; Ozdemir-Kaynak, Qutub and Yesil-Celiktas, 2018). For paediatric GBM, the median survival time is 14 months with less than a 20% five-year survival rate.

1.1.4. Current treatments and challenges

In addition to the late diagnosis, there are various challenges which result in a poor prognosis of GBM (Ozdemir-Kaynak, Qutub and Yesil-Celiktas, 2018). The standard of treatment includes the surgical resection of the bulk of the tumour followed by radiotherapy and concomitant chemotherapy with temozolomide (TMZ) (Stupp *et al.*, 2005, 2009; van Linde *et al.*, 2017). Complete surgical excision is limited by the infiltrative and diffusive nature of GBM which makes it distinct from LGG and results in tumour cells dispersed in the healthy brain parenchyma (Armento *et al.*, 2017). TMZ is

an oral alkylating agent which gets activated in a more alkaline environment, such as the brain. Its highly reactive byproducts methylate DNA bases including at O6-guanine positions and result in cytotoxic effects (Tiek *et al.*, 2018). Although TMZ demonstrated a moderate overall improvement, chemotherapeutic resistance is almost inevitable. This is believed to be due to the DNA repair mechanism involving O6-methylguanine-DNA methyl transferase (MGMT) protecting tumour cells against alkylating drugs (Stupp *et al.*, 2009; Martin, Janouskova and Dontenwill, 2012).

GBMs also display inter- and intra-tumour heterogeneity, meaning there is heterogeneity between tumours of different patients and within the same tumour. The framework to describe these phenomena is that tumour cells resist therapies by varying from dormant to quiescent or proliferative states (Roy *et al.*, 2015). Importantly, this limits the effectiveness of approaches targeting a single oncogenic protein and further drives therapy-resistant subclonal variants (Robertson *et al.*, 2019). Therapeutic resistance is involved in the almost inevitable tumour recurrence after a median interval of 32-36 weeks (Roy *et al.*, 2015). However, there is high variability in tumour recurrence definition and treatment timelines and other causes remain largely undefined. Furthermore, the development of effective therapies to fight the highly infiltrative GBM cells is limited by the blood-brain barrier (Cuddapah *et al.*, 2014; Kim *et al.*, 2015; Armento *et al.*, 2017).

1.2. GBM heterogeneity and classification

As previously mentioned, GBMs comprise inter- and intra-heterogenous populations of tumour cells exhibiting extensive differences in molecular profiles, cellular phenotype and malignancy grade (Claes, Idema and Wesseling, 2007; Aubry *et al.*, 2015). The driver mutations of GBM occur at distinct levels and response to therapy highly varies between subtypes. This sub-chapter will summarise the various high-dimensional profiling studies made to classify GBM in subtypes and correlate the biology to the clinical presentation and prognosis, summarised in Table 1.1.

1.2.1. Inter-tumoural heterogeneity: Genetic subtypes

The Cancer Genome Atlas (TCGA) network catalogued recurrent genomic abnormalities in GBM in a large-scale multi-dimensional analysis in 2008 which was further expanded in 2013 (McLendon *et al.*, 2008; Brennan *et al.*, 2013). Initially, in 206 patient samples, the gene expression analysis pinpointed the roles of Erb-B2 Receptor Tyrosine Kinase 2 (ERBB2), Neurofibromin 1 (NF1), Tumour Protein P53 (TP53), Phosphoinositide-3-Kinase Regulatory Subunit 1 (PIK3R1) as well as MGMT as drivers of malignant transformation and drug resistance mechanism (McLendon *et al.*, 2008). In 2013, the analysis of over 500 GBM tumours allowed for new and revised molecular classification schemes (Brennan *et al.*, 2013). The landscape identified novel relevant mutated genes such as epidermal growth factor receptor (EGFR) and platelet-derived growth factor receptor alpha (PDGFRA). Furthermore, they provided new insights into the role of Telomerase reverse transcriptase (TERT) promoter in elevated mRNA expression and telomerase reactivation (Brennan *et al.*, 2013). Comprehensive molecular profiling has further revealed different glioma molecular subsets based on the Isocitrate dehydrogenase 1 (IDH1) mutation which allowed the prediction of prognosis (Ceccarelli *et al.*, 2016). IDH-wildtype indicates the absence of IDH mutations in primary tumours, whereas IDH-mutant is present in the vast majority of secondary GBM (Ceccarelli *et al.*, 2016; Liu *et al.*, 2016).

Based on the molecular classification with aberrations and gene expression, bulk tumour sequencing defined three different GBM subtypes with distinct clinical features and prognosis: classical, proneural, and mesenchymal (Verhaak *et al.*, 2010; J. Wang *et al.*, 2017; Neftel *et al.*, 2019). Initially, it was suggested that there were four GBM subtypes which included the neural subtype (Verhaak *et al.*, 2010; Zhang *et al.*, 2020). In a later revision, the neural subtype was removed due to its association with the tumour margin and its similar gene expression patterns to normal tissue (Gill *et al.*, 2014; Q. Wang *et al.*, 2017; Neftel *et al.*, 2019; Zhang *et al.*, 2020).

The classical subtype is associated with chromosome 7 amplification and loss of chromosome 10. High-level amplification of EGFR was reported in 97% of cases of the

classic subtype (Verhaak *et al.*, 2010). The classical subtype also distinguishes itself by a lack of TP53 mutations which are frequently mutated genes in GBM (McLendon *et al.*, 2008). The proneural subtype is characterized by high-level amplifications in PDGFRA and point mutations in IDH1 as well as the loss of TP53. Other overexpressed genes in the proneural subtype include genes related to the proneural and oligodendrocytic development such as Oligodendrocyte transcription factor 2 (OLIG2) and Sry-type HMG box (SOX) genes. The mesenchymal subtype is characterized by deletions in the 17q11.2 region, containing the gene NF1. Along with NF1, loss of Phosphatase and tensin homolog (PTEN) is also observed and affects the AKT pathway (Verhaak *et al.*, 2010). The mesenchymal also display mesenchymal markers such as Mesenchymal epithelial transition factor receptor (MET) related to the epithelial-mesenchymal transition (EMT) (Phillips *et al.*, 2006). Finally, genes related to tumour necrosis and the Nuclear factor kappa-light-chain-enhancer of activated B cells (NF-κB) pathway such as Tumour necrosis factor receptor type 1-associated DEATH domain (TRADD) are overexpressed and associated with the high necrosis level and inflammatory infiltration (Verhaak *et al.*, 2010).

These coherent molecular subclasses emphasized the inter-tumour heterogeneity such as the different responses to aggressive therapy with the classical and proneural subtypes having the greatest potential, better prognosis and delayed mortality compared to the mesenchymal subtype. However, this needs to be further verified as it depends on the drug therapy target. Correlative analyses indicated that MGMT DNA methylation may be a predictive biomarker for the treatment response of the classical subtype whereas the survival advantage of the proneural subtype is related to the IDH mutation (Brennan et al., 2013). It was also reported that this classification is dynamic where the proneural subtype often evolves into a mesenchymal subtype, a process termed proneural-to-mesenchymal transition (Ozawa *et al.*, 2014; Fedele *et al.*, 2019; Bhaduri *et al.*, 2020). This poses challenges for treatment responses, for example, drugs targeting the proneural subtype may not impact the mesenchymal subtype resulting in a treatment-resistant mesenchymal subpopulation. To counteract this, approaches have been developed using Janus kinase 2/signal transducer and activator of transcription 3 (JAK2/STAT3) inhibitors to prevent the proneural-to-mesenchymal transition through

early intervention or to revert the mesenchymal to proneural subtype and limit the invasive nature of the disease (Lau *et al.*, 2015; Fedele *et al.*, 2019).

Interestingly, single-cell RNA sequencing within the same tumour has revealed intra-tumour heterogeneity with multiple TCGA subtypes which highlight the concern of objectively characterising GBM (Verhaak et al., 2010). The complexity of the inter- and intra-tumour heterogeneity of GBM is an important barrier to therapeutic development and has become a notable area to research to tackle the disease (Dirks, 2010; Gimple, Bhargava, Dixit, & Rich, 2019; Wurdak et al., 2010).

1.2.2. Intra-tumoural heterogeneity: Cellular states

The first level of heterogeneity we described reflected the inter-tumoural heterogeneity in the genetic subtypes which also varies within the same tumour. In addition to the heterogeneity in the molecular signature, GBM is also heterogenous in the developmental state. Indeed, Neftel et al. characterised those cellular states as the neural progenitor cell-like (NPC-like), oligodendrocyte progenitor cell-like (OPC-like), astrocyte-like (AC-like) and mesenchymal-like (MES-like) states (Neftel *et al.*, 2019).

The AC-like state is associated with EGFR aberrations. Their results suggested that high levels of EGFR favour a high frequency of AC-like cells which is also consistent with reports suggesting the involvement of EGFR as a regulator of astrocytic differentiation. It is also characterized by the expression of astrocytic markers (S100B, GFAP, SLC1A3, GLAST and MLC1). Similarly, the OPC-like state is associated with high-level amplifications of PDGFRA as well as expression of oligodendroglia lineage genes (OLIG1, OMG, PLP1, PLLP, and TNR). High-level amplifications of Cyclin-dependent kinase 4 (CDK4) are associated with the NPC-like state. It is further divided into NPC1 (OLIG1 and TNR) and NPC2 (STMN1) in relation to their potential differentiation towards OPC-like or neurons, respectively. Finally, the MES-like state is characterized by NF1 alterations. This state is also subdivided into hypoxia-independent (MES1) and -dependent (MES2) based on the Hypoxia Inducible Lipid Droplet Associated (HILPDA) expression.

This model agrees with Verhaak et al. (2010) model where both shared similar genetic aberrations and cell-types interactions, including intra-tumour heterogeneity (Verhaak *et al.*, 2010; Neftel *et al.*, 2019). Similarly to genetic subtyping, this classification is also dynamic as the cellular states are influenced by the genetic drivers and the tumour microenvironment, exhibiting plasticity (Neftel *et al.*, 2019). The heterogeneity and the plasticity of the cellular states further highlight why there has not been a successful therapeutic agent for GBM and emphasizes the need to dissect the cellular states' response to treatments. Indeed, the maintenance of those heterogeneous cellular states and the origin of GBM have been associated with a subset of cells which governs GBM, called the glioblastoma stem cells (GSCs) (Geribaldi-Doldán *et al.*, 2021).

Table 1.1 GBM classification and characterization

A) Intra-tumoural heterogeneity represented by the genetic subtypes (Verhaak et al., 2010).
B) Inter-tumoural heterogeneity represented by the cellular states (Neftel et al., 2019).

A

Intra-tumoural heterogeneity - Verhaak	
Genetic subtypes	**Characterisation**
Classical	EGFR amplification
Proneural	Loss of TP53, PDGFRA/IDH1 mutations
Mesenchymal	loss of NF1 and PTEN, overexpression of mesenchymal markers, increase NFKB and tumour necrosis pathway

B

Inter-tumoural heterogeneity - Neftel	
Cellular states	**Characterisation**
OPC-like	PDGFRA amplification
AC-like	EGFR amplification
NPC-like	CDK4 amplification
MES-like	NF1 alteration, Immune cells, Hypoxia

1.3. Glioblastoma stem cells (GSCs)

Single-cell transcriptomics performed at the tumour core and the surrounding tissue revealed a subset of neoplastic cells called the GSCs (Nishikawa *et al.*, 2018; Garnier *et al.*, 2019). The GCSs share properties of self-renewal, stemness markers and multi-lineage differentiation. It was reported that GBM arises from neural stem cells (NSCs) in the subventricular zone as GSCs. However, the exact cell of origin is elusive and it has also been proposed that differentiated astrocytes may give rise to GBM (Gimple *et al.*, 2019). GSCs are chemo-resistant and this evasion of treatment further enables them to initiate a secondary tumour. The ability of GSCs to support tumour growth and migration also results in the recurrence of the tumour. Furthermore, the secondary tumour was

shown to recapitulate tumour heterogeneity with a similar molecular signature and mismatch repair genes. In this sub-chapter, we will summarise the molecular and cellular aetiology that GBM use for the maintenance and progression of GSCs and discuss the migration of GSCs in the next chapter.

1.3.1. Intrinsic factors

The epigenetic and genetic profiles contribute to the classification of the glioma subgroups. Nonetheless, cells from the same tumours may express distinct expression signatures at the same time, as previously mentioned (Patel et al., 2014). GBM harbour frequent genetic alterations resulting in amplifications, insertions, deletions or point mutations which can affect the growth, proliferation, and migration. This section will review the main transcriptional and epigenetic modifications in GBM which play a key role in the development of progression and the maintenance of GSCs.

The genes which are commonly mutated in GBM include EGFR, ERBB2, PDGFRA/IDH1, PIK3CA, and PIK3R1 as well as MET and TERT promoters (Liu *et al.*, 2016; Romani, Pistillo and Banelli, 2018). Those proteins stimulate downstream molecules of the RAS/ERK and AKT/PI3K signalling pathways leading to increase proliferation and growth (Robertson *et al.*, 2019). Mutations in the TERT promoter are found in 76% of IDH wild-type GBM cases (Eckel-Passow *et al.*, 2015). However, the gain of function seen for EGFR, PDGFR and MET are regularly activated in distinct ways within the same tumour emphasising the intra-tumour heterogeneity (Furnari *et al.*, 2015; Robertson *et al.*, 2019). Other recurrent gene expression mutations or deletions were reported in the tumour suppressors CDKN2A, TP53, RB1, PTEN and NF1 (Lathia *et al.*, 2015). Commonly mutated genes in cancer such as TP53 and PTEN are frequent in GBM but are not of prognostic importance.

Epigenome-wide mapping has identified several individual genes involved in the disruption of the same multiprotein complexes (e.g. BAF/PBAF) (Brennan *et al.*, 2013). As previously mentioned, the epigenetic methylation MGMT gene is of clinical relevance as it correlates with the chemotherapeutic resistance to TMZ (Hegi *et al.*, 2005; Romani, Pistillo and Banelli, 2018). Indeed, Stupp et al. demonstrated in their trials that TMZ

treatment benefited patients with a methylated MGMT promoter but could be detrimental in patients with unmethylated MGMT (Hegi *et al.*, 2005; Hegi and Stupp, 2015). This leaves patients with unmethylated MGMT in need of a better treatment (Hegi and Stupp, 2015). This is particularly significant in recurrent tumours which show a decrease in MGMT methylation as this removes TMZ as a valuable treatment option. Other potential epigenetic targets include altered expression of IDH1 protein or histone methyltransferases and demethylases. Alterations such as IDH1/2 mutations can interfere with the "epigenetic modifier" enzymes (Ceccarelli *et al.*, 2016; Romani, Pistillo and Banelli, 2018). The mutations of the histone 3 variants H3.1 and H3.3 can affect the overall levels of H3K27me3. Potential targets for these alterations are currently being tested in preclinical and clinical trials.

Chromosome instability is also found in GBM with whole-chromosome gains and losses which renders the cancer highly aneuploid with distinct karyotypes (Robertson *et al.*, 2019). Indeed, extrachromosomal DNA often derives from oncogene amplification further driving the heterogeneity (Turner *et al.*, 2017; Robertson *et al.*, 2019)

In addition, the epigenetic landscape is involved in the shifting of the developmental states promoting the maintenance and propagation of the GSC state through chromatin remodelling and the core set of neurodevelopment transcription factors POU3F2, SOX2, SALL2, OLIG2 (Suvà *et al.*, 2014), particularly in the proneural subtype. GSCs specifically display NSC markers such as nestin (Nes) and CD133 (Singh *et al.*, 2004; Robertson *et al.*, 2019). Other stemness markers expressed by GBM which play a key role include the neurodevelopmental transcription factors such as the HOX, and FOX genes which sustain the self-renewal capacity of GSCs and drive the disease (Suvà *et al.*, 2014; Bulstrode *et al.*, 2017; Singh *et al.*, 2017; Robertson *et al.*, 2019). Indeed, GSCs have a similar transcriptional profile to the foetal progenitors of the outer sub ventricle radial glia, a proliferating subset of progenitors in the cortex of the developing human brain (Patel *et al.*, 2014; Pollen *et al.*, 2015). Those cells display a more invasive nature than the more differentiated subset which will be described in further detail in the GBM invasion section.

1.3.2. Extrinsic factors

The tumour microenvironment plays a key role in the regulation and maintenance of the GSCs. Firstly, the local niche regulates the balance of the range of proliferative vs non-cycling/quiescent states by GSCs (Patel *et al.*, 2014; Hambardzumyan and Bergers, 2015). The quiescent state and preferential activation of the DNA damage response could explain the radioresistance (Bao *et al.*, 2006). The vasculature also mediates signals maintaining the quiescent state and promoting the self-renewal, proliferation, and survival of GSCs (Gilbertson and Rich, 2007; Ottone *et al.*, 2014).

The local niche has limited access to nutrients such as glucose and oxygen which drive the cancer cells to adapt and alter their metabolism (Hoang-Minh *et al.*, 2018). This is known as the Warburg effect, which is characterized by a metabolic shift to aerobic glycolysis to generate energy from glucose fermentation (Warburg, 1956). This stimulates glucose uptake through the upregulation of Glucose transporter 3 and 4 (GLUT3 and GLUT4) expression. Another hallmark of the GBM niche is the hypoxic conditions resulting in the activation of Hypoxia-inducible factor-2α (HIF-2α) and the Notch pathways (Garnier *et al.*, 2019). Indeed, Notch signalling plays a crucial role in the maintenance of stemness, along with the up-regulation of the BMP, NF-κB and Wnt pathways (Garnier *et al.*, 2019). The upregulation of the Wnt pathway is also involved in the invasiveness of GBM (Lee *et al.*, 2015).

1.4. GBM motility and invasion

In addition to stem cell maintenance and treatment resistance infiltrative nature of GBM is arguably the most challenging cell behaviour that renders recurrency inevitable. Darmanis et al. indicated that GSCs shared a common mechanism of infiltration between different tumours and are likely responsible for the increased invasive potential (Singh *et al.*, 2004; Darmanis *et al.*, 2017; Nishikawa *et al.*, 2018; Garnier *et al.*, 2019). GSCs diffusively infiltrate the neuropil of the patient's brain individually or in small groups (Claes, Idema and Wesseling, 2007; O'Neill *et al.*, 2010; Fortin Ensign *et al.*, 2013). Single-cell migration seems to be preferred by gliomas as they invade long distances in the brain by following existing anatomical structures (de Gooijer *et al.*, 2018). GSCs invade

via the extracellular matrix (ECM), the endothelial cells of the vascular system, and the axons of the white matter tracts (Figure 1.2) (Armento *et al.*, 2017; Cha and Kim, 2017; de Gooijer *et al.*, 2018). Notably, the brain anatomy is a major regulator in the invasion and there are common intrinsic mechanisms of infiltration such as the upregulation of surface receptors or migration-associated changes in the cytoskeleton.

This corroborates with observations of the GBM mesenchymal subtype which is enriched in highly invasive and therapy-resistant cells (de Gooijer *et al.*, 2018). Nishikawa et al. also reported that the expression of CD44 is upregulated in GSCs and may correlate with poor prognosis, another characteristic of the mesenchymal subtype (Nishikawa *et al.*, 2018). Therefore, it is proposed that targeting the GSCs population of the mesenchymal subtype will prevent tumour invasion. As it is still unclear how the tumour microenvironment can influence the single-cell infiltration of GSCs, cellular and environmental conditions promoting the migrating phenotype and driving the GSCs away from the tumour niche should be investigated (Armento *et al.*, 2017; Nishikawa *et al.*, 2018; Robertson *et al.*, 2019). This sub-chapter will elucidate the different mechanisms from the cytoskeleton changes to the use of migratory substrates as we investigate the GBM migration on axons in this project.

1.4.1. Cytoskeleton change

GSCs acquire mutations which help the tumour progression and metastasis such as in receptor tyrosine kinases and the Transforming growth factor beta (TGF-β) signalling (Massagué, 2012). Indeed, SMAD2/3 mutations, the core transcription factors in TGF-β signalling, enable the EMT previously mentioned (Massaous and Hata, 1997). Mesenchymal migration is characterized by enhanced motility, chemoresistance, and stem-like properties (Massaous and Hata, 1997; O'Neill *et al.*, 2010). It is a highly dynamic process which induces by migration-associated changes in the cytoskeleton. That polarized extension of membrane processes in the direction of the cell migration resulted in the formation of pseudopodia, filopodia, and lamellipodia.

The small GTPases are responsible for the regulation of the cytoskeleton. RhoA regulates the contractility at the cell body and the cell rear and leads to increased GBM invasion

(Fortin Ensign *et al.*, 2013). In GBM, Pleiotrophin (PTN) and its receptor PTPRZ1 are involved in the tumour invasion with the Rho/Rho-kinase (ROCK) signalling pathway (Fujikawa *et al.*, 2017; Qin *et al.*, 2017). RAC-1 and CDC42 are involved in cell protrusion formation and cell polarity respectively and their activity is enhanced in infiltrating GSCs (Hirata *et al.*, 2012; Fortin Ensign *et al.*, 2013). Several proteins are involved in the actin polymerization and this includes Cofilin which is highly expressed in migrating GBM cells. Furthermore, GBM can overexpress proteins such as Twist, Snail, Slug and Zeb, and Cadherins, involved in EMT, to interact with existing structures in the brain and migrate (Armento *et al.*, 2017).

The extensions allow the cells to move and penetrate the surrounding environment whilst new focal adhesion forms at the cell front and adhesion contacts disassemble at the rear, known as adhesion turnover (O'Neill *et al.*, 2010). The focal adhesion complexes (FACs) are a downstream effect of integrin signalling which leads to cell migration. They provide traction with the ECM and propel the cell forward under retrograde flows of actin (Boquet-Pujadas, Olivo-Marin and Guillén, 2021).

In addition to the molecular and cellular components, the cytoskeleton changes can be promoted by the tumour microenvironment. For example, the hypoxic environment can also drive the EMT in GBM cells in addition to the activation of transcription factors and signalling pathways mentioned above (Cha, Kang and Kim, 2016; Manini *et al.*, 2018).

1.4.2. Autocrine and paracrine signalling

Cells in the surrounding microenvironment and GSCs also promote migration by secreting growth factors and chemokines (Hoelzinger, Demuth and Berens, 2007). In an autocrine loop, oncogenic EGFR signalling released by neurons, astrocytes, microglia, and reactive astrocytes promotes GBM proliferation, invasion, and resistance. It also induces CD44 localization which further promotes cell migration (Hoelzinger, Demuth and Berens, 2007; Xiao, Sohrabi and Seidlits, 2017). TGF-α is also involved in oncogenic EGFR signalling and promotes a stem cell phenotype (Ramnarain *et al.*, 2006; Hoelzinger, Demuth and Berens, 2007). Another positive feedback loop is created with the autocrine

glutamate signalling involving the glutamate receptors, upregulated in GBM, which promotes invasion (Lyons *et al.*, 2007).

The paracrine signalling between GBM cells and glial cells through multiple signalling pathways can promote tumour invasiveness (de Gooijer *et al.*, 2018). Indeed, neurons secrete the synaptic protein neuroligin-3 to promote GBM cell proliferation (Venkatesh *et al.*, 2015). Secreted proteins in the tumour microenvironment such as C-X-C Motif Chemokine Ligand 12 (CXCL12) and PDGF can also promote migration. CXCL12 interacts with CXCR4 and is normally involved in neuronal guidance in normal brain development. In GBM, both genes are overexpressed and promote the NSC migration towards the tumour increasing the invasive capacity of GBM cells (Barbero *et al.*, 2002; Hoelzinger, Demuth and Berens, 2007). PDGF interacts with PDGFRα, which as mentioned previously is overexpressed in GBM and is involved in stem cell maintenance and proliferation, as well as angiogenesis (Hoelzinger, Demuth and Berens, 2007; Verhaak *et al.*, 2010; Neftel *et al.*, 2019). In contrast, BMP4 is a secreted protein which drives the differentiation of GSCs, hence decreasing migration and proliferation (Xi *et al.*, 2017; Sachdeva *et al.*, 2019).

The autocrine and paracrine signalling of secreted growth factors and cytokines may also enhance the GBM migration on anatomical structures such as axons and blood vessels, allowing the cells to invade longer distances.

1.4.3. Extracellular matrix

GSCs tend to migrate toward a stiffer ECM area, a process termed mechanotaxis (Armento *et al.*, 2017). In the normal brain, the expression of the matrix metalloproteinases (MMP), secreted or membrane-anchored endoproteinases which degrade the ECM, is low. However, MMPs are overexpressed and overactivated in GBM (Beliën, Paganetti and Schwab, 1999; Könnecke and Bechmann, 2013). In particular, the overexpression of MMP-2 and MMP-9 activates the pro-migratory cytokine TGF-β. This, in turn, creates a feedback loop which induces MMP-2 and upregulates integrin avβ3 further promoting the mesenchymal phenotype and migration (Armento *et al.*, 2017; Liu *et al.*, 2018). Other integrins such as integrin α9β1, a5β1, and αvβ5 are

overexpressed in GBM cells and can lead to an enhanced MMP-9 or MMP-2 expression or the activation of TGF-β (Bello *et al.*, 2001; Guo and Giancotti, 2004; Brown *et al.*, 2008; Xiao, Sohrabi and Seidlits, 2017). The integrins are transmembrane receptors involved in cell adhesion and interaction with the ECM. The ECM-integrin binding leads to the downstream activation of focal adhesion kinase (FAK) which promotes migration and further induces the expression of MMP-9 (Hu *et al.*, 2003; Anderson and Galileo, 2016; Jiang *et al.*, 2020). Also, FAK is overexpressed in GBM and it correlates with the tumour grade (Mitra, Hanson and Schlaepfer, 2005; Mitra and Schlaepfer, 2006).

In GBM, many ECM proteins and a hyaluronic acid-enriched matrix with associated proteoglycans and glycoproteins are involved in the increased migration of GBM. The fibrous glycoproteins laminin, fibronectin, and collagen are normally found at the basement membrane but are enriched in GBM. GSCs may also remodel the ECM by producing stiffness-promoting factors such as fibrous glycoproteins to migrate (Cuddapah *et al.*, 2014; Armento *et al.*, 2017; de Gooijer *et al.*, 2018). Fibronectin interacts with integrin α5β1, αvβ3, and αvβ5 and promotes collective invasion of basement the membrane (Martin, Janouskova and Dontenwill, 2012; Serres *et al.*, 2014; Malric *et al.*, 2017). On the other hand, laminin interacts with integrin α6β1, overexpressed in GSCs, and enhances the migration on myelinated axons through netrin, an axonal guidance molecule (Kawataki *et al.*, 2007; Delamarre *et al.*, 2009).

Interestingly, other ECM components overexpressed in GBM such as chondroitin and heparan sulphate proteoglycans can lead to the activation of TGF-β but are also involved in Sema5A axon guidance molecule attachment (Kantor *et al.*, 2004; Chédotal, Kerjan and Moreau-Fauvarque, 2005). Those proteoglycans support cell adhesion through integrin binding and examples of it are the versican, brevican, syndecan 1, as well as tenascin-C (Kawataki *et al.*, 2007; Armento *et al.*, 2017; J. W. E. Chen *et al.*, 2018). Tenascin-C binds to Toll-like receptor 4 (TLR4) and integrin αvβ1/6, α2/6/9β1 and is not normally found in normal neuropil (Brösicke and Faissner, 2015; Xia *et al.*, 2016; Ellert-Miklaszewska *et al.*, 2020). Its expression in the brain correlates with GBM malignancy grade and prognosis and is involved in cell adhesion and migration on blood vessels. Syndecan-1 interacts with co-receptors for FGF-2, fibronectin, and talin modulating

integrin signalling and actinin to regulate cytoskeletal organization. The expression of syndecan-1 was reported to be increased in the GBM mesenchymal subtype (Longley *et al.*, 1999; Wade *et al.*, 2013; Kerrisk, Cingolani and Koleske, 2014). Brevican binds to EGFR, hyaluronic acid, and fibronectin to promote migration (Hu *et al.*, 2008; Xiao, Sohrabi and Seidlits, 2017; Belousov *et al.*, 2019). Versican interacts with hyaluronic acid, CD44, and TGF-β to promote cell migration (Wade *et al.*, 2013; Rao *et al.*, 2014; Xiao, Sohrabi and Seidlits, 2017). Finally, hyaluronic acid binds CD44, and both are overexpressed in GBM, which enables the migration of GBM cells on a hyaluronic acid matrix (Koochekpour, Pilkington and Merzak, 1995; Park, Kwak and Lee, 2008; Belousov *et al.*, 2019)

All this results in an increase in the density and stiffness of the matrix. Importantly, there is also heterogeneity in the microregional extracellular matrix which can alter the GBM invasion. For example, the ECM proteins, hyaluronan, vitronectin, and tenascin-C, are unregulated at the border of the spreading GBM (Bellail *et al.*, 2004; Koh *et al.*, 2018). This emphasizes that GBM migration is a complex mechanism influenced by diverse signalling cascades and the surrounding environment. In addition, ECM stiffness-based cues also regulate and maintain GSCs through specific Rho GTPases we have previously mentioned (Fortin Ensign *et al.*, 2013).

1.4.4. Axonal Guidance Molecules

As previously mentioned, GSCs can invade long distances within the brain by interacting with pre-existing structures such as white matter tracts composed of myelinated axons (de Gooijer *et al.*, 2018). The GBM migration along myelinated axons is modulated by axonal guidance molecules such as semaphorins and netrins and through a hyaluronic acid-rich matrix (Chédotal, Kerjan and Moreau-Fauvarque, 2005; Cha, Kang and Kim, 2016; Armento *et al.*, 2017; de Gooijer *et al.*, 2018). Those axonal guidance molecules can be secreted, oligodendrocyte membrane-anchored, and transmembrane proteins (Giese *et al.*, 1996; Tessier-Lavigne and Goodman, 1996). They are composed of a multitude of proteins involved during neural development but that is hijacked by GBM

to migrate along the myelinated axons. Example of it are semaphorins, netrins, and ephrins.

Semaphorins play a key role in the cytoskeleton regulation involving RhoA, RAC-1, and cofilin previously described. Semaphorins activate RAC-1 through its interaction with EGFR and PDGFRα. Conversely, Sema3F negatively regulates RhoA and its inhibition leads to cell motility (Li and Lee, 2010; Li, Law and Lee, 2011). Netrin 1 is an axon guidance receptor which binds to the UNC5-family dependence receptor. It is associated with the enhancement of stemness and invasion through Notch signalling and its expression is associated with poor prognosis (Lee *et al.*, 2008; Ylivinkka *et al.*, 2013). The secreted Slit proteins regulate axon guidance and the migration of neural progenitor cells by sending chemorepulsive signals onto cells expressing the Robo receptors (Mertsch *et al.*, 2008; Xu *et al.*, 2010; Kouam *et al.*, 2018). In GBM, the expression of Slit-2 is low whereas Robo1 is overexpressed, leading to an increase in migration (Mertsch *et al.*, 2008; Xu *et al.*, 2010; Kouam *et al.*, 2018). Finally, there is also an increased expression of receptors to ephrins (Eph), ligands affecting cell migration, adhesion, differentiation, proliferation, and survival through Jun-N-terminal kinase (JNK), STAT3, PKB/AKT, and Rho GTPase pathways. For example, Eph Receptor B1 (EphB1) is overexpressed and can act as a regulator of the “Go or Grow” behaviour of GBM (Wei, Wang and Ji, 2017).

The corpus callosum is the largest white matter tract in the brain and is the main highway for GSCs to cross into the other hemisphere. The continuous extension of the tumour in both hemispheres through the bilateral corpus callosum results in the distinctive butterfly pattern on axial view, termed ‘butterfly GBM’ (Bellail *et al.*, 2004; Claes, Idema and Wesseling, 2007; de Gooijer *et al.*, 2018). As the surgical resection has a poor risk-to-benefit ratio, the butterfly GBM is associated with a poor prognosis. Hence, it is crucial to decipher the mechanism of axonal guidance molecules to prevent the invasion of axons.

1.4.5. Perivascular Space

GBM cells can also migrate using the blood vessels as migratory substrates. Indeed, the rigidity of the perivascular space and chemoattractants released by endothelial cells such as bradykinin promote migration. GBM also secrete CXCL12 which then hijacks the Olig2-Wnt7 signalling pathway to further drive invasion along blood vessels (Barbero *et al.*, 2002).

1.4.6. Immune response

Finally, the compromised blood-brain barrier allows circulating immune cells in the GBM tumour microenvironment such as monocytes, T cells, and neutrophils. Despite the abundant presence of immune cells, the infiltrative GBM cells avoid any sort of immune response by secreting immunosuppressive factors, known as 'stealth invasion of the brain' (Claes, Idema and Wesseling, 2007). As such, they suppress T cells through the secretion of T cell checkpoint molecule Programmed death-ligand 1 (PD-L1) and favour the immunosuppressive phenotype of tumour-associated microglia (resident macrophages of the brain) by secreting TGF-β and interleukin-10 (IL-10) (Wu *et al.*, 2010; Prosniak *et al.*, 2013; Ricklefs *et al.*, 2018). Along with tumour-associated microglial cells, the immune cells secrete pro-angiogenic and immunosuppressive factors which further promote maintenance of the GBM cells and their escape from immune surveillance.

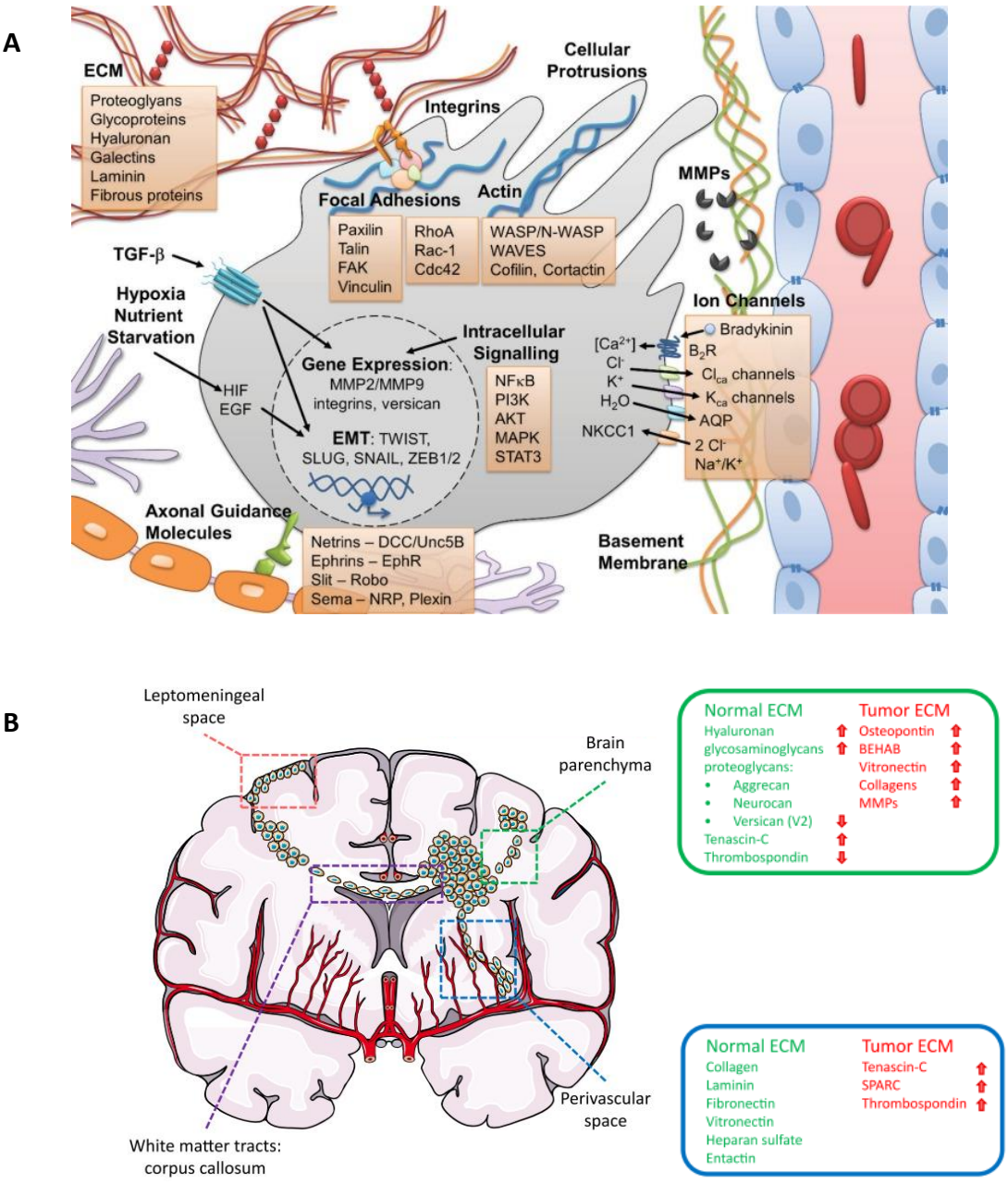

Figure 1.2 GBM migration and invasion

A) Mechanisms of GBM migration and invasion such as cellular signalling cascades and interactions with environmental features (Armento *et al.*, 2017). **B)** Routes of GBM invasion including the brain parenchyma, the perivascular space, the white matter tracts, and the leptomeningeal space and the ECM changes between the tumour (red) and normal brain (green) (de Gooijer *et al.*, 2018).

1.5. *In vitro* GBM models to study migration

Consequently, the appreciation of context-dependent invasion signalling contributed to the rise of relevant *in vitro* models recapitulating the complexity of GBM. They aim to define the interactions between the GBM cells and the various components of the brain microenvironment to target GBM migration and invasion. As we aim to develop an *in vitro* model to study the GBM migration, this sub-chapter will describe the evolution of models from established to patient-derived cell lines as well as from monolayer to 3D cultures (Table 1.2).

1.5.1. Cell Lines

Different classic tumour cell lines have been established including, but not limited to, U251, U87MG, T98G, and G11 (Allen *et al.*, 2016). These traditional lines are grown in serum-supplemented media and have been routinely used to study the development and various mechanisms of GBM. The challenge with these cell lines is that the serum-supplemented media promotes astrocytic differentiation and genetic aberrations over time (Lee *et al.*, 2006). Therefore, those cells may diverge genetically or epigenetically to a point where they fail to recapitulate the phenotype of the human disease (Robertson *et al.*, 2019). There is also the risk of harbouring non-parental genotypic mutations. Many research laboratories have since moved away from traditional cell lines to patient-derived lines as traditional cell lines do not accurately reflect the infiltrative and stem-cell characteristics of GSCs (Xie *et al.*, 2015).

Patient-derived tumour cell lines accurately recapitulate the stem-cell characteristics of GCS, and thus the *in vivo* features of GBM. They are grown in neural stem-cell culture conditions (supplemented with growth factors such as EGF and FGF and in the absence of serum). Primary cultures/explants from human tissue can also be maintained in suspension or on an adherent (laminin) surface for a long period (Galli *et al.*, 2004; Singh *et al.*, 2004; Pollard *et al.*, 2009). Examples of such widely used patient-derived cells include the GBM1, GBM4 and GBM20 cell lines and the GNS cell lines (Wurdak *et al.*, 2010; Polson *et al.*, 2018). These cells, unlike the traditional serum-cultured lines, retain the genetic and transcriptional state of the parental tumour despite frequent passaging

(Lee *et al.*, 2006). Moreover, these cell lines are disease-relevant and maintain the molecular genotype, phenotype and heterogeneity of the original tumour *in vitro* and *in vivo*. This has notable potential for personalised precision medicine because we can now quantify differences between patient tumours with therapeutic development in mind (O'Duibhir, Carragher and Pollard, 2017).

This project focuses on the Wurdak lines, GBM1 and GBM20. GBM1 was first presented by Wurdak et al. in 2010 and characterised as a primary tumour from a proneural subtype (Wurdak *et al.*, 2010; Polson *et al.*, 2018). GBM20 was later added to the set by Polson et al. in 2018 and is derived from a pre-treated recurrent tumour of a mesenchymal subtype (Polson *et al.*, 2018).

Finally, other *in vitro* cell models include *in vitro* engineered tumour-initiating cells (Robertson *et al.*, 2019). As GSC display similar molecular markers to subventricular zone NSCs (Pollen *et al.*, 2015), NSCs were previously obtained via the differentiation of human pluripotent stem cells (Conti *et al.*, 2005). With the introduction of induced pluripotent stem cells (iPSC), many protocols have been established with human iPSC-derived neural progenitor cells modelling GSCs (Sancho-Martinez *et al.*, 2016). By engineering driver mutations *in vitro* in cells to be transplanted *in vivo*, they showed that iPSC-derived NSC has been transformed into glioma-initiating cells. Another study reported that postnatal primary cortical astrocytes and NSC harbouring GBM-associated oncogenic protein EGFR will generate tumours in their xenograft model (Singh *et al.*, 2017).

1.5.2. 2D models

Various models to study GBM have been developed from *in vitro* simple reductionist approaches to complex organoids to study the cell's intrinsic and extrinsic properties (Robertson *et al.*, 2019). In reductionist approaches, cells are cultured in a simple monolayer on glass or plastic substrates functionalized with the substrate of interest such as ECM by coating or by adding it to the medium. Scratch invasion assays and cell-exclusion zone assays enabled the identification and the study of the role of various ECM molecules and MMP in the initiation and progression of the disease (Beliën, Paganetti

and Schwab, 1999). An example of it is the hyaluronic acid/CD44 interaction involvement in cell detachment, migration, and invasion (Koochekpour, Pilkington and Merzak, 1995).

However, simple monolayer cultures do not capture all cell-ECM interactions or the interactions with other cells in the tumour microenvironment. For example, Leite et al. investigated the linear cell migration of GBM cells (U-87 MG, SNB-19, and UP-007) with microglia in a live-imaging of scratch wound assays or transwell migration assays (Boyden chamber) (Leite *et al.*, 2020). In a disease which affects the brain and is highly influenced by extrinsic factors, the lack of heterogeneity and essential features such as hypoxia, interstitial fluids pressure, and cytokine concentration gradient can make a model not representable of the disease. The shear stiffness of 1-3.5 kPa of the brain with varying viscoelastic behaviour contributes to the lack of valuable cell models and many laboratories have turned to 2D co-cultures to resolve it.

As cancer research evolved, assays developed from scratch wound assays to random cell migration assays. Random cell migration assays are more adapted to the study of individual cancer cell migration as the scratch wound assays are more relevant to the analysis of wound healing with cells collectively migrating toward each other to form tight junctions. However, scratch wound assays are still performed to study the mechanism of resistance against drugs. For example, Tiek et al. showed how TMZ-resistant cell lines adapted a strategy to increase migration (Tiek *et al.*, 2018).

1.5.3. 3D models

The introduction of 3D models for migration assays has enabled labs around the globe to better recapitulate the complexity of GBM and mimic its microenvironment. This allowed the generation of patient-specific GSC-derived model types, including glioma spheres or tumour organoids, and co-cultures with several other cell types (Pine *et al.*, 2020). Neurosphere-based models are semi-3D *in vitro* models able to maintain the stemness of GBM cells (Singh *et al.*, 2004). Aubert et al. co-cultured spheroids of glioma cells (GL15) with astrocytes to investigate the role of gap junctions in the migration of glioma cell spheroids on substrates of collagen and primary astrocytes (Aubert *et al.*,

2008). In line with our project, Zepecki et al. developed a co-culture of GBM neurospheres on dorsal rat myelinated axons (Zepecki *et al.*, 2019). Using high-content imaging, they demonstrated the real-time migration of patient-derived GBM cells on their axons.

More complex modelling can be achieved with organoids. The use of organoids allowed for a better study of the brain tumour microenvironment and the necrotic centre of organoids is ideal to mimic the hypoxic gradient environment of brain cancer (Azzarelli, 2020). For example, da Silva et al. developed early-stage cerebral organoids and demonstrated an increase in infiltration with the patient-derived GBM1 spheroids compared to the neural progenitor's spheroids (da Silva *et al.*, 2018). The authors concluded that the early-stage cerebral organoids may be a useful model for the identification of anti-GBM invasion strategies (da Silva *et al.*, 2018).

1.5.4. Tissue-engineered 3D models

The brain tumour microenvironment is unique due to its composition of the parenchyma with distinct ECM and the blood-brain barrier. This is difficult to mimic *in vitro* and poses a problem for treatment. With the evolution of tissue engineering and synthetic models, biomaterials can be used to mimic the mechanical and topography of the brain. These range from polymer-based protein delivery systems, micro/nanoparticles, hydrogel, and porous scaffolds. Protein delivery systems allow the incorporation of protein molecules into appropriate matrices for the gradual release of the protein cargo as well as the prevention of rapid protein degradation by limiting its exposure to proteases or neutralizing antibodies. Fibrous scaffolds refer to scaffolds made of fibres with varying diameters from micro- to nanometres. They create a 3D structure which can be used to imitate structures of the brain such as white matter tracts or axons.

For example, hydrogels are used to encapsulate a glioma spheroid and electrospun fibres to imitate axon white matter tracts (Johnson *et al.*, 2009; Rao *et al.*, 2013; Haji Mansor *et al.*, 2018). Diao et al. used a 3D model consisting of micro-chamber arrays containing natural collagen to analyse invasion patterns of the GBM cell lines – LN229, SNB19, U87, and U251. This assay could potentially be applied to patient-derived cells

(Diao *et al.*, 2019). Ngo, Karvelis, and Harley assembled 3D endothelial networks on U87MG cells encapsulated in gelatin hydrogels to investigate the role of various secreted factors on the GBM cell number, migration, and resistance to TMZ (Ngo, Karvelis and Harley, 2020). In other drug resistance assays, Leite et al. cultured primary tumourspheres seeded on Geltrex with a hyaluronic acid-gelatin hydrogel to investigate cell migration in response to oxaliplatin with intra-tumour heterogeneity (Gudbergsson *et al.*, 2019; Leite *et al.*, 2020).

Further 3D models focus on mimicking the vascular system with Ozturk et al. generating a 3D bioprinted model with perfused vascular channels with high-content imaging (HCI) system which enabled the non-invasive monitoring of a 3D culture viable for up to 70 d (Ozturk *et al.*, 2020). Whereas Bayat et al. used label-free HCI and a phase-contrast microscope to image a 3D co-culture with U87 spheroids and Human Umbilical Vein Endothelial cells in fibrin gel (Bayat *et al.*, 2018).

1.5.5. HiPSC-derived models

A challenge when studying the brain is that there are many differences between brain structures in animals and humans, and there is limited access to tissue from the human brain. The use of human iPSCs (hiPSC) for disease modelling has proven to have a lot of potential for GBM and this could benefit personalised medicine as well as quicker and safer drug development.

HiPSCs are stem cells that can be generated ("induced" or "reprogrammed") by reprogramming adult somatic cells to a pluripotent state (Takahashi *et al.*, 2007; Moradi *et al.*, 2019). They have the potential to self-renew indefinitely in culture and differentiate into any specialized cell type. Specific transcription factors: Oct3/4, Sox2, Klf4, and c-Myc, known as the Yamanaka factors, are introduced by retroviral transduction into adult fibroblast cells (Takahashi *et al.*, 2007; Yamanaka, 2007; Park *et al.*, 2008), causing them to become more similar to embryonic stem cells. Additionally, these cells can then be differentiated into cell types of the three germ layers (Takahashi *et al.*, 2007). iPSCs have become a valuable tool for medical research because they offer a way to study human disease and develop new therapies without the ethical and

practical limitations associated with the use of embryonic stem cells (Moradi *et al.*, 2019). They can also be used to create personalized treatments, as they can be generated from a patient's cells and then used to replace damaged or diseased tissues.

Commonly, hiPSCs are differentiated with the introduction of small molecules to direct iPSCs into cortical lineages but this is a challenging and long process, and its efficiency can be variable (Moradi *et al.*, 2019). Accurate modelling has now been achieved using transcription-factor mediated differentiation known as forward reprogramming. This involves the generation of a transgenic iPSC line with a doxycycline-inducible transcription factor at a safe-harbor loci which we will elaborate further in the Results Chapter 2 (Fernandopulle *et al.*, 2018). The culture and genetic engineering of these lines are straightforward and have been applied to different neuronal lineages including cortical neurons (Fernandopulle *et al.*, 2018).

Valuable cell models able to capture the invasiveness of GBM are critically needed to develop innovative therapies that target migrating GBM cells. As the efficacy of conventional therapies is limited in eliminating the highly infiltrative GBM cells, more research on glioma motility is critically needed to develop a more targeted therapeutic approach (Cuddapah *et al.*, 2014; Kim *et al.*, 2015; Armento *et al.*, 2017).

Table 1.2 Various *in vitro* GBM models to study migration

Inter-tumoural heterogeneity is represented by the cellular states (Neftel et al., 2019).

		Production		GBM cell population			Analysis		What can be studied			
Model		simple	low-cost	self-renewable cells	homogenous	heterogenous	high-throughput	live-imaging	ECM	multi-cellular	axons	blood vessels
2D monolayer	Scratch wound	✓	✓	✓	✓		✓	✓	✓			
	Random cell migration	✓	✓	✓	✓		✓	✓	✓			
3D model	Transwell migration	✓	✓	✓	✓		✓		✓	✓		
	Co-culture		✓			✓	✓	✓		✓	✓	✓
	Neurophere			✓			✓	✓		✓		
	Microfluidic systems					✓		✓	✓	✓		✓
	Organoids/spheroids					✓				✓	✓	✓
3D tissue engineered model	Biomaterial scaffolds			✓	✓		✓	✓	✓	✓		
	Electrospun nanofibres			✓	✓		✓	✓			✓	✓

1.5.6. Imaging challenges

Although the introduction of organoids can provide more relevancy with immune cell co-cultures, vascularisation, and tissue engineering, it is highly variable, lengthy, and laborious (Robertson *et al.*, 2019). Furthermore, another challenge with using organoids is the imaging due to their size. The bigger the organoid (larger than 1 mm^2) the harder it is to image the middle cells using live-imaging approaches and traditional imaging technologies like fluorescence microscopy (Ozturk *et al.*, 2020). The limited field of view, the shallow depth penetration, and the risk of photobleaching result in the need for cryosection and confocal imaging. Tissue clearing can be an option and was done previously on brain organoids (Renner *et al.*, 2017). Organotypic slices cultured in the air-liquid interface can also be imaged with live imaging (Giandomenico *et al.*, 2019). Nevertheless, the increase in complexity of the model renders the dissection of each mechanism difficult due to factors such as heterogeneity of cell types and necessitates HCI and fast deep-tissue imaging techniques to image *in vitro* 3D models (Bian *et al.*, 2018; Robertson *et al.*, 2019).

1.6. High-content imaging

HCI, also known as high-content screening or analysis is an advanced approach which combines automated imaging and quantitative data analysis for cell-based screening in drug discovery (Liu and Nolan, 2014; Bon, Si and Arimondo, 2020). The application of automated imaging and multiparameter algorithms allows the visualisation and quantification of the cell phenotype, behaviour, and morphology at the single-cell level (Usaj *et al.*, 2020). Various assays can be exploited for the screening and identification of candidate drugs or biomarkers as well as the characterisation of a panel of cell lines in cell profiling assays which is why it is relevant to this thesis (Danovi *et al.*, 2013; Usaj *et al.*, 2020; Veschini *et al.*, 2021). HCI is also suitable for a high-throughput format in large-scale applications in endpoint and live assays (Liu and Nolan, 2014; Singh, Carpenter and Genovesio, 2014; Bon, Si and Arimondo, 2020).

1.6.1. Tracking cells

HCI involves using bioimage analysis, the process of translating image data into features of biological significance that are quantifiable (Boquet-Pujadas, Olivo-Marin and Guillén, 2021). The first apparent feature is the morphology feature of the cell which is aided by a reliable segmentation to separate the cells from the background using the spatial or frequency distribution of image brightness (Boquet-Pujadas, Olivo-Marin and Guillén, 2021). This gives information on the cell viability, adhesion, as well as means for motility. The segmentation also allows the tracking of migrating cells and the study of invasion assay in tumour cells (Boquet-Pujadas, Olivo-Marin and Guillén, 2021).

1.6.2. Cell migration assays

Different imaging techniques are used for cell migration assays. The main one is fluorescence microscopy as it increases contrast for better tracking of the cells and identification of markers. This is used for fixed and sectioned cultures for structural imaging, but also for drug response with analysis of cell proliferation. The combination of wide-field fluorescence microscopy with live-cell imaging further enables the studies of tracking properties such as the speed, persistence, displacement, and directionality of the cells.

Label-free imaging is a good option to avoid fluorescence-based tracking which may be phototoxic and can alter normal cell function including migration. This includes phase contrast and differential interference contrast commonly used for 2D monolayer cultures and live cell imaging.

1.6.3. Personalised Medicine

The evolution of HCI has benefitted the progress towards personalised medicine approaches. The technology named ‘pharmacoscopy’ enables the discovery and prediction of suitable drugs to which patients would respond via high-throughput and HCI. *Ex vivo* drug screening of patient biopsies will predict the drug response and therefore improve treatments. This offers new possibilities for comparison across genotype, phenotype, and clinical trial stratification. In cancers such as leukaemia, initial

promising results have been obtained by extracting patient-derived cells and testing their response to a panel of drugs *ex vivo* (Snijder *et al.*, 2017). The identification of effective therapies based on precision medicine is essential to improve GBM prognosis. Similar approaches are now being attempted in diverse GBM models to identify relevant molecular markers in GBM (Garrett, Lastakchi and McConville, 2020; Lee *et al.*, 2022). In 2022, Lee et al. developed an *in silico* drug screening on more than 1 million compounds using machine learning and multi-omics profiling (Lee *et al.*, 2022). They present the GBM oncogenesis and the neural activity-dependent signalling as tumour-intrinsic neural vulnerabilities and opportunities for clinical translation. More recently, Migliozzi et al. used integrative multi-omic networks to evaluate the association of therapeutic response with GBM subtypes and to inform patient classification in future clinical trials. They identified Protein Kinase C delta (PKCδ) and DNA-PK as GBM subtype-specific therapeutic targets (Migliozzi *et al.*, 2023).

1.7. PhD project

Following the shift towards models involving patient-derived cells which can recapitulate some aspects of the tumour microenvironment, we found a lack of effective models for GBM migration using patient-derived GBM cells on human axons. It has not been previously confirmed that GBM cells interact with axon bundles and migrate towards an hiPSC-derived cortical neural spheroid. We hypothesise that patient-derived GBM cells will migrate towards the neural spheroid using axons and that the migration could be mediated by several migratory cues such as the axonal structure, the axonal guidance molecules, and soluble growth factors/cytokines released by the neural spheroid.

In the next chapters, I will describe how I developed an *in vitro* model mimicking the GBM microenvironment by co-culturing patient-derived GBM cells and human iPSC-derived cortical neural spheroids with radiating axons (Figure 1.3). Using HCI, I generated robust pipelines to study the infiltration of GBM cells in endpoint assays as well as migratory properties such as the speed, displacement, directionality and persistence in live-imaging assays.

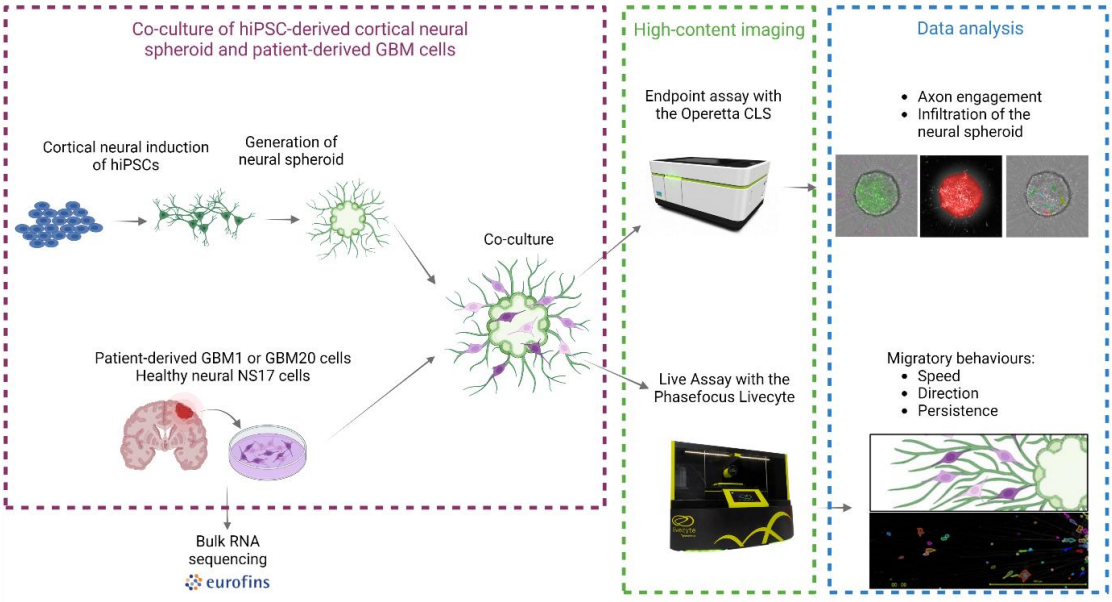

Figure 1.3 Graphical abstract

Schematic diagram summarising the co-culture of hiPSC-derived cortical neural spheroid and patient-derived GBM cells (purple box), the endpoint or live assays using HCI, and the data analysis and pipelines. Created with BioRender.com.

2. MATERIALS AND METHODS

2.1. Cell culture

2.1.1. GBM cells culture

Nunc™ EasYFlask™ Cell Culture T75 and T25 flasks (Thermo Scientific 156472 and 156340) were coated with poly-L-ornithine (PLO) (Sigma P3655-50MG) diluted in H_2O at 5 µg/mL for 1 h at room temperature (RT) followed by coating with laminin (Thermofisher 23017015) diluted in Phosphate Buffered Saline (PBS, Sigma P4474) at 2 µg/mL overnight at RT. The patient-derived GBM1 and GBM20 cell lines were derived under informed consent according to ethical approvals (LREC 115/ES/0094; courtesy of Dr Heiko Wurdak, University of Leeds (Wurdak *et al.*, 2010; Polson *et al.*, 2018). GBM1 and GBM20 cell lines were derived respectively from a primary tumour of a 58-year-old female patient and a 50-year-old male patient with a recurrent GBM, previously treated with Radiotherapy, TMZ and IMA950. The cell models maintain the stem cell-like characteristics of GBM under adherent culture conditions (Wurdak *et al.*, 2010; da Silva *et al.*, 2018; Polson *et al.*, 2018).

Cells were cultured in Neurobasal Medium (Invitrogen 21103049) supplemented with 0.5X B27 (Invitrogen 17504044), 0.5X N2 (Invitrogen 17502048), 40 ng/mL Epidermal growth factor (EGF) (R&D Systems 236-EG-200), and 40 ng/mL basic-fibroblast growth factor (b-FGF) (Invitrogen PHG0026) as described in Table 2.1. The cells were given at passage 12 and cell banks were created by growing the cells from a T25 to T75 and batch freezing at early passages. The cells were passaged every week when approximately 80% confluency was reached. The passages were kept between passage numbers 14 to 20 for each experiment. Following a rinse with PBS, the cells were detached with incubation with TrypLE Express Enzyme (1X), no phenol red (Gibco 12604013) for 4 min at 37°C and resuspended in Neurobasal medium in a T75 laminin-coated flask.

Table 2.1 Components of the neurobasal media for GBM cells

Component	Manufacturer	Catalogue n°	Stock	Medium
Neurobasal Media	Invitrogen	21103049	/	/
B27 Supplement	Life Technologies	17504044	50X	0.5X
N2 Supplement	Life Technologies	17502048	100X	0.5X
Epidermal growth factor (EGF)	R&D Systems	236-EG-200	400 µg/mL	40 ng/mL
Basic fibroblast growth factor (b-FGF)	Invitrogen	PHG0026	100 µg/mL	40 ng/mL

2.1.2. Neural stem cells

T75 or T25 flasks were coated with PLO and laminin as previously described in section 2.1.1. The cells GCGR.NS17ST_A (shorten to NS17) from the Glioma Cellular Genetics Resource (GCGR) was acquired under informed consent according to local ethical approvals (08/S1101/1) (Al Shboul *et al.*, 2021). They were kindly provided by Dr Steven Pollard (University of Edinburgh) and cultured according to previously published methods (Pollard *et al.*, 2009). The medium used was DMEM/HAMS-F12 (Sigma D8437) supplemented with Glucose (Sigma G8644), MEM Non-essential Amino Acids (MEM NEAA) 100x (Gibco 11140-035), Pen-Strep (Gibco 15140-122), bovine serum albumin (BSA) 7.5% (Gibco 15260-037), Beta-Mercaptoethanol 50mM (Gibco 31350-010), B27 Supplement 50x (LifeTech/Gibco 17504-044), and N2 Supplement 100x (LifeTech/Gibco 17502-048) as described in Table 2.2. Before use, complete media was also supplemented with EGF to a final concentration of 40 ng/mL and b-FGF to a final concentration of 40 ng/mL. The cells were passaged every week when they reached approximately 80% confluency at a split no lower than 1:6. Following a rinse with PBS, the cells were detached with incubation with StemPro Accutase Cell Dissociation Reagent (Gibco A1110501) for 6 min at RT and resuspended in DMEM/HAMS-F12 in a T75 laminin-coated flask.

Table 2.2 Components of the neural stem cell media for NSC

Component	Supplier	Catalogue n°	Stock	Medium
DMEM/HAMS-F12	Sigma	D8437	/	/
Glucose	Sigma	G8644	100 g/L	1.5 mg/mL
MEM NEAA 100x	Gibco	11140-035	100X	100 µM
Pen-Strep	Gibco	15140-122	5000 U/mL and 5000 mg/mL	50 U/mL and 50 mg/mL
BSA Solution 7.5%	Gibco	15260-037	7.50%	0.01%
Beta-Mercaptoethanol	Gibco	31350-010	50 mM	100 µM
B27 Supplement	Life Technologies	17504-044	50X	0.5X
N2 Supplement	Life Technologies	17502-048	100X	0.5X
EGF	R&D Systems	236-EG-200	400 µg/mL	10 ng/mL
b-FGF	Invitrogen	PHG0026	100 µg/mL	10 ng/mL

2.1.3. Induced glutamatergic neurons cell culture

PAMV1 human iPSCs obtained from the HipSci biobank (www.hipsci.org). For forward reprogramming (Results Chapter 2), cells were transduced by Federica Riccio in Dr Ivo Lieberam's laboratory. She transduced the PAMV1 cells with a doxycycline-inducible Neurogenin-2 transgene following the protocol from the Ward laboratory (Fernandopulle *et al.*, 2018) (Figure 2.1.A). The integration of the transgene was achieved by electroporation and TALEN-mediated integration into the AAVS1 safe-harbour locus. 6-well plates were coated with 4% Vitronectin XF (Stem Cell Technologies 100-0763) diluted in PBS for 1 h at RT. Cells were cultured in feeder-free conditions in supplemented Essential 8 medium (Gibco A1517001) and 1% or 50 U/mL and 50 mg/mL Penicillin/Streptomycin respectively (Life Technologies 15140-122) as described in Table 2.3.A. The medium was changed daily and cells were passaged at approximately 1.5 million cells per well. Cells were rinsed with PBS, incubated with TryplE for 4 min at 37°C and resuspended in E8 medium with 10 µM Y-27632 Rho-kinase inhibitor (ROCK

inhibitor, ENZO Life Sciences ALX-270-333-M005) in 6-well vitronectin-coated plates at approximatively 1.5 million cells per well.

2.1.4. Transcription factor-mediated differentiated cortical neurons

The transcription factor-mediated differentiation protocol (Results Chapter 2), was adapted from the Ward laboratory (Fernandopulle *et al.*, 2018) (Figure 2.1.A). On Day 0, PAMV1 cells were rinsed twice with PBS and dissociated using Accutase at 37°C for 5 minutes. The cells were resuspended with the Induction Medium - DMEM/F12 Hepes (Life Technologies 11330032), supplemented with 100x N2, 100x MEM NEAA (Life Technologies 11140-050), 100x L-Glutamine (Gibco 25030081), Doxycycline (2 µg/ml) (Sigma D9891) and 10 µM Y-27632 ROCKi (1:1000), as described in Table 2.3.B, on GFR Matrigel (bd biosciences 356230) in DMEM (Life Technologies 11966025) (1:50) at a density of 1.5 million cells per well in a 6-well plate. Doxycycline will induce the differentiation into Glutamatergic Excitatory Neurons. On Day 1, nascent neurites began to be evident and the cultures were rinsed twice with PBS and fresh induction media with Doxycycline was added. On Day 2, the medium was replaced with fresh medium. On Day 3, neurites were evident. Cells were dissociated with Accutase to be frozen (1 million cells per vial) or for a neural spheroid generation.

Table 2.3 Components of the medium used in transcription-factor driven differentiation.

A) E8 media for stem cells
B) Neural induction media
C) Cortical neuron maintenance media

A

Component	Manufacturer	Catalog n°	Stock	Medium
Essential 8 (E8) Basal medium	Gibco	A1517001	/	/
E8 supplements	Gibco	A1517001	100X	1X
Penicillin-streptomycin	Life Technologies	15140-122	5000 U/mL and 5000 mg/mL	50 U/mL and 50 mg/mL

B

Component	Manufacturer	Catalog n°	Stock	Medium
DMEM/F12 Hepes	Life Technologies	11330032	/	/
N2 supplements	Life Technologies	17502-048	100X	0.5X
MEM Non-essential amino acid solution	Life Technologies	11140-050	100X	100 µM
l-Glutamine	Gibco	25030081	200 mM	2 mM
Doxycycline	Sigma	D9891	2 mg/mL	2 µg/ml

C

Component	Manufacturer	Catalog n°	Stock	Medium
BrainPhys neuronal medium	Stemcell Technologies	5790	/	/
B27 supplements	Life Technologies	17504-044	50X	0.5X
BDNF	PeproTech	450-02	10 µg/mL	10 ng/mL
NT-3	PeproTech	450-03	10 µg/mL	10 ng/mL
Laminin	Thermofisher	23017015	1 mg/mL in PBS	1 µg/mL

2.1.5. Generation of neural spheroids

A 96-well V-bottom plate was treated with 5% Pluronic F127 (Sigma-Aldrich P2443) according to the in-house protocol (Alsehli *et al.*, 2021) at RT for 1 h (Figure 2.1). The addition of the V-bottom 96-well plate as well as the coating of pluronic acid facilitated the aggregation of the cells and the reproducibility of similar sizes neural spheroids. Following dissociation, cells were resuspended in the induction media and were seeded at a density of 10 000 cells/well in the V-bottom plate after a PBS wash. The plate was centrifuged for 2 min at 200 g to aggregate the cells at the bottom of the well. The cells were left for 48 h with daily half-medium changes.

2.1.6. Maturation and generation of axon bundles

On day 6, the neural spheroids were transferred to laminin-coated 24-well or 96-well glass bottom plates (Cellvis P24-0-N and P96-0-N) in Cortical Neuron Culture Medium - BrainPhys neuronal medium (Stemcell Technologies UK Ltd 5790) supplemented with 50x B27 supplements, 10 ng/mL Brain-Derived Neurotrophic Factor (BDNF) (PeproTech 450-02), 10 ng/mL Neurotrophin-3 (NT-3) (PeproTech 450-03) and 1 µg/mL Laminin as described in Table 2.3.C. The cells were checked daily for the presence of cell debris and morphological changes with bi-weekly half-medium changes.

2.1.7. Co-culture of GBM cells with neural spheroids

On Day 11, BioTracker 488 Green Nuclear Dye (Sigma-Aldrich SCT120) at 1000X was diluted to a final concentration of 1X in cell culture medium and was used to stain the neural spheroids for 20 min at 37°C followed by two medium washes. GBM cells were labelled with BioTracker 655 Red Cytoplasmic Membrane Dye (Sigma-Aldrich SCT108) (final concentration of 1X in cell culture medium) in suspension for 20 min at 37°C and washed three times by centrifugation. The GBM cells were seeded on top of the neural spheroids at a density of 5 000 cells/well in a 24-well plate or 840 cells/well in a 96-well plate with a 50/50 medium (Figure 2.1).

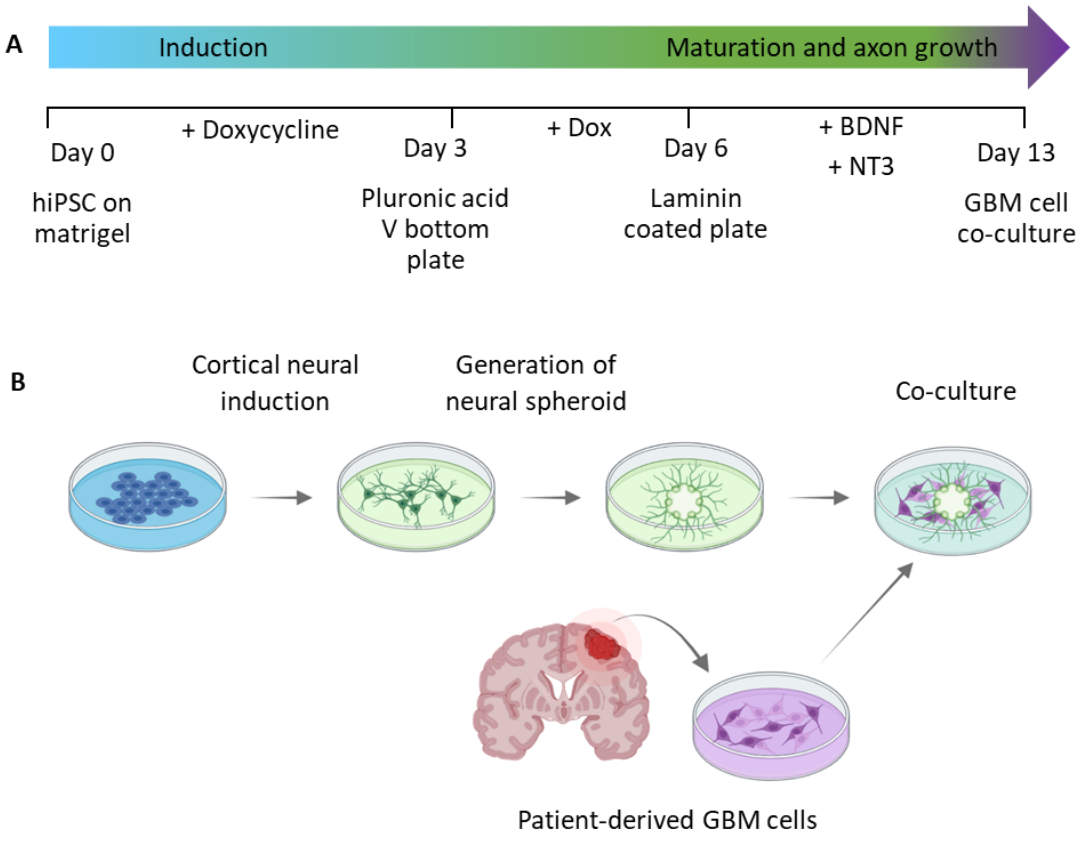

Figure 2.1 Timeline for neural induction and co-cultures

A) Timeline for inducing the transcription-factor mediated differentiation for cortical neurons (protocol from Fernandopulle et al., 2018. Laboratory of Michael Ward), generating neural spheroids using pluronic acid coated V bottom plates and co-culturing the NS with patient-derived cells.

B) Schematic diagram of the neural spheroid and GBM cell co-culture.

2.1.8. Extrinsic factor-driven neural differentiation of hiPSC (previous protocol)

While initially developing both approaches, I later settled on the transcription factor rather than extrinsic-factor-driven differentiation for its efficiency and reproducibility (Results Chapter 1 and Results Chapter 2). PAMV1 human iPSCs were differentiated into cerebral cortical neurons according to the protocol from Shi et al. (Shi, Kirwan and Livesey, 2012). Neural induction was performed by culturing the hiPSC colonies in Neural Maintenance Medium - DMEM/F-12 GlutaMAX (Life Technologies 31331-028),

Neurobasal medium, 1x B27 (with RA), 1x N2, 5 µg/mL insulin (Sigma I9278), 100 µM NEAA, 100 µM beta-mercaptoethanol (Life Technologies 31350), 2 mM L-Glutamine (Life Technologies 25030-024), Sodium pyruvate (Sigma S863650), 1% Penicillin/Streptomycin, supplemented with 1 µM Dorsomorphin (Tocris 3093) and 10 µM SB431542 (Tocris Bioscience 1614) as described in Table 2.4. Once a neuroepithelial layer was formed (days 8-12), the cells were passaged using PluriSTEM Dispase-II Solution (Sigma SCM133) in aggregates in neural induction medium onto laminin-coated dishes and sustained in the neural medium the next day. Once neural rosettes were visible (days 12-17), the neural stem cells were further expanded with 20 ng/mL of FGF-2 (F20) for 2–4 days. Between days 20-30, considerable neurogenesis should occur, and the neural rosettes can be cryopreserved for future use.

2.1.9. Generation of neural spheroids with axon bundles (previous protocol)

The rosette structures were grown and following incubation with PBS + EDTA (Life Technologies 15575020) for 3 min at RT, they were detached as a sheet with 50/50 medium using a P1000 pipette. After the transfer to a 15 mL falcon tube using the P10mL, the cells were centrifuged at 0.8 rcf for 3 min. The pellet was resuspended in clumps with proliferation medium (F20) and was then transferred to a suspension 6-well plate and placed on a shaker at 50 rpm in the incubator for the formation of aggregates. After 2 days, the medium was replaced with a 50/50 medium as described in Table 2.4. The neural spheroids were transferred laminin-coated TC plate and left to outgrow axons.

Table 2.4 Components of the medium used in extrinsic factor-driven differentiation.

A) Cortical neural maintenance media
B) Cortical neural induction media
C) Freezing media

A

Component	Manufacturer	Catalog n°	Stock	Medium
DMEM/F-12, GlutaMAX	Life Technologies	31331-028	/	50%
Neurobasal Media	Invitrogen	21103049	/	50%
B-27 supplement with vit A	Life Technologies	17504-044	50X	1X
N-2 supplement	Life Technologies	17502-048	100X	0.5X
Insulin	Sigma	I9278	10 mg/mL	5 µg/mL
MEM Non-essential amino acid solution	Life Technologies	11140-050	100X	100 µM
2-Mercaptoethanol	Life Technologies	31350	50 mM	100 µM
Sodium pyruvate	Sigma	S8636	100 mM	50 µM
Penicillin-streptomycin	Life Technologies	15140-122	5000 U/mL and 5000 mg/mL	50 U/mL and 50 mg/mL
l-Glutamine	Life Technologies	25030-024	200 mM	2 mM

B

Component	Manufacturer	Catalog n°	Stock	Medium
Neural Maintenance Media	/	/	/	/
SB431542	Tocris Bioscience	1614	10 mg	10 µM
Dosomorphin	Tocris	3093	10 mg	1 µM

C

Component	Manufacturer	Catalog n°	Stock	Medium
Dimethyl sulfoxide	Sigma	D2650	100%	10%
Fibroblast growth factor 2	PeproTech	100-18B	10 µg	20 ng/mL

2.2. FACS sorting of CFP+ GBM1 cells

GBM1 were previously transfected with a plasmid with Cyan fluorescent protein (CFP) and Neo resistance gene using the T2A system and the FuGENE HD Transfection Reagent. Geneticin (InvivoGen G418) treatment was used to select the cells. The CFP+ GBM1 cells and untransfected GBM1 cells (negative control) were prepared for FACS sorting following a PBS rinse and lifted using TrypLE. The cells were rinsed in FACS buffer (PBS w/o Ca2+/Mg2+, 0.5% BSA, 5U/ml DNaseI, 0.2% glucose) and centrifuged at 1200 rpm for 4 min. The supernatant was discarded, and the cell pellet was resuspended in the FACS buffer. The samples were divided into two separate tubes where a live/dead stain Zombie Near Infra-Red (NIR) Fixable Viability Kit (BioLegend 423105) was added to half of the tubes. The cells were then transferred and filtered using 40 µm strainer cap FACS tubes. They were kept on ice and brought to the BRC Advanced Phenotyping Platform where they were sorted using the BD FACS Aria cell sorter 2 and analysed with the FACSDIVA software.

2.3. Staining and Imaging

2.3.1. Immunostaining

Neural spheroids were fixed at 4% PFA/PBS at RT for 20 min. The cells were rinsed with PBS twice and placed in fresh PBS at 4°C until staining. The cells were permeabilized with 3% BSA/0.1% Triton-X-100/PBS for 1 h at RT and incubated with primary antibodies diluted in 3% BSA/0.1% Triton-X-100/PBS overnight at 4°C in the dark (Table 2.5). The next day, primary antibodies were rinsed away 3x with 3% BSA/PBS for 5 min. The cells are incubated with secondary antibodies diluted (Table 2.5) (1:500) in 3% BSA/0.1% Triton-X-100/PBS at RT for 45 min at RT and rinsed 2x with PBS for 5 min away from light. To stain the nucleus, the cells are incubated with Hoechst 10 µM (1:1000 in PBS from 10mM stock solution) for 10 min at RT and rinsed with PBS once. Finally, the cells were incubated with 80% glycerol as a clearing agent for 1 h min at RT and rinsed with PBS three times before being placed in fresh PBS at 4°C until imaging.

2.3.2. Confocal microscopy

Confocal images were acquired using a Leica TCS SP8 Confocal laser scanning microscope, using a 10x dry objective and viewed with the Leica software. Each fluorochrome was excited with the corresponding laser line (DAPI, UV (355 nm); AF488, Green (530 nm); AF594, Red (639 nm) laser line). Immunofluorescence data were analysed in Fiji open-source software (2.0.0-rc-64/1.51s version). The brightness/contrast of the image was adjusted using the histogram. Images from different fields were tiled and stitched and the maximum projection was obtained using the Z stack.

Confocal images were also acquired using the Operetta CLS Imaging System (PerkinElmer) with the brightfield, 488 nm, and 639 nm channels. The PreciScan Intelligent Acquisition plug-in for Harmony software was used to locate the neural spheroid within the well (Figure 2.2). The plug-in allows the accurate target of the region of interest (ROI) and significantly reduces acquisition and analysis times. Once the PreciScan was performed and the region of the neural spheroid was located, a Z-stack of 10 images over 20 µm (distance 2 µm) was acquired.

Table 2.5 Primary (A) and secondary (B) antibodies used in immunofluorescence.

A

Antigen	Expression	Host	Dilution	Supplier	Catalog n°
Foxg1	Primary progenitors	rabbit	1/500	abcam	ab18259
Ki67	proliferation	mouse	1/500	bdbiosciences 550609	550609
MAP2	dendrites	rabbt	1/500	cell signal	8707
Pax6	primary progenitors	rabbit	1/500	Biolegend 278P	901301
Tau	axons	sheep	1/500	abcam	ab62639
Tuj1 (beta-III Tubulin)	axons	mouse	1/1000	R&D systems	MAB1195

B

Antigen	Fluorophore	Host	Dilution	Supplier	Catalog n°
anti-mouse	AF 488	goat	1/500	Invitrogen	A-11029
anti-sheep	AF 488	donkey	1/500	Invitrogen	A-11015
anti-rabbit	AF 594	donkey	1/500	Invitrogen	A-21207

2.4. Imaging assay

2.4.1. Live-cell imaging of labelled cells

CFP+, nuclear dyed, membrane dyed GBM cells or NS17 were imaged on the Operetta Mark 1 High Content Analysis System (PerkinElmer). Images were acquired using Harmony Software. Regions of interest were selected and live cell imaging was performed with the brightfield and far-red channel every 30 min for 24 h.

2.4.2. Live-cell imaging of non-labelled cells

Live-cell imaging of non-labelled cells was performed on the Livecyte quantitative phase imager (Phasefocus). ROIs (10 mm x 25 mm) on the right and the top of the neural spheroids were selected and images were acquired every 10 min for 16 h.

2.4.3. Endpoint assay

Co-cultures of patient-derived GBM cells and hiPSC-derived cortical neural spheroids were imaged every 24 h at Day 0, 1, 2, and 3 using the Operetta CLS High Content Analysis (PerkinElmer) with the brightfield, 488 nm and 655 nm channels. To locate the

neural spheroid within the well, the PreciScan Intelligent Acquisition Plug-in for Harmony software was used as previously described (Figure 2.2). Once the PreciScan was performed and the region of the neural spheroid was located, a Z-stack of 10 images over 20 µm (distance 2 µm) was acquired.

2.4.4. Inhibitor screen

Inhibitors were added to the co-culture at a final concentration of 1 µM. Following a 6 h antagonist treatment, images were acquired using Operetta CLS Imaging System. This was repeated for the next two days.

Analysis Sequence "PreciScan Spheroid"

Input Image	**Input**		
	Flatfield Correction : None Brightfield Correction **Stack Processing :** Maximum Projection **Min. Global Binning :** Dynamic		
Find Image Region	**Input**	**Method**	**Output**
	Channel : Alexa 488 **ROI :** None	**Method :** Common Threshold Threshold : 0.6 Split into Objects Area : > 0 px²	Output Population : Neural Spheroid Output Region : Neural Spheroid
Calculate Intensity Properties	**Input**	**Method**	**Output**
	Channel : Alexa 488 **Population :** Neural Spheroid **Region :** Neural Spheroid	**Method :** Standard Mean	Property Prefix : Intensity Image Region Alexa 488
Select Population	**Input**	**Method**	**Output**
	Population : Neural Spheroid	**Method :** Filter by Property Intensity Image Region Alexa 488 Mean : > 1500	Output Population : Intensity Filtered
Calculate Morphology Properties	**Input**	**Method**	**Output**
	Population : Intensity Filtered **Region :** Neural Spheroid	**Method :** Standard Area Roundness	Property Prefix : Neural Spheroid
Select Population (2)	**Input**	**Method**	**Output**
	Population : Intensity Filtered	**Method :** Filter by Property Image Region Area [µm²] : > 30000 Image Region Roundness : > 0.6 Boolean Operations : F1 and F2	Output Population : Morph filtered
Determine Well Layout	**Input**	**Method**	**Output**
	Population : Morph filtered **Region :** Neural Spheroid	**Method XY :** Multiple Objects Rescan Magnification : 20x Max No of Fields : Object Margin : 100 µm Field Overlap : 2 % **Method Z :** None	Output Population : Well Layout
Define Results	**Results**		
	Method : List of Outputs **Population : Morph filtered** Number of Objects **Object Results** Population : Intensity Filtered : None Population : Neural Spheroid : None Population : Morph filtered : Use Selected Well Results		

Figure 2.2 Analysis sequence pipeline to locate the neural spheroid using PreciScan

The pipeline was developed using the plug-in PreciScan in Harmony Software of the Operetta CLS to identify the ROI.

2.5. Image analysis

2.5.1. Live-cell imaging analysis of the Operetta Mark 1

Live-imaging assays acquired from the Operetta Mark 1 Imaging System (PerkinElmer) were analysed using the Harmony Software or extracted to be analysed using the plug-in Trackmate in Icy.

2.5.2. Live-cell imaging assay analysis using the Phasefocus Livecyte

Images were analysed using the built-in Analysis Software, Morphology and Motility Assay on the Livecyte quantitative phase imager (Phasefocus) (Figure 2.3.C). Using the built-in applications, the cells were identified and tracked, and the tracking properties were calculated to generate cell morphology and migration parameters (Table 2.6).

2.5.3. Endpoint assay analysis using Icy

The brightfield channel was extracted, a median filter was applied, and the image was inverted (Figure 2.3.A). The image contrast was threshold using the HK-Means plug-in (an increase of intensity to 10, min and max object size change) to detect clustered objects. The holes in the ROI were filled and active contours blocks were applied to identify the neural spheroid as an ROI. Along with it, the 655 nm channel was extracted and a median filter was applied. Using the wavelet spot detector block to detect objects, the GBM cells were identified, the holes in the ROI filled, and active contours blocks were applied again to select the GBM cells to present within the ROI.

2.5.4. Endpoint assay analysis using Harmony

Images were analysed using the built-in Harmony HCI and Analysis Software on the Operetta device (Figure 2.3.B). The maximum projection of the Z-stack was taken, and the neural spheroid was stained with the BioTracker 488 so was identified as an ROI using the green channel, the GBM cells stained with the BioTracker 655 in the ROI were identified and segmented cells using the far-red channel (Segmentation Method C in Harmony Software) (Figure 2.4).

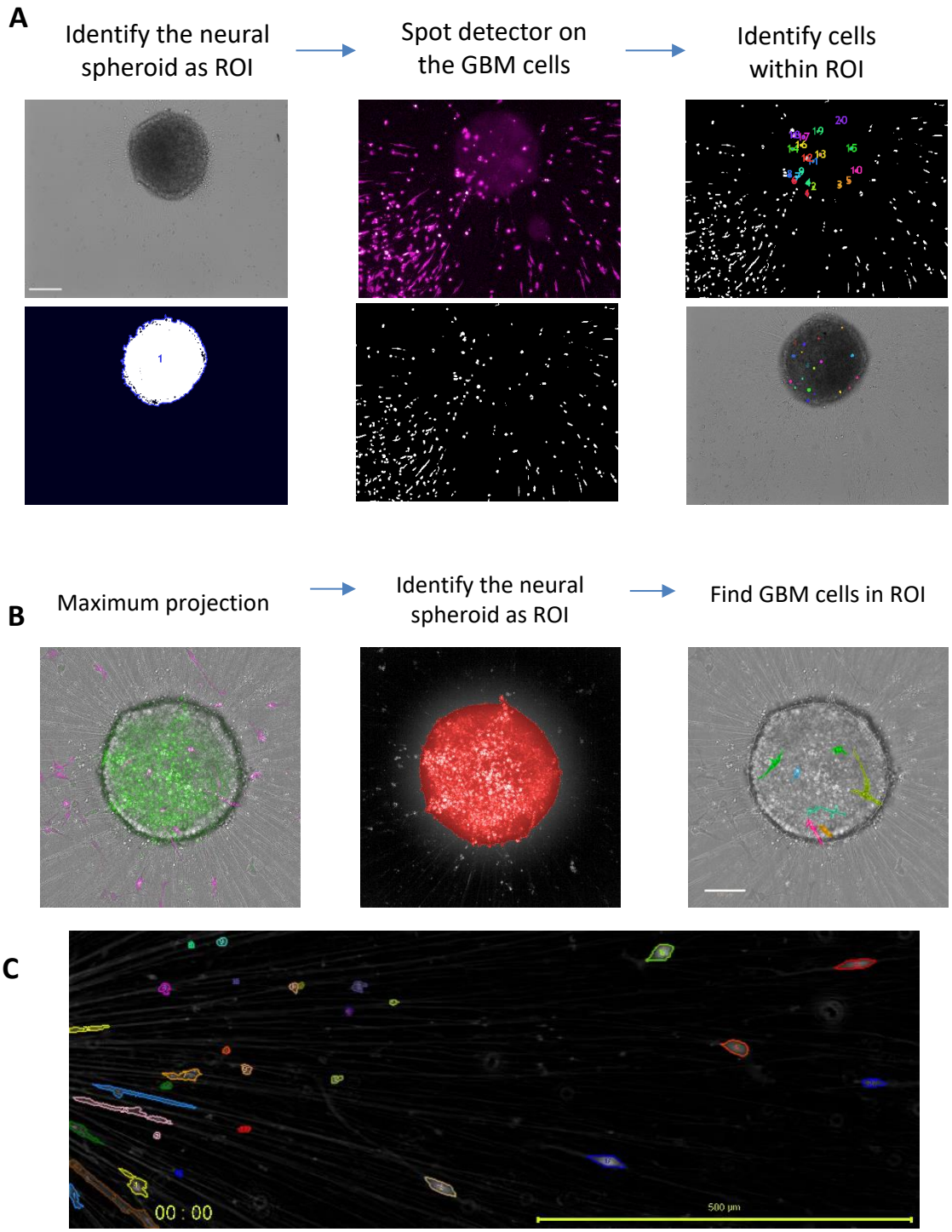

Figure 2.3 HCI pipelines

Analysis pipeline to quantify the GBM cells within the neural spheroid from images acquired on the Operetta CLS and analysed using Icy **(A)** or Harmony **(B)**. Scale bars = 100 µm.
C) Co-culture of GBM cells on axons with the hiPSC-derived neural spheroid on the left, acquired on the Phasefocus livecyte. The cell mask represents the cell id of the tracked cells. Scale bar = 500 µm.

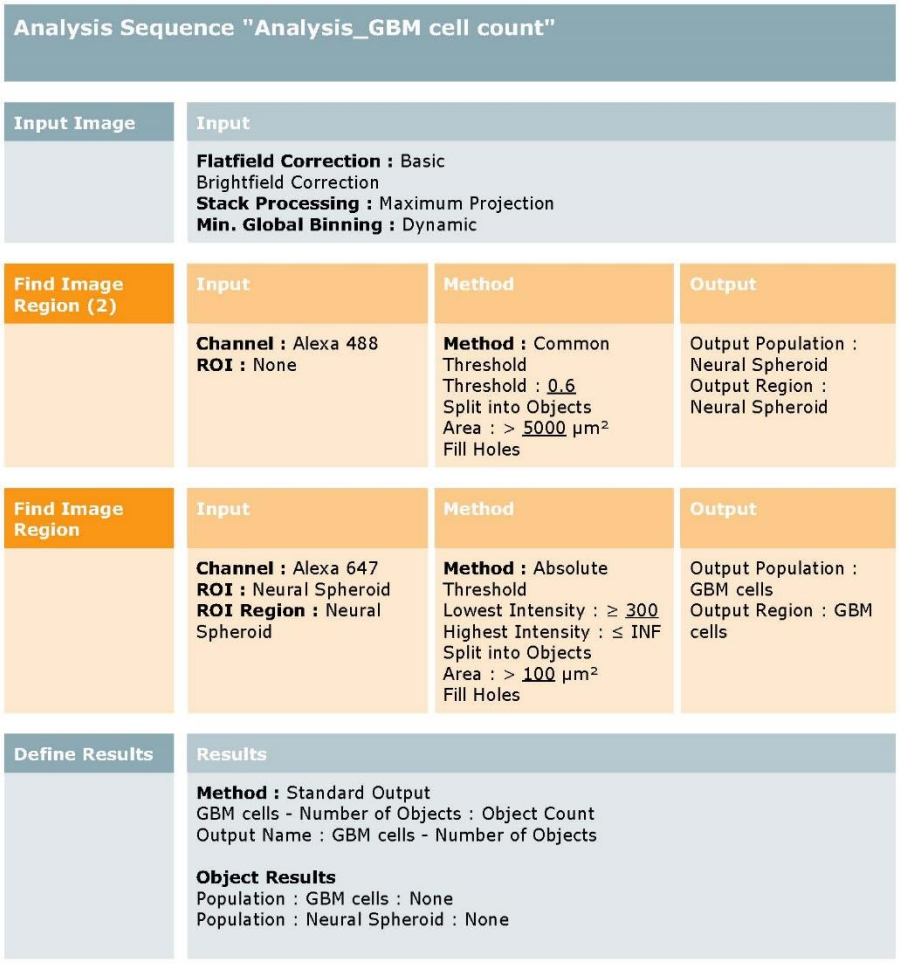

Figure 2.4 Analysis sequence pipeline for the GBM cells infiltration

Pipeline developed using the Harmony Software on the Operetta CLS to quantify the number of GBM cells infiltrated in the neural spheroid.

Table 2.6 Morphology and migration parameters obtained from the Phasefocus Livecyte

The value and description are noted

	Parameter	Value	Description
Morphology	Median cell area	µm^2	The middle value of the surface area of the cells
	Median cell sphericity	A value between 0 and 1	The middle value of the sphericity of the cells. A value close to 1 represents a perfectly spherical cell compared to a value close to 0 with elongations.
Migration	Track speed	µm/s	The average speed of a cell, which is calculated by the total distance travelled divided by the track duration
	Instantaneous velocity	µm/s	The mean velocity for all cells at all time points for each frame, represented in a violin plot
	Persistence	A value between 0 and 1	The total cell displacement is divided by the total distance travelled. A value close to 1 represents a movement in a direct line compared to a cell moving in a randomized direction
	Directionality	polar histograms	The length of the segment is proportional to the number of instances cells moved in this direction

2.5.5. Statistical analysis

All experiments were performed in technical triplicates and were repeated at least three times to perform statistical analysis. All statistical analyses were performed using GraphPad Prism software (version 9.2). Results represented as means with standard deviation (SD) and different ANOVA tests with multiple comparisons between control and other conditions were performed to calculate the statistical significance of multiple experimental conditions. A p-value below 0.05 was considered significant and was indicated with an asterisk: *p≤0.05, **p≤0.01, ***p≤0.001. The number of biological replicates for each experiment is indicated in the figure legend as N.

2.6. RNA sequencing

The GBM1 and GBM20 cell lines were prepared for RNA sequencing. They were rinsed once with PBS, detached with TrypLE and snap-frozen in pellets of 10^6 cells. The cells were submitted to Eurofins Genomics, Germany, under Project ID: NG-29040. Raw sequencing data were pre-processed using the fastp software to generate clean data termed quality control (Figure 2.5). This involves checking the quality of the raw sequencing filtering for high-quality reads to remove poor-quality bases (below Phred Quality 20) (S. Chen *et al.*, 2018).

High-quality sequence reads were aligned using the STAR (Spliced Transcripts Alignment to a Reference) to the reference genome UCSC Homo sapiens version hg38 (Dobin *et al.*, 2013). Gene-wise quantification was achieved to inspect the transcriptome alignments using the RSEM tool (Li and Dewey, 2011). For the differential gene expression between cell lines, genes with less than 10 average reads were removed. Using the R/Bioconductor DESeq2 package, the abundance counts of each gene were then used to perform differential gene expression (Love, Huber and Anders, 2014). This pre-processing was provided by Eurofins Genomics.

Further analysis was performed on R studio using the ggplot2 package to generate a volcano plot of the differential gene expression (Figure 2.6). The values of the sample-wise comparison foldchange and significant foldchange values (log2_foldChange and p-value) provided by Eurofins Genomics were used in this analysis.

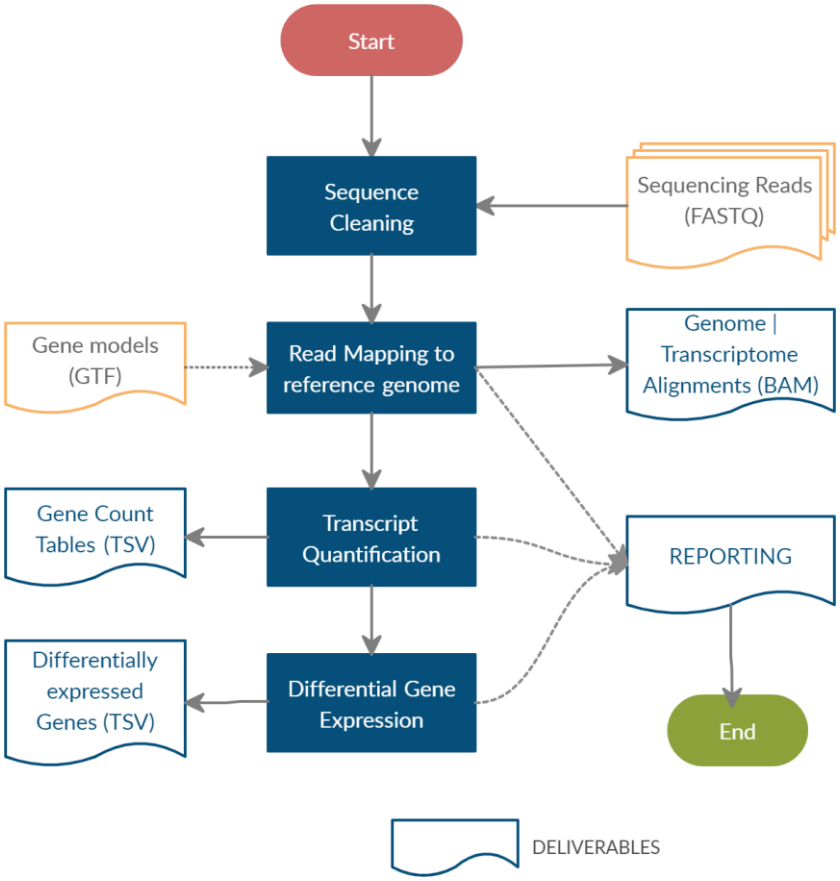

Figure 2.5 RNA sequencing pipeline

Quality control of the RNA sequencing results provided by Eurofins Germany which include the sequence cleaning, read mapping to reference genome, transcript quantification, and differential gene expression.

A

```
# The basic scatter plot: x is "log2FoldChange", y is "pvalue"
ggplot(data=GBM2O_vs_GBM1_fold_change_id_sig, aes(x=log2_foldChange, y=p_value)) + geom_point()

# Convert directly in the aes()

p <- ggplot(data=GBM2O_vs_GBM1_fold_change_id_sig, aes(x=log2_foldChange, y=-log10(p_value))) + geom_point()

# Add more simple "theme"
p <- ggplot(data=GBM2O_vs_GBM1_fold_change_id_sig, aes(x=log2_foldChange, y=-log10(p_value))) + geom_point() + theme_minimal()

# Add vertical lines for log2FoldChange thresholds, and one horizontal line for the p-value threshold
p2 <- p + geom_vline(xintercept=c(-0.6, 0.6), col="red") +
  geom_hline(yintercept=-log10(0.05), col="red")

plot(p)

plot(p2)
```

B

```
# 1. by default, it is assigned to the categories in an alphabetical order):
p3 <- p2 + scale_color_manual(values=c("#990099", "#33CCCC", "black"))

# 2. to automate a bit: ceate a named vector: the values are the colors to be used, the names are the categories they will be assigned to:
mycolors <- c("#990099", "#33CCCC", "black")
names(mycolors) <- c("Enriched in GBM1", "Enriched in GBM2O", "NO")
p3 <- p2 + scale_colour_manual(values = mycolors)
plot(p3)

# Now write down the name of genes beside the points...
# Create a new column "delabel" to de, that will contain the name of genes differentially expressed (NA in case they are not)
GBM2O_vs_GBM1_fold_change_mig$delabel <- NA
GBM2O_vs_GBM1_fold_change_mig$delabel[GBM2O_vs_GBM1_fold_change_mig$diffexpressed != "NO"]
<- GBM2O_vs_GBM1_fold_change_mig$gene_name[GBM2O_vs_GBM1_fold_change_mig$diffexpressed != "NO"]

ggplot(data=GBM2O_vs_GBM1_fold_change_mig, aes(x=log2_foldChange, y=-log10(p_value), col=diffexpressed, label=delabel)) + geom_point()+ theme_minimal() + geom_text()

# Finally, we can organize the labels nicely using the "ggrepel" package and the geom_text_repel() function
install.packages("ggrepel")
# load library
library(ggrepel)
# plot adding up all layers we have seen so far
ggplot(GBM2O_vs_GBM1_fold_change_mig, aes(x=log2_foldChange, y=-log10(p_value), col=diffexpressed, label=delabel)) +
  geom_point() +
  theme_minimal() +
  geom_text_repel() +
  scale_color_manual(values=c("#990099", "black", "#33CCCC" )) +
  geom_vline(xintercept=c(-1, 1), col="red") +
  geom_hline(yintercept=-log10(0.1), col="red")
```

Figure 2.6 R scripts

R script using the ggplot2 package for the **(A)** generation of the volcano plot and **(B)** to highlight the genes involved in the inhibitor screen

3. RESULTS CHAPTER 1 - DEVELOP A CO-CULTURE OF EXTRINSIC FACTOR-DRIVEN DIFFERENTIATED HIPSC-DERIVED NEURAL SPHEROID AND PATIENT-DERIVED GBM1 CELLS

This project aims to develop an *in vitro* model mimicking the GBM microenvironment to study the migration of patient-derived GBM cells on axons. The model comprises a co-culture of patient-derived GBM cells which mirror the relevant tumour-maintaining cells and hiPSC-derived cortical neural spheroid with radiating axons, which mirror the microenvironment of migrating tumour cells. Using HCI analysis, I have developed robust pipelines to quantify the migratory cell behaviour in endpoint and live image-based assays. This experimental system may be further developed to serve as a screening tool to identify new treatments for GBM based on specific inhibition of cell migration.

The patient-derived GBM1 cells, studied in this work, were established by Polson et al. 2018 and Wurdak et al. 2010 (as described in the Materials and Methods). The GBM1 cell line was derived from a primary tumour of a classical/proneural GBM phenotype. It was cultured as dissociated cells under adherent conditions and maintained stem cell-like characteristics. In this chapter, I will report how I tested several HCI platforms and techniques to identify, track, quantify, and characterise the migration of labelled or non-labelled patient-GBM cells in 2D endpoint and live assays.

Cortical neurons can be obtained with many different protocols ranging from primary cells to stem cell-derivation protocols via extrinsic factor (with soluble factors) or transcription factor-driven differentiation (forward reprogramming with transduction of transcription factors) (Shi, Kirwan and Livesey, 2012; Fernandopulle *et al.*, 2018). I generated cortical neurons using extrinsic factor-driven differentiation based on the protocol published by the Livesey group (Shi, Kirwan and Livesey, 2012), as well as using the transcription factor-driven differentiation based on the Ward laboratory protocol (Fernandopulle *et al.*, 2018). Once I obtained cortical neurons, I aggregated them

together to form neural spheroids which can develop axons all around. Before settling on one protocol, I compared both protocols based on the morphology of the neural spheroid and the axon development, and I also optimized the aggregation of the neural spheroid.

Throughout my PhD project, I have tried several methods of hiPSC reprogramming, spheroid aggregation, and imaging methods. This chapter reports the first pilot experiments including the imaging of single patient-derived GBM1 cells, the generation of the cortical neural spheroid with radiating axons using extrinsic factor-driven differentiation followed by the co-culture of patient-derived GBM cells and hiPSC-derived cortical neural spheroid. In Results Chapter 2, I will cover the successful development of hiPSC-derived cortical neural spheroid using transcription factor-driven differentiation and the co-culture with patient-derived GBM1, GBM20 cells and non-cancer NS17 cells.

Finally, different high-content imaging platforms were used throughout the project such as the Operetta Mark 1 High Content Imaging System (PerkinElmer) and the Livecyte quantitative phase imager (Phasefocus). The Operetta Mark 1 Imaging System is a platform commonly used in the fields of cell biology, drug discovery, and genomics. It combines automated microscopy, advanced image analysis, and data visualization capabilities to provide researchers with detailed and quantitative information about cellular processes. The key features of the Operetta Mark 1 Imaging System include high-throughput, multimodal, and live cell imaging. The Phasefocus Livecyte imager is a label-free imaging device, which uses ptychographic quantitative phase imaging to capture high-resolution phase images of cells. This label-free imaging method allows for non-invasive observation of live cells without the need for exogenous labels or dyes resulting in lower risks of phototoxicity. It generates images by recording a data set consisting of interference patterns scattered from an object of interest relative to an illumination field. The data is processed and inverted into an image contrast. Similarly to the Operetta Mark 1, it also allows for automated analysis and time-lapse imaging as well as accurate single-cell tracking and image-based cytometry.

This aim is divided into different objectives using extrinsic factor-driven differentiation: (1) generate hiPSC-derived cortical neurons, (2) develop a hiPSC-derived cortical neural spheroid with radiating axons, (3) characterise the cortical neuron identity and axon bundles via specific markers, and (4) co-culture the hiPSC-derived cortical neural spheroid with patient-derived GBM cells.

3.1. Investigate patient-derived GBM1 single cells in 2D live assays

3.1.1. Sorting CFP+ GBM1 cells

I set to develop a live image-based assay able to identify, track, and quantify the migratory behaviour of patient-derived GBM1 cells on the hiPSC-derived axons from the neural spheroid. One common method to facilitate the identification and tracking of cells is to overexpress a fluorescent marker. Hence, the GBM1 cells were transfected with CFP using the T2A system and geneticin treatment was used to select the cells.

I sorted CFP+ GBM1 cells by flow cytometry to get a homogenous culture. Hence, the cell vials were thawed and cultured, and prepared for sorting using a live/dead stain in NIR and FACS buffer as described in the methods chapter. The cells were sorted using the Aria 2 sorter. The FACS plot generated shows the gates for unstained GBM1 cells, GBM1 cells stained with a live/dead stain and two samples of CFP+ GBM1 cells stained with a live/dead stain (Figure 3.1). The cells were gated as the following: “Scatter” using the side and forward scatter, “Single cells” to eliminate doublets, “Live/Dead” to select live cells, and finally the “CFP+ GBM cells” were selected based on their CFP AmCyan expression. Although 3 million cells were sorted for the two samples, only 2% of the GBM1 cells were CFP+ which totalled to 50 000 cells.

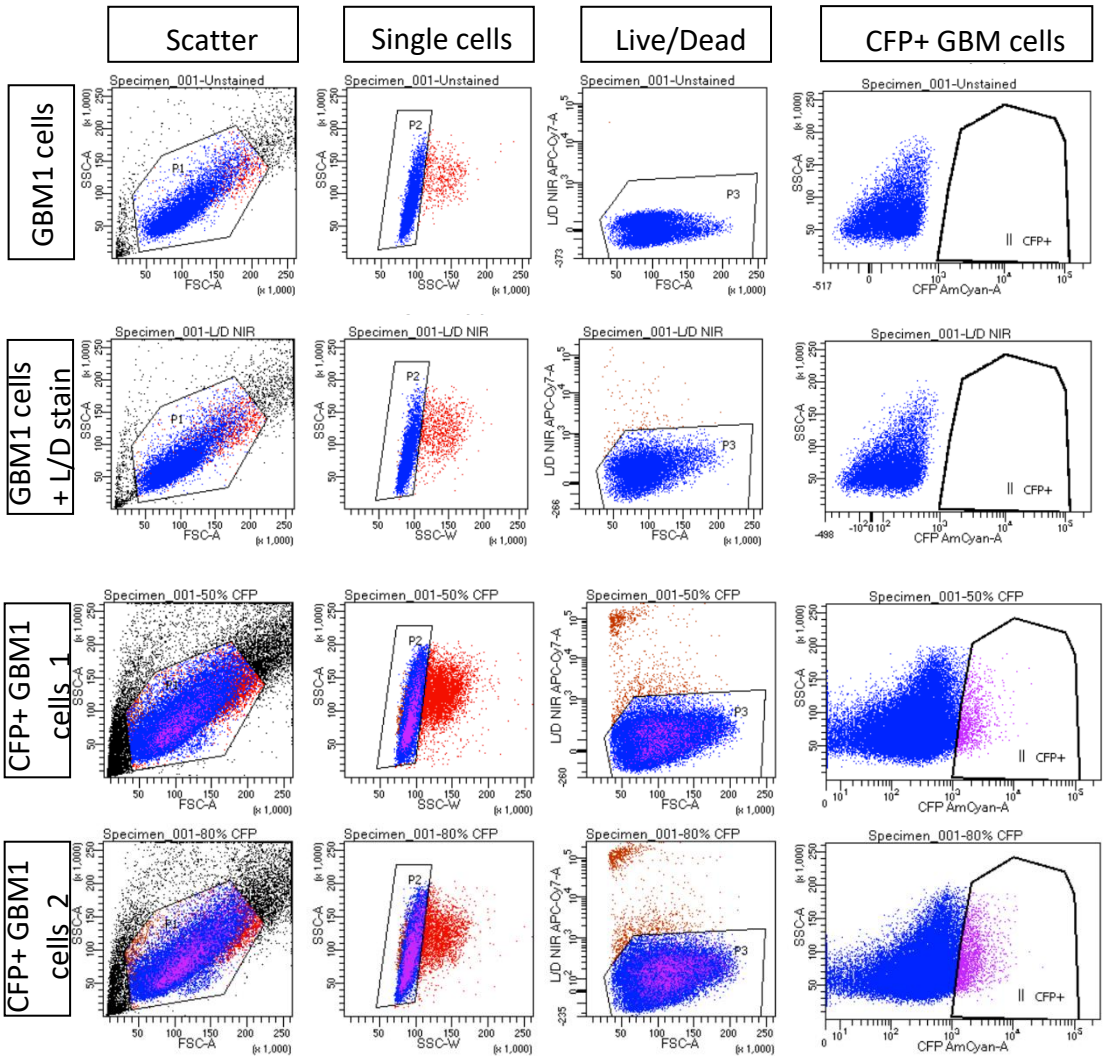

Figure 3.1 FACS sort of CFP+ GBM1 cells

FACS plots of non-transfected GBM1 cells, non-transfected GBM1 with the L/D stain, and two samples of CFP+ GBM1 cells. The cells were sorted based on the side and forward scatter and the singlets were selected. The cells were gated with the L/D stain and expression of CFP.

3.1.2. Tracking CFP+ and nuclear-stained cells from the Operetta Mark 1 images

In line with my objective to develop a live-image-based assay to identify, track, and quantify the migratory behaviour of patient-derived GBM cells on the hiPSC-derived

axons from the neural spheroid, I set out to image and track them as single cells. Accordingly, I tested and compared different imaging methods to identify and track the GBM1 cells including the FACS-sorted CFP+ GBM1 cells and non-labelled GBM1 cells stained with Hoechst and NucRed.

I plated the CFP+ GBM1 cells and non-labelled GBM1 cells in a laminin-coated glass 6-well plate. The non-labelled GBM1 cells were stained with Hoechst or NucRed once adhered and rinsed with PBS. Live-cell imaging was performed on the Operetta Mark 1 every 30 min for 48 h with the brightfield, green, blue, and red channels. As Cyan and Green cannot be separated without spectral unmixing, the green laser was used. Tracking the CFP+ GBM1 cells using the Harmony software was not ideal as only a small proportion of the CFP+ GBM1 cells were detected (Figure 3.2). Moreover, the introduction of the nuclear dyes Hoechst and NucRed seemed to be toxic to the cells as they started to die after less than 10 h from staining. Acquired images of CFP+ GBM1 cells were extracted and analysed with Trackmate in ImageJ. The plug-in enabled the modification of more variables and the ability to skip frames when the cell goes out of focus. Trackmate identifies the GBM cells in the brightfield channel and I labelled each cell track by the duration of the track. However, the changes in cell morphology rendered the cells difficult to identify and resulted in a high number of short tracks.

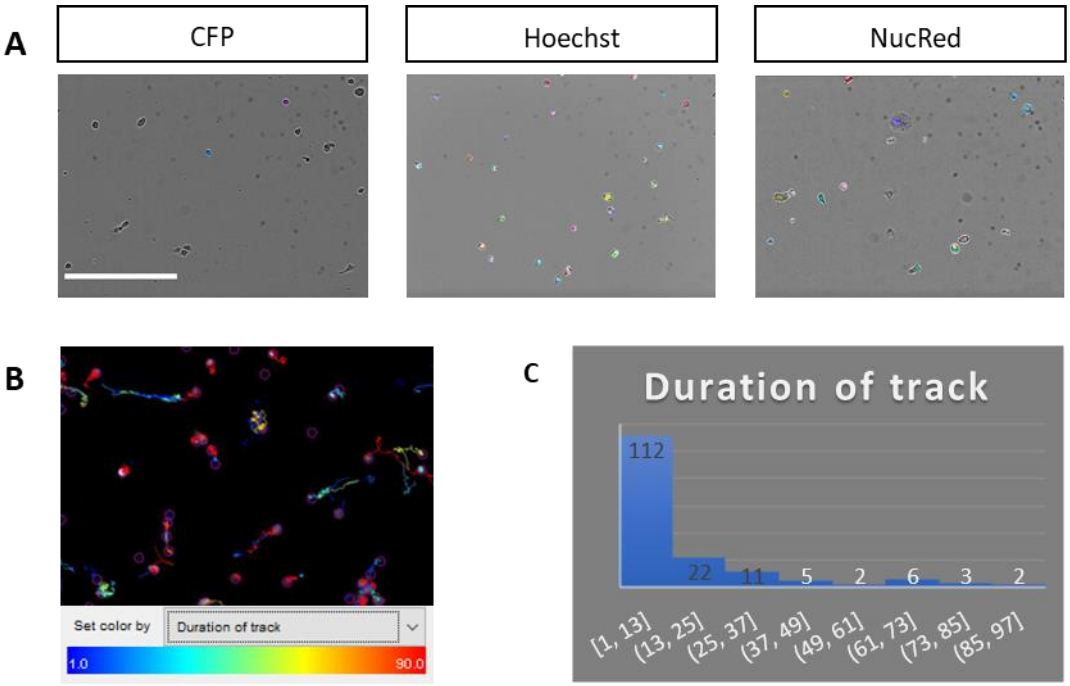

Figure 3.2 Tracking CFP+ or nuclear stained GBM1 cells from the Operetta Mark 1 images

A) Snapshots showing the CFP+ GBM1 culture, Hoechst, and NucRed nuclear stainings at the 10 h timepoint with the colour representing each cell track. Scale bar = 100 µm.
B) Tracking of GBM1 cells using Trackmate on ImageJ. Image representing a snapshot of the video using Trackmate on ImageJ with the track colour representing the duration of tracks by several timepoints.
C) Histogram showing the tracks generated. Only two cells were tracked through the whole 90 timepoints and most of the tracks are shorter than 20 timepoints.

3.1.3. Lipophilic dye staining enabled an accurate identification of the GBM cells

I aimed to screen multiple cell lines from patients whilst improving cell identification, and segmentation, tracking, and decided to use separate imaging devices for endpoint and live assays. For endpoint assays, I reasoned that using lipophilic dyes would be better than nuclear dyes or transduction of fluorescent genetic markers as they are less toxic and do not interfere with the replication/transcription. Also, this allows to readily screen multiple cell lines from large panels. Instead of using the Hoechst or NucRed stained or CFP+ GBM1 cells, GBM1 cells were stained with BioTracker AF655 in suspension and seeded on laminin-coated glass bottom plates. The dye is a lipophilic

membrane dye suitable for long-term labelling and cell tracking. Once stained, the images were acquired on the Operetta Mark 1 the following day. The images represent the GBM1 cells stained with BioTracker AF655 in the 655 nm channel only, and the 655 nm and brightfield channels combined. From the observations, the BioTracker AF655 stains the cells clearly and accurately and there are different sizes and shapes composing the GBM1 cell line (Figure 3.3.A and B).

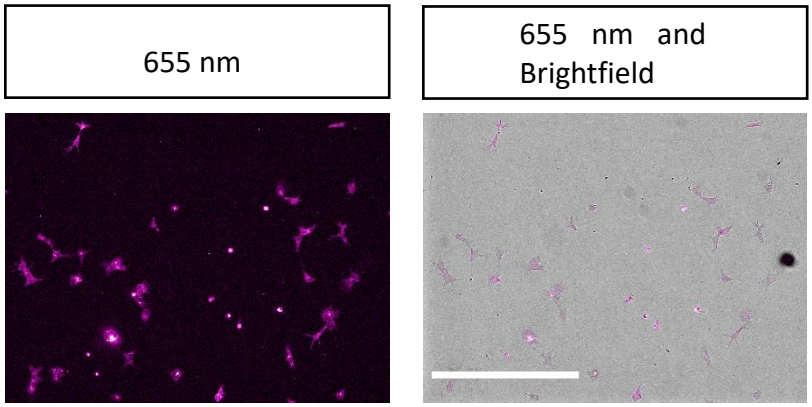

Figure 3.3 Patient-derived GBM cells can be stained with BioTracker AF655
Example images with GBM1 cells stained using BioTracker in far red cultured on a laminin-coated glass bottom plate. Merged channels on the right side. Scale bar = 100 µm.

3.1.4. The Phasefocus Livecyte allowed long-term cell tracking in live assays

As the live imaging and tracking of labelled cells using the Operetta was challenging, I attempted to image the cells with a label-free imaging device, the Phasefocus Livecyte. The Livecyte uses quantitative phase imaging and ptychography to create a phase contrast image with lower risks of phototoxicity (see Materials and Methods). Images of GBM1 cells were acquired for 48 h every 15 min. Using the built-in analysis software, accurate cellular segmentation was performed and a cell mask was created (Figure 3.4.A). With this approach, I was able to visualize the cells and accurately identify and track individual cells.

3.1.5. The cell density affected the speed and velocity

I set to standardise and optimise the cell density to identify an ideal cell density for a migration assay. The cell density should allow the appropriate space between the GBM cells so they can proliferate and move freely, be identified and be tracked.

Different densities of cells from 3,000 to 8,000 cells were seeded in a 24-well plate. The built-in motility application software from Livecyte was used to determine the migratory parameters from the individual cell metrics of each time-lapse video. The following parameters, the track speed, the instantaneous velocity, the persistence, the directionality, and the displacement were determined for each cell density condition (Figure 3.4.B, C, D, E, and F).

Cells seeded at a density higher than 6,000 cells moved faster than with a density lower than 5,000 cells, as shown by the track speed and the instantaneous. The track speed and instantaneous velocity were also similar for the densities from 6,000 to 8,000 cells. Moreover, the density of the cells did not affect the persistence and the cells kept an indirect motion, even in the highest density seeded of 8,000 cells.

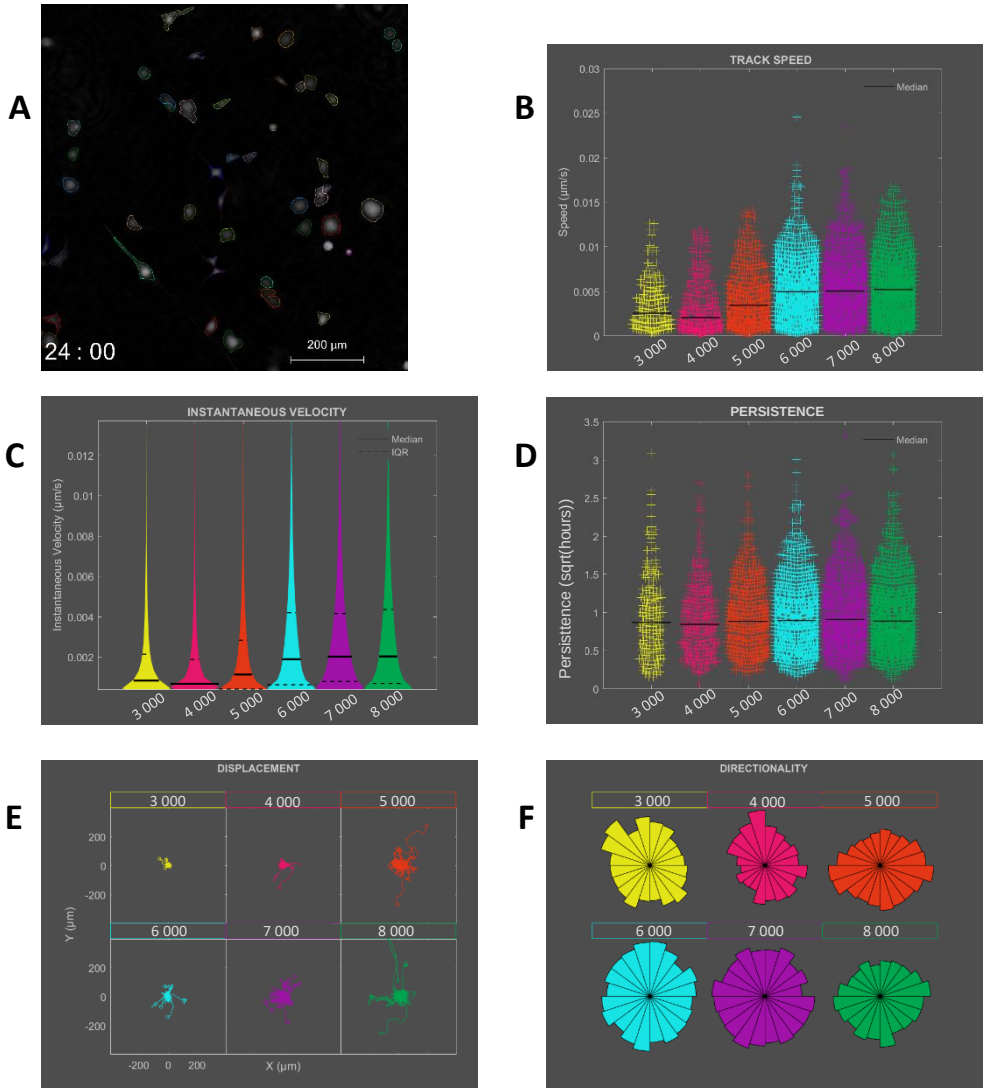

Figure 3.4 The Phasefocus Livecyte gave an accurate cellular segmentation and tracking of the GBM1 cells at a different cell density

A) Image showing the cell segmentation and cell mask coloured by track id at the 24 h timepoint. GBM1 cells were seeded in a 24-well plate at a density of 3000-8000 cells. Scale bar = 200 µm.

The motility assay application tracked the cells and generated graphs based on the data for the **(B)** track speed (total distance/track duration), **(C)** instantaneous velocity, **(D)** persistence (total cell displacement/total distance travelled), **(E)** displacement and **(F)** directionality.

3.2. Extrinsic factor-driven differentiation of cortical neurons

3.2.1. Differentiation of PAMV1 iPSCs to create a dense neuroepithelial layer

I first aimed to obtain cortical neurons using an extrinsic factor-driven differentiation. The hiPSCs PAMV1 were differentiated into cortical neuron progenitors with BMP-signalling agonists Dosomorphin and TGF-β inhibitor SB431542 according to the protocol from Shi et al. and as described in the Materials and Methods (Shi, Kirwan and Livesey, 2012). Firstly, the PAMV1 cells were plated on Matrigel on Day 0 and treated from Day 1-8 with the neural induction media composed of neural maintenance media supplemented with Dorsomorphin and SB431542 (Figure 3.5.A). To confirm the successful differentiation of the hiPSC into cortical neurons, I monitored the cells daily and observed their morphological changes. After 8 days of Dorsomorphin and SB431542 treatment, the cells were confluent and created a dense neuroepithelial sheet required for a successful differentiation (Figure 3.5.B). The progenitors were grown for 4 days in a proliferation medium, a process named the FGF-2 pulse. After 4 days, I observed the 3D rosette-like structures in a culture where the neural stem cells are arranged radially like the neuroepithelial cells in the neural tube; this is a developmental signature of neuroprogenitors (Figure 3.5.B).

3.2.2. Generating a cortical neural spheroid using the rotating shaker resulted in different sizes of neural spheroid

Following the differentiation of the cortical neurons, I set to aggregate the cells into spheroids and generate axons. On day 14, I resuspended the 3D rosette-like structures in a suspension 6-well plate which was placed on a shaker at 50 rpm in the incubator to form aggregates. After 2 days, the neural spheroids appeared perfectly round and smooth and the medium was replaced with a 50/50 medium. The formation of spheroids in suspension via the rotating shaker resulted in a range of random variable sizes as seen in the image (Figure 3.5.B).

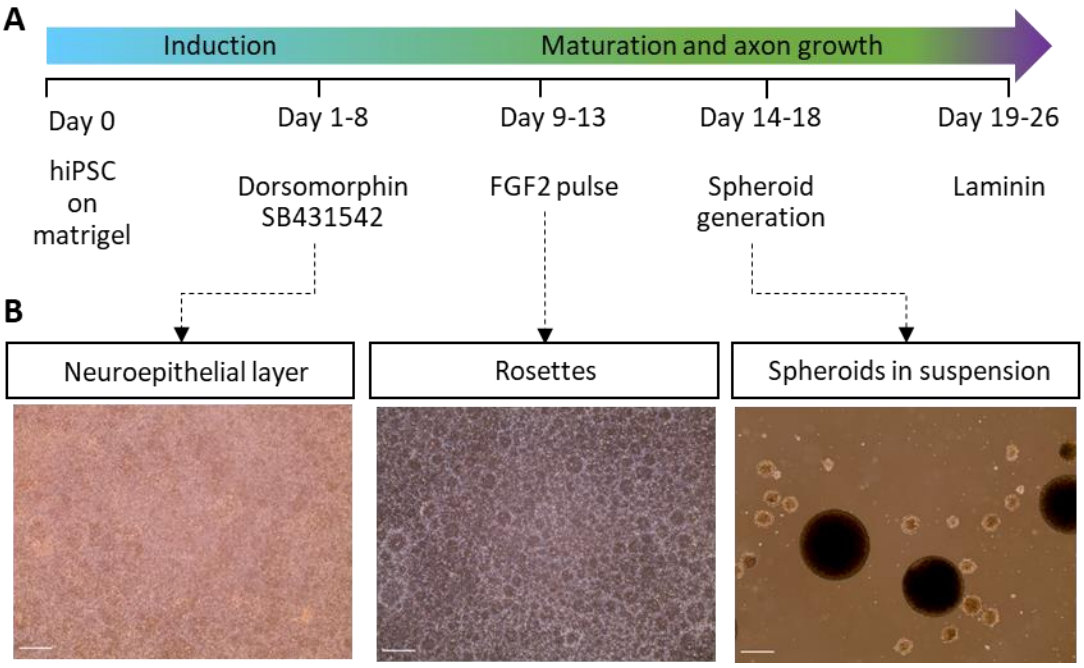

Figure 3.5 Timeline for normal differentiation

A) Timeline for inducing the normal differentiation of hIPSC into cortical neurons (protocol from Shi et al., 2012. Laboratory of Frederick J Livesey) using dosomorphin and SB431542 and generating neural spheroids using suspension plates on a rotating shaker. Scale bars = 250 µm.

B) Images captured on the x10 microscope representing stages of the differentiation with the neuroepithelial layer, the rosettes, and the spheroids in the suspension plate

3.2.3. The sizes of neural spheroid affected axon outgrowth and density

I then sought to generate the axons from the neural spheroids. On Day 19, the neural spheroids were transferred to a laminin-coated plate and left to adhere for 7 days. During this period, they were monitored daily and checked for the development of axons and the morphology of the spheroid. The images of the neural spheroids captured with the x10 cultured summarise the development of the axon and variable size from small, medium and large of diameter 400 µm, 600 µm and 1100 µm (Figure 3.6.A). Day 19 is indicative of the spheroid's transfer to laminin and there were already visible axons

present for all the different sizes. The axons were more abundant for the smallest spheroid and more sparse for the largest spheroid.

As part of the optimisation, I continued to monitor the growth of the axons for 5 days and the axons grew even longer. During this time, the neural spheroids appeared to flatten out on the borders and expanded (Figure 3.6.B). I also observed that a small clump of rosettes detached and formed long networks between different aggregates (Figure 3.6.B).

As the overall diameters of the neural spheroids ranged from 500 to 1500 µm, I wanted to know if this affected the length of axons that the neural spheroid will develop. To measure the size of the neural spheroids, they were fixed and imaged on the JuLI stage (Figure 3.7.A). The acquired images were extracted and analysed using Fiji where the area of the spheroid and the length of axons were measured and put into bins. The neural spheroids with an area of 1-1.5 mm^2 had a higher number of long axons compared to the larger ones of more than 2.5 mm^2 (Figure 3.7.B).

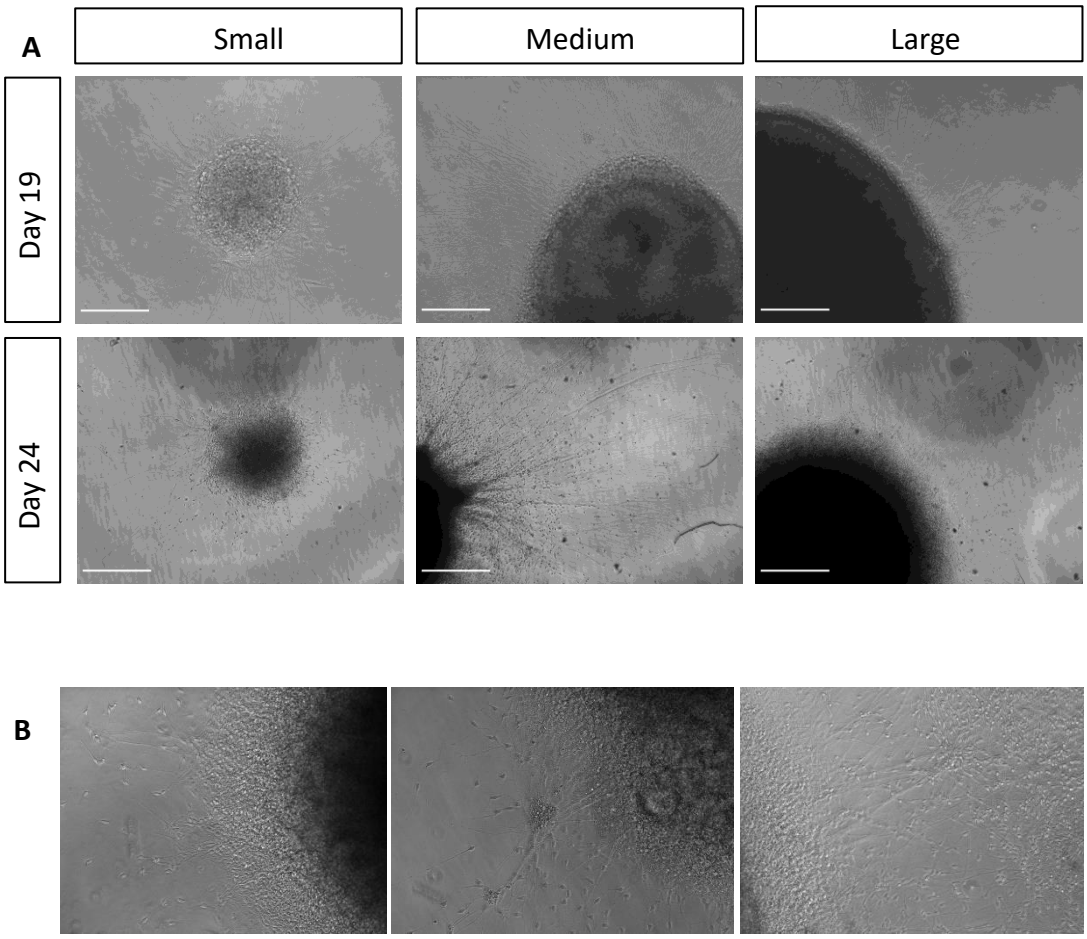

Figure 3.6 Development of different sizes of neural spheroids

A) Images captured on the x10 microscope representing different sizes of neural spheroids and the generation development of axons. Scale bars = 250 µm.

B) Regions of interest captured on the x20 microscope representing the expansion of the neural spheroid.

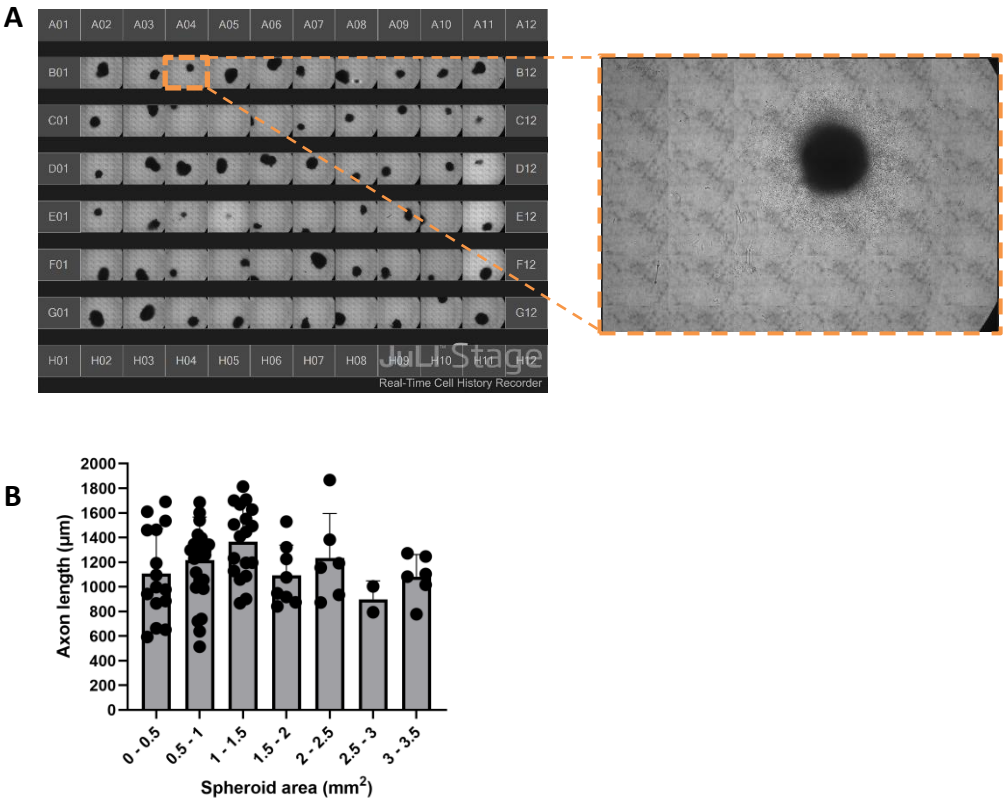

Figure 3.7 Comparison of the size of the neural spheroids

A) Images acquired on the Juli stage of fixed neural spheroids in a 96-well plate and the close-up image of well B04.

B) Graph representing the spheroid area in mm^2 to the axon length in µm. Each point represents a neural spheroid and the data represents the mean ± SD. This was a single experiment N = 1.

3.2.4. Using a pluronic acid-coated V-bottom 96-well plate to generate reproducible neural spheroids

It would be advantageous to rely on a consistent number of axons and spheroids of a similar size for the co-culture. Therefore, I aimed to optimize the size of the neural spheroid obtained. Instead of using the rotating shaker which resulted in variable sizes, I aggregated the cells with a pre-coated hydrophobic lipidure U-bottom 96-well plate or a pluronic acid V-bottom 96-well plate. Lipidure and pluronic acid are anti-fouling coatings which inhibit cell adhesion to the surface and promote the self-aggregation of spheroids. The cortical neural progenitors are usually always passaged in clusters so I

had to test the dissociation into single cells to seed a specific number of 10,000 cells per well and obtain neural spheroids of 1-1.5 mm^2 area.

The cells were left to aggregate for 2 days in the V- or U-bottom plate, and the spheroids were transferred to laminin and cultured to enable the axons to develop for 7 days. The images were taken on the x10 microscope and allowed the comparison between the V- and U-bottom plates (Figure 3.8). The U-bottom plate showed an aggregate without clear round outlines and in some instances, the borders of the aggregate will open and cells will escape. I also observed more cellular debris around the aggregate compared to the V-bottom plate. Our results indicated that using the pluronic acid-coated V-bottom 96-well plate allowed us to obtain spheroids of consistent shape and size as well as a consistent length and number of neurites.

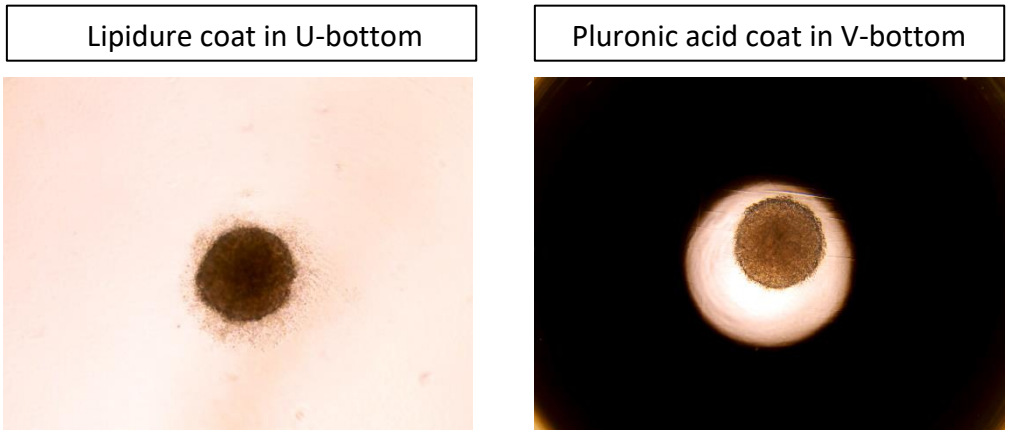

Figure 3.8 Optimisation of the size of the neural spheroids
Images captured on the x10 microscope representing a neural spheroid aggregated using a lipidure-coated U bottom (A) or a pluronic acid-coated V bottom (B) 96-well plate.

3.2.5. Characterisation of cortical neuron identity and axon bundles

Following the successful neural induction and generation of the axon, I set to characterize the neural spheroids with immunofluorescence staining. First, I tested whether the obtained neurites were axons or dendrites. Accordingly, I stained for the cytoplasmic neuronal axonal marker beta-tubulin (TUBB/Tuj 1) and the dendrites marker MAP2 (Figure 3.9.A). The confocal images show a positive staining for Tuj1 in

green and I also observed a positive signal for MAP2 in red. I confirmed that the neurites observed are axons (green), but that shorter dendrites may also be present (red).

I then sought to confirm the presence of cortical neurons with the neural precursor marker FoxG1. The signal is present in the rosettes, the area where the primary progenitors are located which confirmed the presence of cortical neurons (Figure 3.9.B). Finally, I also stained for Ki67 to check that the cells were still proliferating and to ensure they were not dying. Indeed, the rosettes were Ki67 positive which means that they are still proliferating (Figure 3.9.C).

Because I previously obtained neural spheroids of different sizes using the suspension plate, I wanted to confirm which neural spheroid will generate the most and longer neurites. I repeated the stainings of Tuj1 and MAP2 for different sizes of neural spheroids, one of 640 µm diameter and another of 1070 µm (Figure 3.10.A). Indeed, I observed that neural spheroids of 640 µm diameter gave more and longer neurites (Figure 3.10.B).

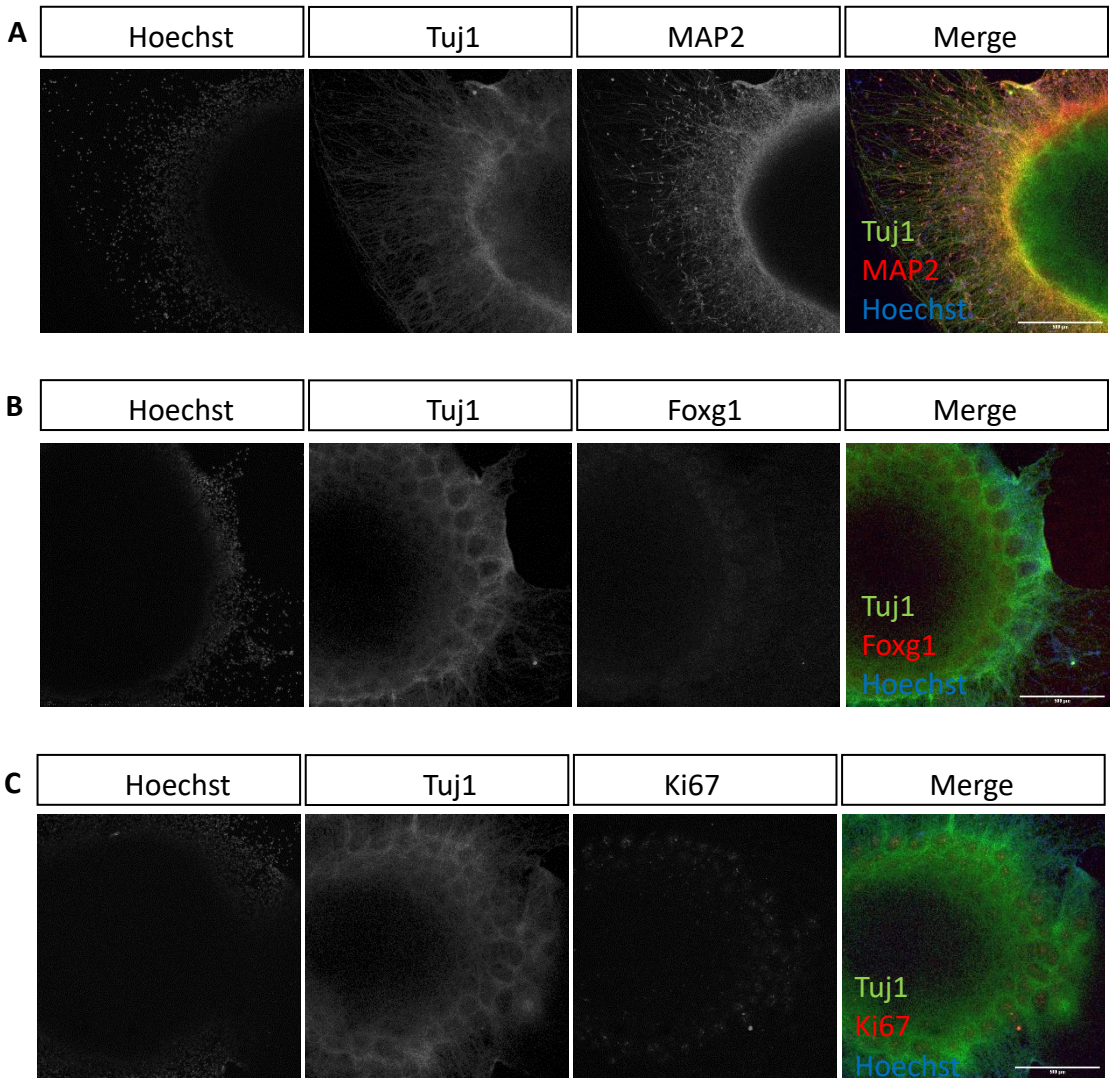

Figure 3.9 Characterisation of neural spheroids

Immunostaining of the neural spheroid neurites demonstrating they are axons **(A)** (Tuj1 in green, MAP2 in red, nucleus in blue), the presence of cortical neurons **(B)** (Tuj1 in green, FoxG1 in red, nucleus in blue), and proliferating cells within rosettes **(C)** (Tuj1 in green, Ki67 in red, nucleus in blue). Scale bars = 500 µm.

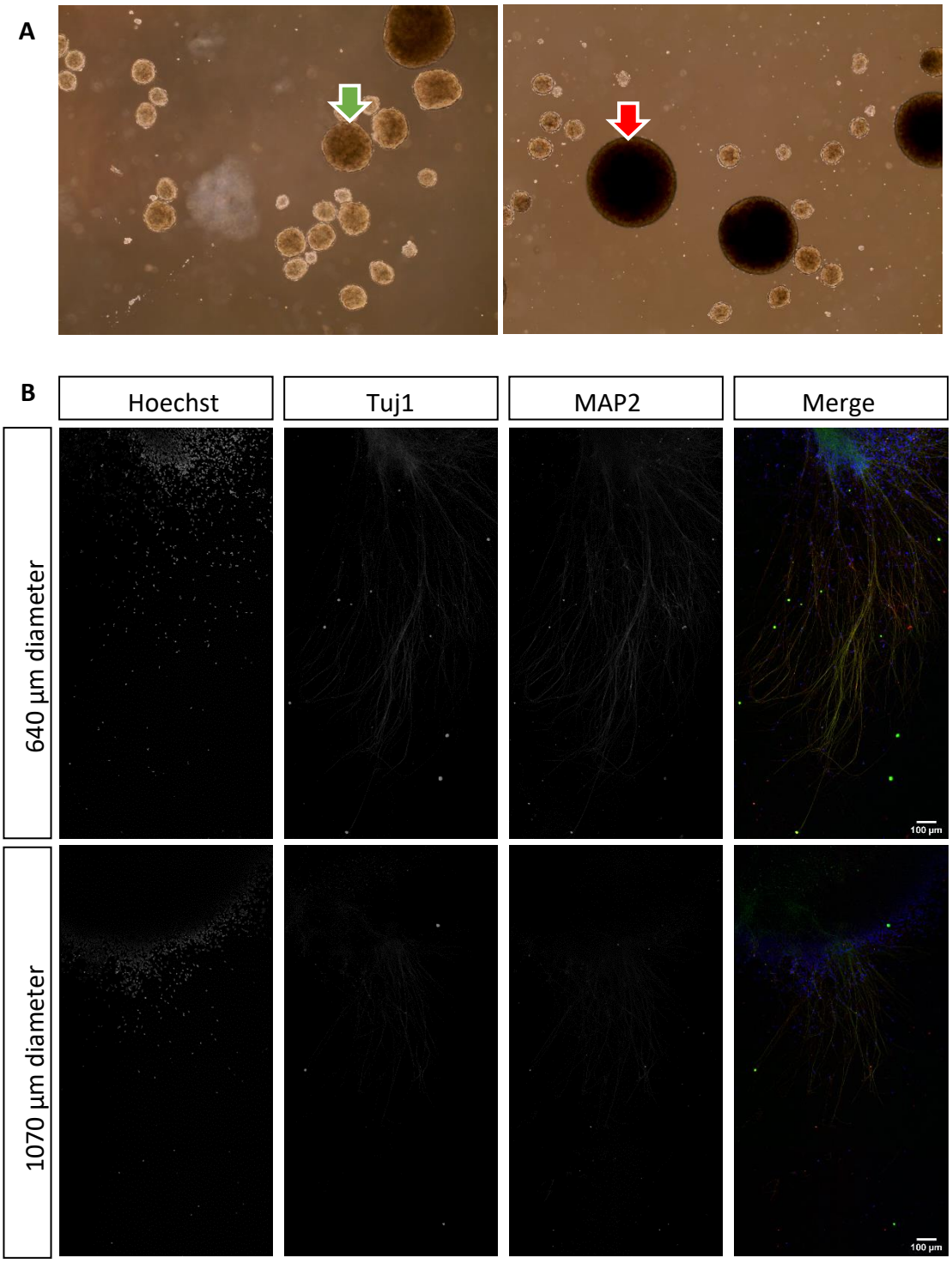

Figure 3.10 Characterisation of the neural spheroids of different sizes

A) Images captured on the x10 microscope representing the spheroids in the suspension plate with the arrows pointing to a spheroid of 600 µm diameter (green) and another of 1000 µm (red)

B) Characterisation of the neural spheroid neurites (Tuj1 in green, MAP2 in red, nucleus in blue) of different diameters: 640 µm and 1070 µm. Scale bars = 150 µm.

3.2.6. Batch freezing the neural rosettes

Taken together, these results indicated I was able to differentiate hiPSCs into cortical neurons and grow out axons in the neural spheroid cultures. However, the protocol was time-consuming with a minimum of 26 days where daily monitoring, media changes, and splitting may be required. Therefore, a solution to facilitate the protocol is the batch freezing of differentiated cortical neurons which could allow the time needed to generate neural spheroids to be divided into two parts. This would allow the batch freezing of differentiated cortical neurons obtained after 14 days and the thawing of each sample at the time when I need to generate neural spheroids which would take another 12 days (Figure 3.11.A). Hence, I froze the cells at the rosettes stage of an extrinsic factor-based differentiation. The rosettes were expanded for 2-3 days to obtain the most rosettes. After 6 days, long narrow structures formed which could mean they are terminally differentiated neurons (Figure 3.11.C). The rosettes were frozen on day 20. When thawed, the cortical neurons rearranged themselves into rosettes which were visible depending on the density of the cells (Figure 3.11.C and D). This is a good sign that they retain their cortical neural signature and should be able to generate the neural spheroids.

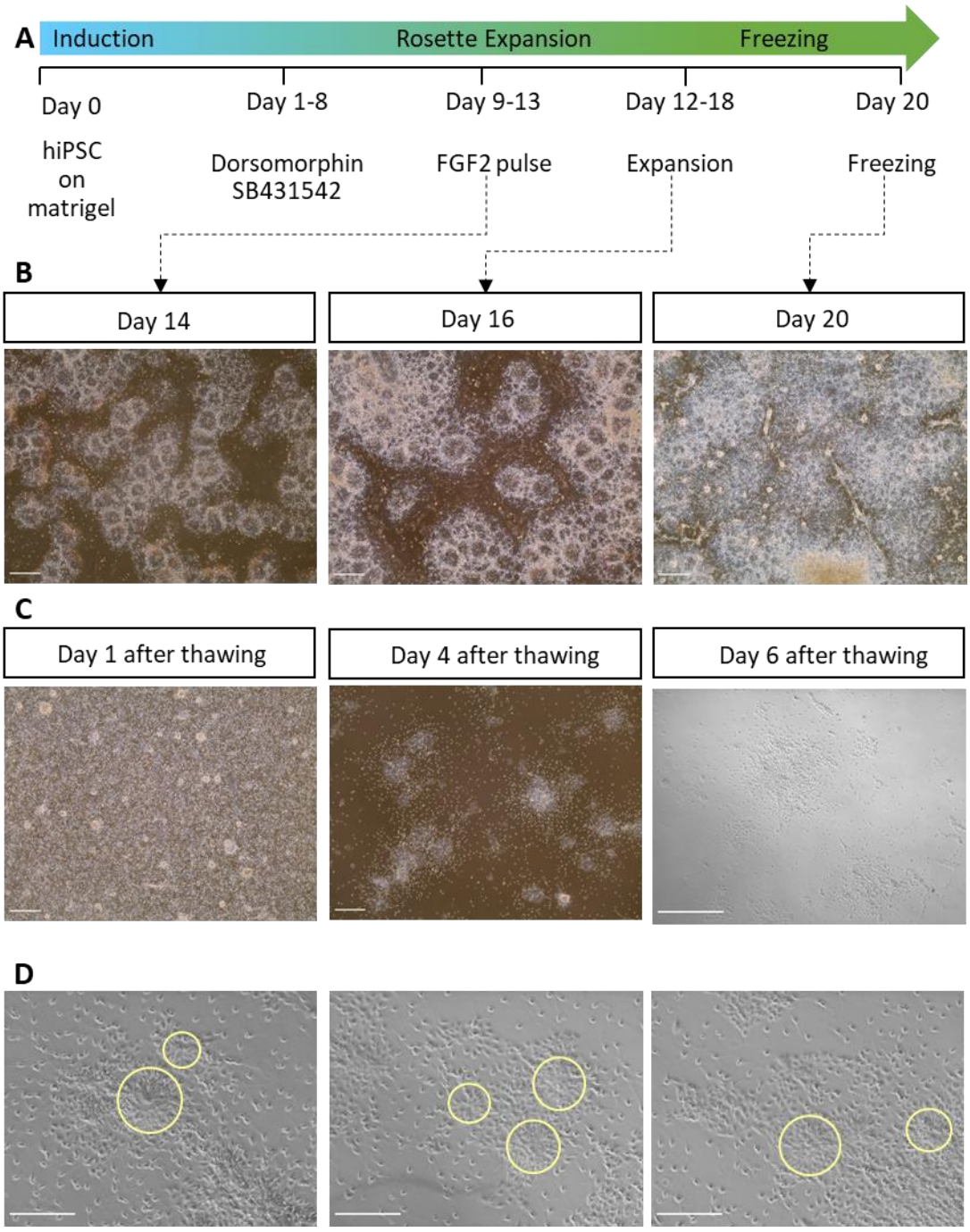

Figure 3.11 Batch freezing the neural rosettes

A) Timeline for expanding and freezing the differentiated cortical neurons.

B) Images captured on the x10 microscope representing the expansion of rosettes before freezing. Scale bars = 250 µm.

C) Images captured on the x10 microscope representing the thawing of the frozen cortical neurons

D) Images captured at x20 showing the rearrangement of the cells into rosettes

3.3. Co-culture of hiPSC-derived cortical neural spheroids with axons and patient-derived GBM cells

3.3.1. Preliminary results

Ongoing research has been focusing on the development of an *in vitro* model to capture the invasiveness of GBM such as organoid models and biomimetic strategies (Cha and Kim, 2017). To mimic the GBM microenvironment, the Danovi laboratory has previously set up pilot experiments co-culturing patients-derived CFP+ GBM1 cells with neural spheroids from hiPSCs with radiating axons (Figure 3.12.A, Cell Phenotyping group). Each GBM1 cell was identified and their migration on axons was tracked. Preliminary observations indicated that GBM1 cells could engage with the axon and migrate into the neural spheroid. The quantitative analysis of 30 GBM1 cells indicated that 28 GBM1 cells had migrated towards the soma of the neural spheroid (Figure 3.12.B and C).

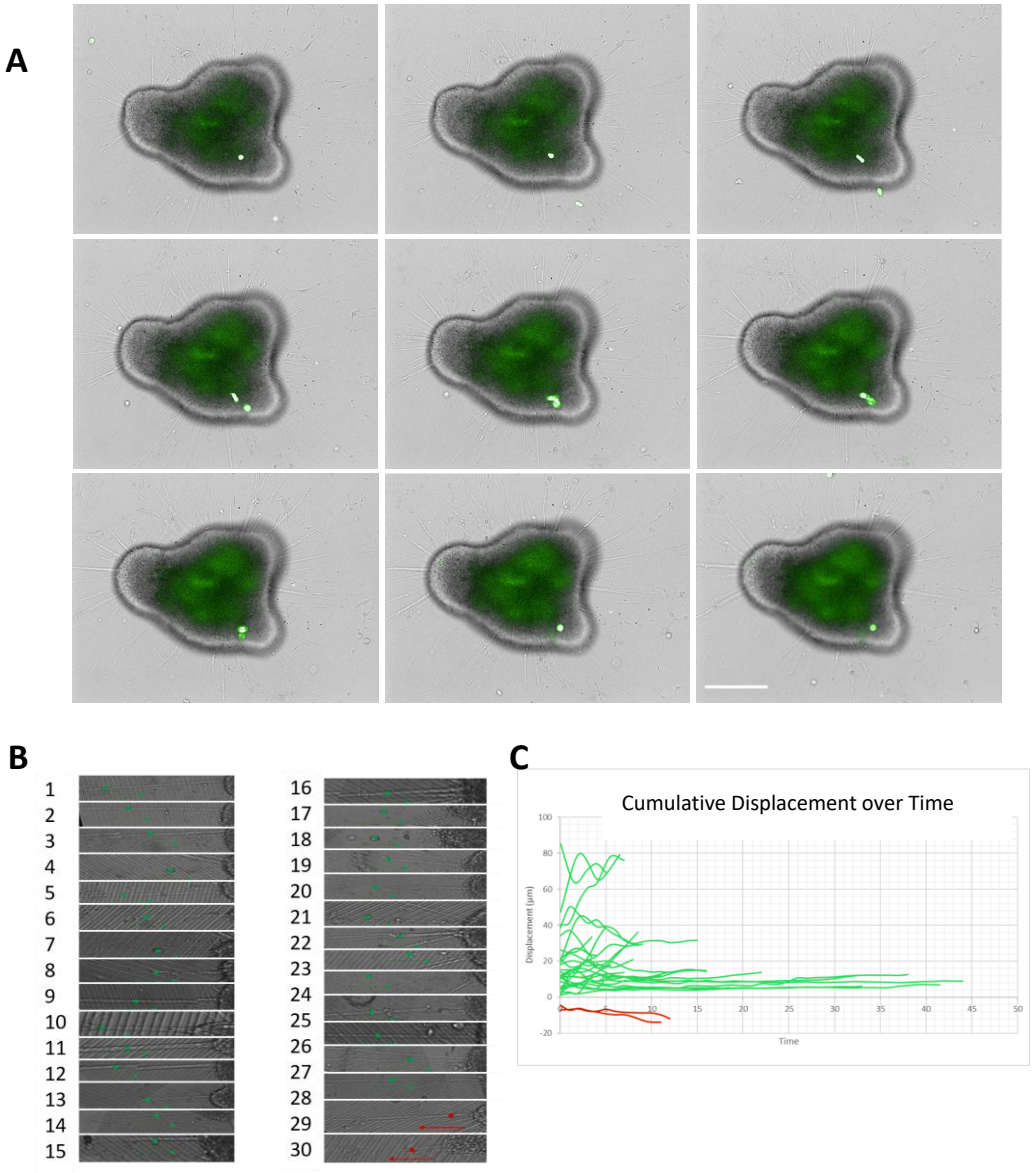

Figure 3.12 Preliminary data showing GBM1 cell engaged on an axon and migrated towards the hiPSC-derived neural spheroid

A) Neural spheroid were co-cultured with patients-derived GBM1 cells transduced CFP. Images were acquired using the Operetta Mark1 every 30 min (Images courtesy of Oluwaseun Adegbite). They are presented at every 5 h interval starting from the top left panel. One round cell was visible inside the neural spheroid and one cell (in the bottom right of each field) engaged on an axon to migrate inside the neural spheroid. Scale bar = 250 µm.

B) The cropped images represent GBM1 cells engaged on axons (Images courtesy of Cybill Ann Cherian) tracked using TrackMate. There was a tendency for the GBM1 cell to migrate towards the soma of the neural spheroid (red) rather than away from it (green).

C) Cumulated corrected displacement of GBM1 cell displacement on the axons plotted over time. The quantitative analysis counted that 28 cells migrated towards the soma (green) and 2 migrated away (red).

3.3.2. Harmony software did not accurately tracked CFP+ GBM1 cells by the when migrating the neural spheroid

To mimic the GBM microenvironment and repeat the preliminary experiment, the CFP+ GBM1 cells used in the pilot experiments were co-cultured with the neural spheroids obtained with extrinsic factor-driven differentiated cortical neurons (Figure 3.13.A). The co-culture was imaged for 24 h every 30 min on the Operetta Mark 1 (Figure 3.13.A). It is possible to observe the rosettes within the neural spheroid and the axons emerging from it. We observed a GBM cell going in, extending inside the aggregate and moving around. Using Harmony, the built-in image analysis on the Operetta, the CFP+ GBM cells were identified. However, the Harmony software was unable to recognise a cell from frame to frame and this resulted in inaccurate tracking of the CFP+ GBM cells.

3.3.3. Trackmate did not accurately tracked CFP+ GBM1 cells by the when migrating the neural spheroid

Since the Harmony software of the Operetta Mark 1 was not able to accurately track the CFP+ GBM cells, the data from the Operetta Mark 1 was also extracted and analysed using the Fiji plugin Trackmate. We set out to use Trackmate to identify and track the CFP+ GBM1 cells to quantify the migratory properties such as the speed, direction, and meandering index. Trackmate identifies the GBM cells in the 445 nm channel and labels each cell track with a new track ID (Figure 3.13.B). When I labelled each cell track by the duration of the track, there was a high number of short tracks meaning a cell is not able to be tracked for the duration of the video.

The identified cells and tracks were used as a basis for analysis and quantified the cells present in over 25 neural spheroids images in different bins based on their directionality: random, away or towards the neural spheroid, going in, already in (Figure 3.13.C). The majority of the cells moved in a random direction. Only a few cells moved away or towards the neural spheroid and a few cells were found already inside the aggregate.

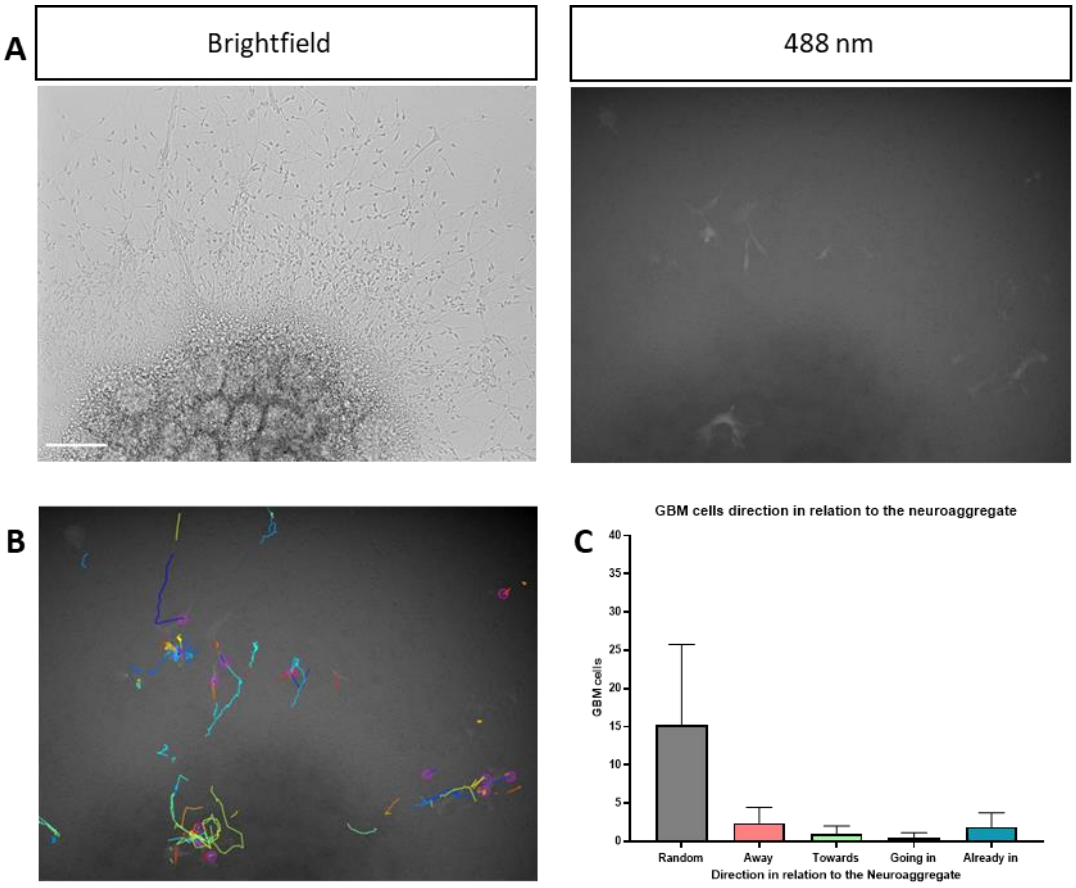

Figure 3.13 Extrinsic-factor driven differentiation cortical neural spheroid co-cultured with GBM1 cells

A) hiPSC-derived neural spheroids were co-cultured with patients-derived GBM1. Images of live cultures were acquired using the Operetta Mark 1 every 30 min for 24 h. The left panel represents the merged image of the brightfield and 488 nm channel. Scale bar = 100 µm.

B) Image representing the tracking done using TrackMate with each colour labelling a new track ID.

C) Graph representing the GBM1 cell direction on the axons plotted over time. The quantitative analysis counted that 28 cells migrated towards the soma (red) and 2 migrated away (green).

3.4. Discussion

3.4.1. Live-imaging of the GBM cells using the Operetta

The first objective of the project was to develop a robust pipeline to investigate cell migration. The initial issue with the low CFP+ GBM cells could arise from the fact that the cells were kept in culture without the drug geneticin for a few passages before freezing or that the drug concentration used was not strong enough to kill all the untransfected cells. I performed an efficient selection from the beginning with the correct concentration of geneticin by doing a kill curve experiment. Although the CFP+ GBM cells were homogenous immediately after the sort and despite the geneticin selection, tracking CFP+ GBM cells on the Operetta was suboptimal.

I encountered challenges in optimising the cell tracking using the Operetta Mark 1 images. The issues included the phototoxicity of Hoechst, the expression of CFP in GBM1 cells at different intensities as well as the variable GBM1 cells morphology. Introducing the nuclear dyes seemed to have led to some levels of toxicity as they intercalate into the DNA and can interfere with replication/transcription. As we observed, the cells remained mobile for less than 10 h following staining. For instance, NucRed has previously been used in live cell assays up to 6 h but its possible toxicity in longer time courses, with the frequent excitation of the dye, is not known (Yui *et al.*, 2014; Gutiérrez-Caballero *et al.*, 2015). In contrast, Purschke et al. have demonstrated that Hoechst can lead to apoptosis (Purschke *et al.*, 2010). To avoid toxicity from dyes, they advised using a low concentration of the dye, a low exposure, and a reduced imaging frequency. As our study involved the accurate tracking of the cells imaged every 15 min over a longer period, the use of nuclear dyes seemed suboptimal. Although CFP and GFP are commonly used to label cells for tracking, the expression of such proteins can lead to cellular toxicity as reported by Ansari et al. in 2016 (Ansari *et al.*, 2016). Those challenges prevented the Harmony software from recognising a cell from frame to frame and suggested that the Harmony software was unable to track the labelled GBM1 cells cultured with the neural spheroid in a live assay.

3.4.2. Live-imaging of the GBM cells using the Phasefocus Livecyte

Given that tracking CFP+ and nuclear-stained cells from the Operetta Mark 1 image was suboptimal, I looked into quantitative phase imaging, a label-free imaging approach, the Phasefocus Livecyte, which enabled the long-term imaging of unlabelled GBM1 cells. It overcomes the challenge of introducing dyes/labels, which may affect cell viability and motility. Quantitative phase imaging offers high-content and high-contrast images resulting in a more robust segmentation and tracking compared to traditional methods (Kasprowicz, Suman and O'Toole, 2017). This enables the generation of individual cell metrics compared to population-level averages and the evaluation of the dynamic phenotypes in the cell-to-cell heterogeneity and temporal changes. The label-free also allows the same cells to be used in further assays. All this has great potential and clinical relevance for drug screening and personalised medicine (Kasprowicz, Suman and O'Toole, 2017).

Using the built-in cellular segmentation and applications of the Livecyte, I demonstrated the ability to perform efficient and reliable cell tracking. While optimising the cell tracking conditions for the Livecyte, I observed the effects of the cell density on the speed or velocity. It has previously been reported that increased cell density mechanically inhibited cell movement and resulted in decreased velocity (Demuth *et al.*, 2001). However, our results implied that cells seeded at higher densities moved faster than cells seeded at lower densities. I believed that a low density led to the proliferation of the cells instead of the migration. In support of our interpretation, Katakowski et al. demonstrated that the migration and proliferation of tumour cells were density-driven (Katakowski *et al.*, 2016). They suggested that cells will proliferate at a low density as conditions are less hypoxic, but that they will migrate in the hypoxic environment near the primary tumour. Therefore, it would be interesting to duplicate the experiment with a wider range of cell density.

All things considered, we were able to confirm that our pipeline can track GBM1 cells and investigate their morphology and motility and a proof of principle that the livecyte able to track and quantify migratory properties of GBM cells more accurately.

3.4.3. Optimisation of the neural spheroid size

In this chapter, I also summarised how the cortical neural spheroid was generated to obtain human axons as migratory substrates. Using the extrinsic factor-driven differentiation protocol based on the Livesey laboratory protocol, the cortical neurons were obtained using soluble factors. Although it was successful, our method for the aggregation of the cortical neurons using the suspension plate resulted in different sizes of the neural spheroid. I sought to optimize the protocol by making the size of the neural spheroids consistent by using the lipidure-coated U-bottom or pluronic acid-coated V-bottom 96-well plate. They both worked and resulted in reproducible neural spheroids and I obtained clearer outlines with the pluronic acid-coated V-bottom 96-well plate so I decided to continue with the latter for a standardized spherical shape.

3.4.4. Characterise the cortical neuron identity and axon bundles

Next, I aimed to characterise the cortical neuron identity and axon bundles. Indeed I demonstrated that the cortical neurons obtained were positive for FoxG1 and Pax6 which confirms the cortical neuronal identity and that the axons developed were positive for the axonal marker Tuj1. Further work could have been achieved by fixing and staining on different days to see the progression of the axon's development from the day of the transfer to laminin to the co-culture.

4. RESULTS CHAPTER 2 - DEVELOP A CO-CULTURE OF TRANSCRIPTION FACTOR-DRIVEN DIFFERENTIATED HIPSC-DERIVED CORTICAL NEURAL SPHEROIDS WITH AXONS AND PATIENT-DERIVED GBM1 AND GBM20 CELLS

As part of our aim to develop an *in vitro* model mimicking the tumour microenvironment to study the GBM migration, we have described the generation of hiPSC-derived cortical neural spheroids using extrinsic factor-driven differentiation and investigated the patient-derived GBM1 cells migration in 2D assays in Results Chapter 1. In this chapter, I describe the development of the co-culture of hiPSC-derived cortical neural spheroids using transcription factor-driven differentiation, and with two patient-derived GBM cells as well as non-cancer neural stem cells.

To represent the transcriptionally heterogeneous primary and recurrent tumours, our panel comprises two patient-derived GBM cell lines. We are using the previously described GBM1 from a proneural subtype in Results Chapter 1 and GBM20 from a recurrent tumour of a proneural/mesenchymal subtype (Polson *et al.*, 2018). I investigated the migration of the patient-derived GBM cells and non-cancer neural stem NS17 cells cultured on axons from hiPSC-derived neural spheroids. I present the robust pipelines developed and optimised using HCI platforms to quantify the engagement of the cells on the axons, the infiltration of the neural spheroid in endpoint assays, and the migratory properties of the cells next to the neural spheroid in live assays such as the direction towards the neural spheroid. Finally, I compared the migratory behaviours of the different patients-derived GBM cell lines and non-cancer neural stem cell lines.

In this chapter, we decided to image the co-cultures using the Operetta CLS High Content Analysis System as it includes more features than the previous Operetta Mark 1 system. In particular, we were interested in using the PreciScan plug-in to easily identify the neural spheroid and to put it in the centre of the ROI. The Operetta CLS also offers faster,

more efficient, and more precise imaging with its high-power LED excitation and one large format sCMOS camera.

Similarly to the previous chapter using extrinsic factor-driven differentiation, the aim of this chapter is divided into the following objectives using transcription factor-driven differentiation: (1) generate hiPSC-derived cortical neurons, (2) develop a hiPSC-derived cortical neural spheroid with radiating axons, (3) characterise the cortical neuron identity and axon bundles via specific markers, and (4) co-culture the hiPSC-derived cortical neural spheroid with patient-derived GBM cells. Here, we also compare the two protocols – extrinsic factor-driven and transcription factor-driven differentiation.

4.1. Results

4.1.1. Generate an iPSC-derived cortical neural spheroids with axons

The previous results describe the cortical neural spheroid developed using an extrinsic factor-driven differentiation. Before I settled on a protocol to generate cortical neurons, I wanted to try generating cortical neurons using transcription factor-driven differentiation. The method I tested to generate cortical neurons involved the forward reprogramming of the iPSCs PAMV1 with a doxycycline-inducible NGN2 transgene as described in the methods section (Figure 4.1.A).

On Day 0, the PAMV1 cells were seeded on Matrigel and induced into cortical neurons using the neural induction media with doxycycline. To develop the spheroid, the cortical neurons were aggregated in a sphere on Day 3 using the pluronic acid-coated 96-well V-bottom plate as previously described. Once transferred to laminin on Day 6, the neural spheroids were monitored daily and checked for the development of axons and the morphology of the spheroid (Figure 4.1.B).

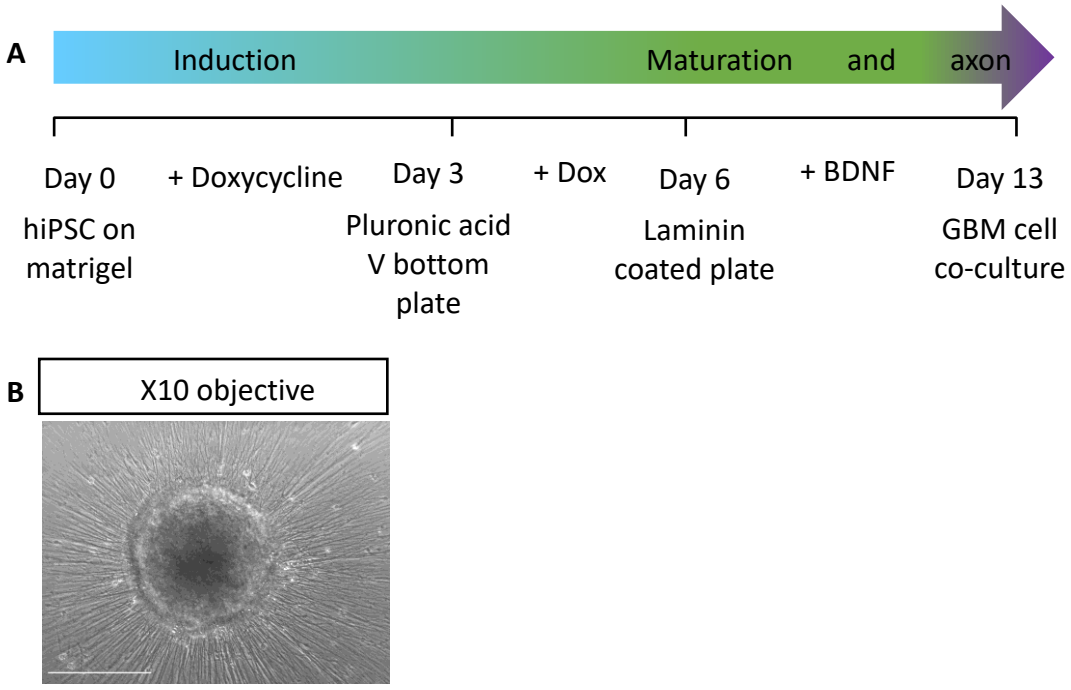

Figure 4.1 Neural spheroids generation through transcription-factor mediated differentiation

A) Timeline for inducing the transcription-factor mediated differentiation for cortical neurons (protocol from Fernandopulle et al., 2018. Laboratory of Michael Ward), generating neural spheroids using pluronic acid coated V bottom plates and co-culturing the NS with patient-derived cells.
B) Image captured on the x10 microscope representing a neural spheroid generated through forward reprogramming. Scale bar = 100 µm.

4.1.2. Characterisation of cortical neuron identity and axon bundles

To confirm the neuronal cell identity, the neural spheroids were tested for the presence of cortical neuron markers Pax6 by immunofluorescence. The presence of this marker is characteristic of the cortical neuron identify from progenitors to mature neurons (Figure 4.2.A). From the staining, the neural spheroid is positive to Pax 6 confirming the successful differentiation and the presence of cortical neurons. I then addressed whether the neurites emerging from the neural spheroids were axons by staining for the presence of the axonal marker Tau and Tuj1 and the dendrite marker MAP2. I concluded that the neurites formed were axons (Figure 4.2.B).

Taken together, these results indicated I had the appropriate culture to model the axons using the forward reprogramming method and that I could proceed to the GBM co-culture.

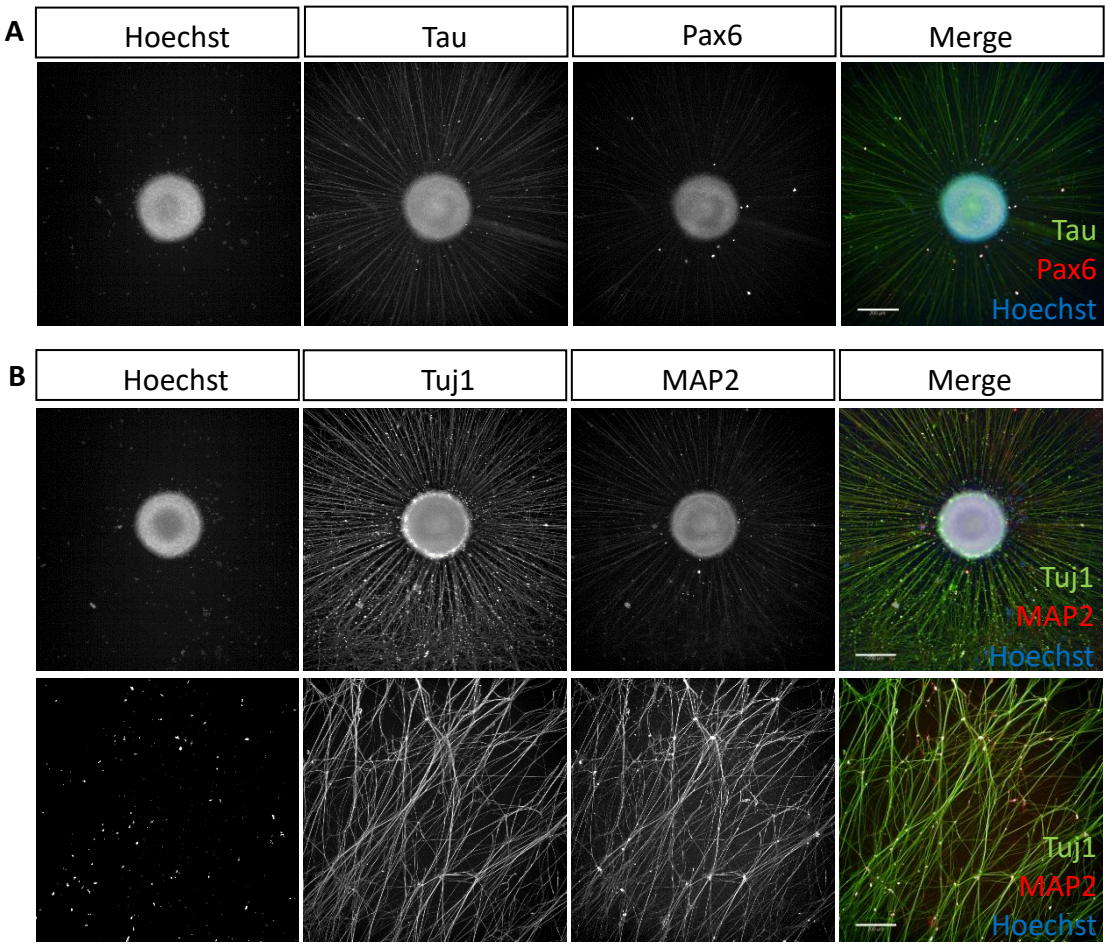

Figure 4.2 Neural spheroids characterisation

A) Characterisation of the neural spheroid with antibodies demonstrating these are cortical neurons (Tau in green, Pax6 in red, nucleus in blue). Scale bar = 200 µm.

B) Characterisation of the neural spheroid neurites demonstrating they are axons (Tuj1 in green, MAP2 in red, nucleus in blue). Scale bar = 200 µm.

4.1.3. Patient-derived GBM1 cells change morphology when engaged on an axon of a neural spheroid

As mentioned in the previous chapter, GBM1 cells were stained with BioTracker AF655 for endpoint assays. They were seeded on laminin-coated glass bottom plates in empty

wells or wells with neural spheroids and axons (Figure 4.3.A and B). The cultures were then imaged on the Operetta Mark 1 and analysed using the Harmony software.

From visual inspection, we noticed that patient-derived GBM1 cells align along the axons when co-cultured on the neural spheroids axons. First, we segmented the cells and created a cell mask to quantify the morphological changes such as the cell area and the cell width-to-length ratio. We found morphological differences of cells on laminin-coated glass or plastic 2D surface compared to a cell 'engaged' on an axon (Figure 4.3.B). At day 0, the GBM cells seeded on axons are significantly larger than the GBM cells in empty wells. The cells on axons are also less round and more elongated. With time, the cell area difference is reduced as the GBM1 cells settle and stretch in empty wells as well as on axons. This is similar to the changes in cell roundness and ratio width to the length I observed with the cells on laminin; these cells also stretched out.

I also noticed that the GBM cells moved along axons, and I set out to quantify whether the direction of the cells was unbiased or biased towards the neural spheroid culture. My initial observation regarding the directionality pointed to the possibility that they were also attracted to the soma of the neurons within the spheroid (Figure 4.3.A).

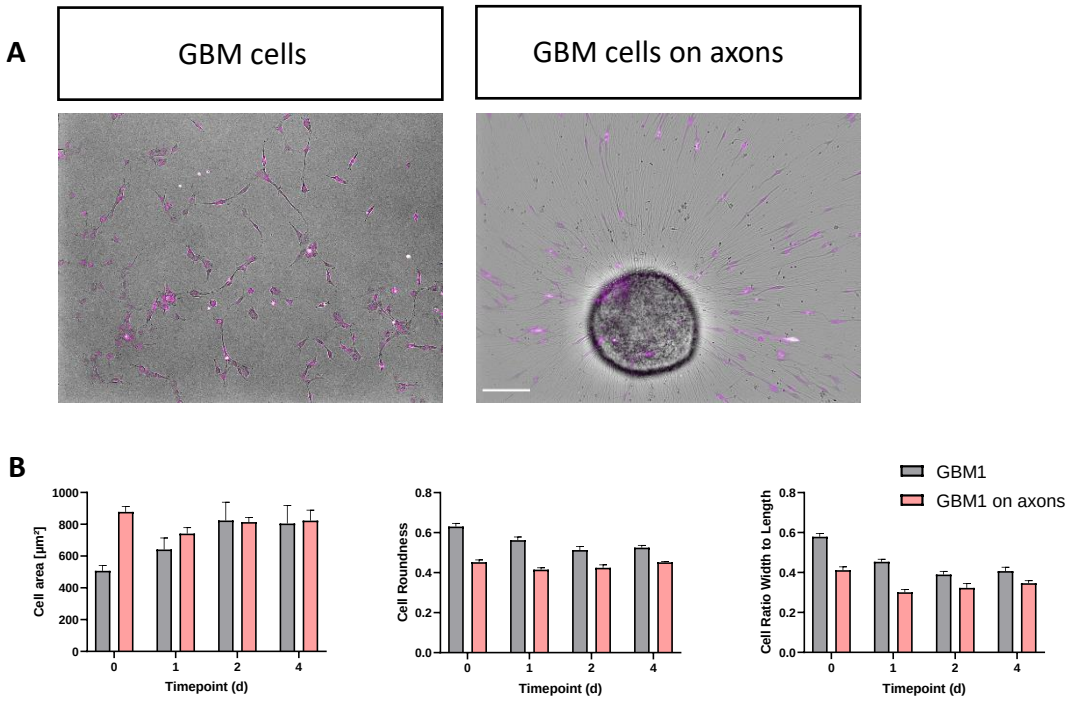

Figure 4.3 Transcription-factor-driven differentiation cortical neural spheroid co-cultured with GBM1 cells

A) hiPSC-derived neural spheroids were co-cultured with patients-derived GBM1. Images of live cultures were acquired using the Operetta Mark 1 every 30 min for 24 h. The left panel represents the merged image of the brightfield and 488 nm channel. Scale bar = 100 µm.
B) Graphs representing the features of the cells such as the area, roundness, and ratio width to length of GBM1 cells alone or GBM1 cultured on axons.

4.1.4. Patient-derived GBM1 cells migrate towards the neural spheroid

To analyse the migration of the unlabelled GBM1 cells towards the neural spheroid, we performed live imaging assays with image acquisition every 15 min for 12 h. The images were acquired on the Phasefocus Livecyte which uses quantitative phase imaging and has an accurate tracking apparatus as mentioned in the Materials and Methods. Using HCI, we developed a robust workflow to identify and track the cells and to analyse the cell's migratory behaviours.

The example images show the GBM1 cells seeded on laminin-coated glass moving randomly or GBM1 cells on axons in an ROI selected on the right of the neural spheroid with the cell mask overlay (Figure 4.4.A). I observed that the cells follow the structure of

the axon underneath and move towards the neural spheroid. The graphs show the random displacements on the x and y axis and the uniform directionality of GBM1 cells on glass. In contrast, when GBM1 cells migrate on axons, the movement becomes more horizontal as the cells follow the structure underneath and the displacement is mainly towards to left where the neural spheroid is.

The videos were used to calculate the tracking properties such as the speed, directionality, displacement and persistence described in the methods (Figure 4.4.A and B). There were no significant differences in the speed or the persistence between cells plated on laminin alone or cells plated on axons (Figure 4.4.B). However, the spread of the data for cells on axons is larger. This confirmed that GBM1 cells engaged on axons and followed the directionality towards the neural spheroid using the axons.

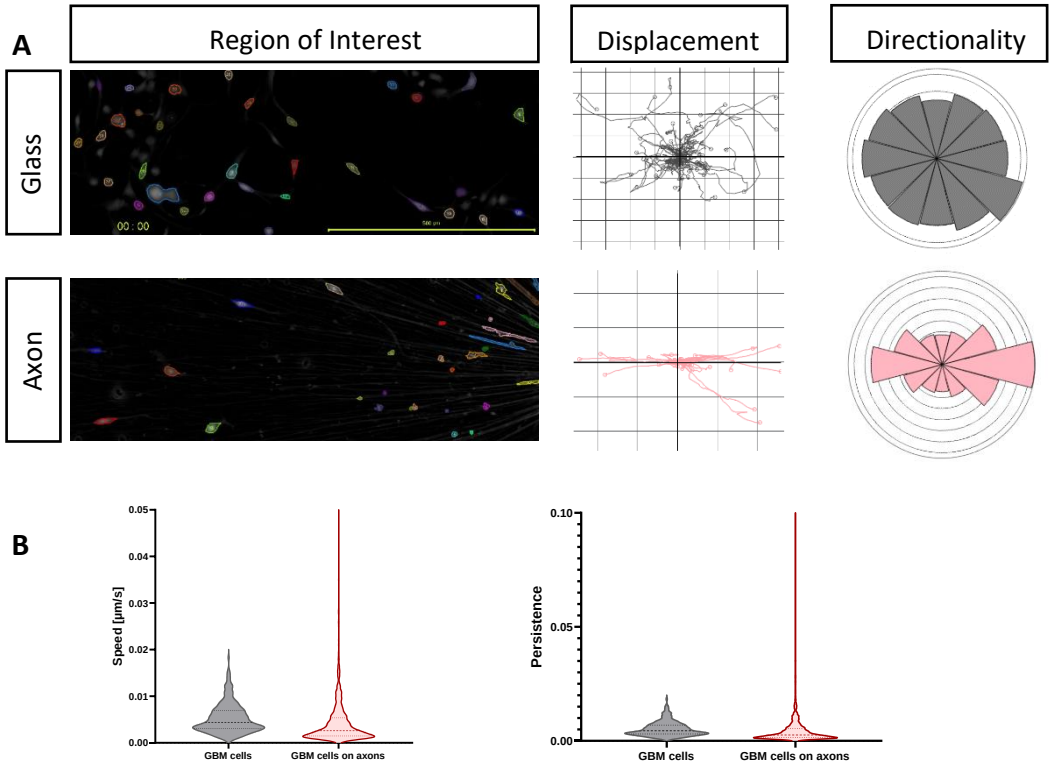

Figure 4.4 Quantification of GBM1 cells migration towards the neural spheroid

A) Videos acquired every 15 min for 12 h on the phasefocus livecyte with the cell mask overlay. Graphs showing the displacements as 0 as a point of origin of the cell track and the directionality along the x and y axis (GBM cells on the laminin-coated glass surface in grey and axons in pink)
B) Violin plot representing the speed and the persistence (definition is summarized in the methods section) n=1.

4.1.5. Both patient-derived GBM1 and GBM20 cell and NS17 lines migrate towards the neural spheroid

To analyse and compare the migration of the different cell lines towards the neural spheroid, we performed live imaging assays with image acquisition every 15 min for 24 h on the livecyte of the different cell lines cultured on laminin-coated glass plates and on axons (Figure 4.5.A). We selected two ROIs around the neural spheroid, one ROI on the left of the neural spheroid and one perpendicular to it (Figure 4.6). This allowed us to analyse two directions and avoid bias in the instrument. The directionality and displacement confirmed our previous findings for the other cell lines (Figure 4.5.B). Cells plated without axons moved in a randomized direction compared to cells on axons which move following the direction of the axons underneath. There was also an increased movement in the direction of the neural spheroid for all cell lines including the NS17 control cell line. There were no significant differences in the instantaneous and mean velocity, speed, or persistence (Figure 4.5.C).

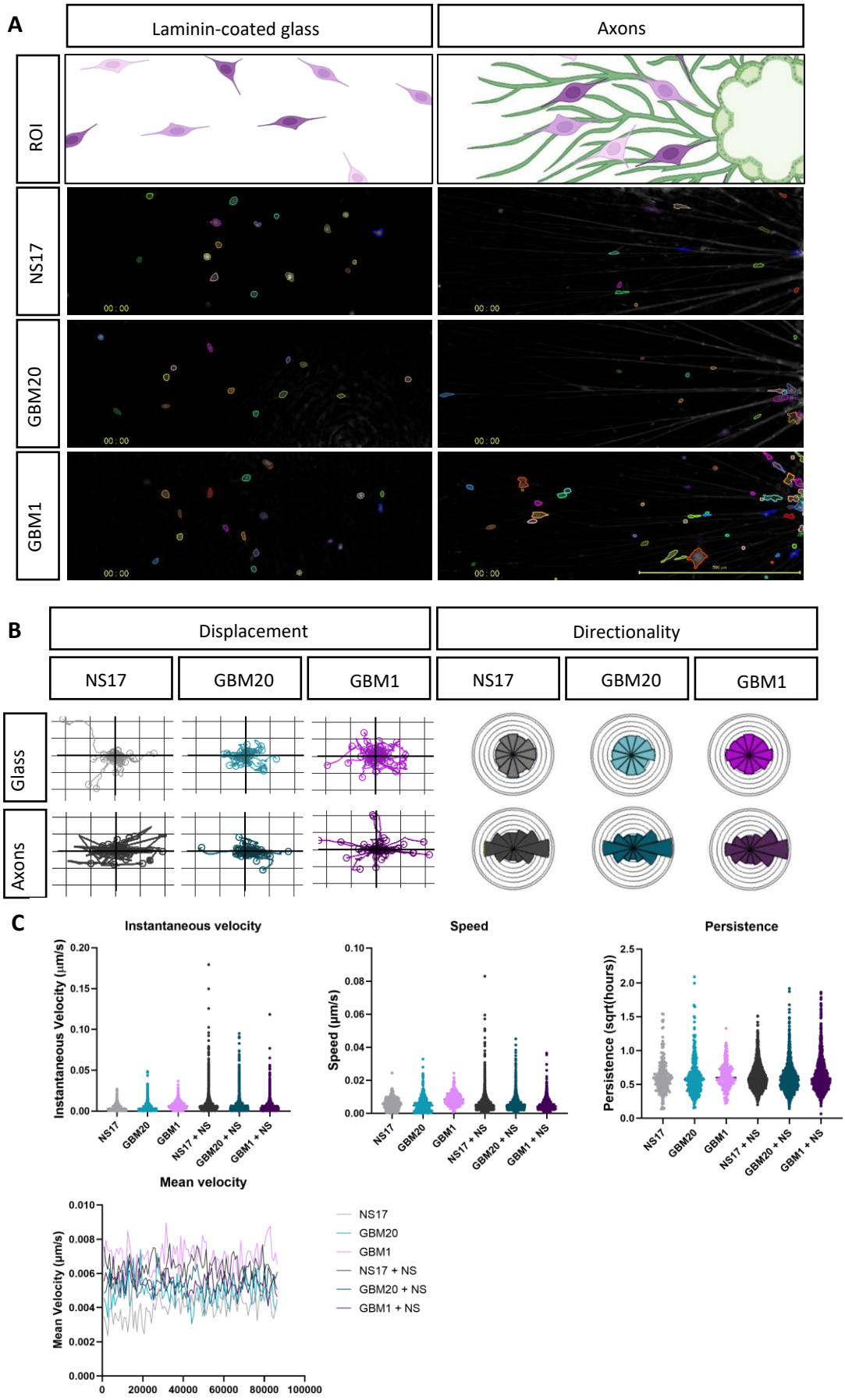
A
Laminin-coated glass
Axons
ROI
NS17
GBM20
GBM1
B
Displacement
Directionality
NS17
GBM20
GBM1
NS17
GBM20
GBM1
Glass
Axons
C
Instantaneous velocity
Instantaneous Velocity (µm/s)
Speed
Speed (µm/s)
Persistence
Persistence (sqrt(hours))
NS17
GBM20
GBM1
NS17 + NS
GBM20 + NS
GBM1 + NS
Mean velocity
Mean Velocity (µm/s)
0
20000
40000
60000
80000
100000

Figure 4.5 Live imaging assays of neural spheroids co-cultured with NS17, GBM20 and GBM1 cells

A) Scheme depicting the layout and Phase-contrast images of the timelapse assay of NS17, GBM20, and GBM1cells alone or co-cultured with neural spheroids at 00:00 with the cell mask overlay.
Quantification of NS17, GBM20, and GBM1 cells **(B)** displacement and directionality, and **(C)** instantaneous velocity, speed, persistence, and mean velocity.

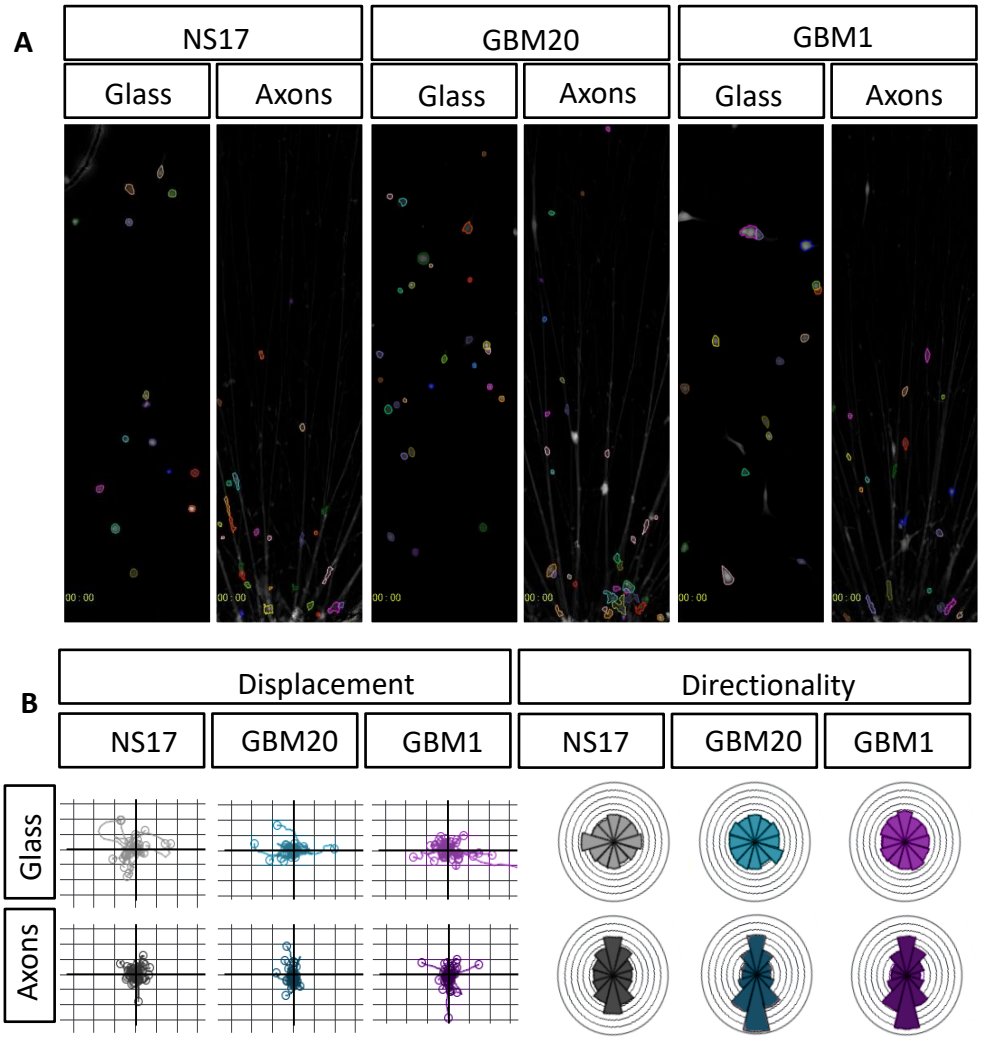

Figure 4.6 Live imaging assays of neural spheroids co-cultured with NS17, GBM20, and GBM1 cells

A) Phase-contrast images of the timelapse assay of neural spheroids co-cultured with NS17, GBM20, and GBM1cells at 00:00 with the cell mask.

B) Quantification of NS17/GBM20/GBM1 cells displacement and directionality.

4.1.6. Patient-derived GBM1 cells infiltrate the neural spheroid

We reasoned that cells migrating towards the neural spheroid would be infiltrating the neural spheroid so we set out to quantify the cell infiltration in terms of invasion of the neural spheroid. We imaged these co-cultures in endpoint assays on Days 1-8 to count the number of GBM1 cells that infiltrated the neural spheroid (Figure 4.7.A). The number of infiltrating GBM1 cells increased significantly after 2 days (Figure 4.7.B) and the number continued to increase for eight days (Figure 4.7.C).

However, we encountered issues with the quantification of the GBM1 cells within the neural spheroid after 5 days of culture. On days 4 and 5, the cells are identifiable and easily segmented (Figure 4.7.D). The problems with the segmentation arise from day 6 onwards. First, there was more debris which made it difficult to count the cells inside the neural spheroid. Secondly, the lipophilic dye staining the GBM1 cells starts to fade. Finally, a rare occurrence which further rendered the analysis difficult was that the neural spheroid will spread and flatten with the rosettes rearranging outside of the neural spheroid initial border (Figure 4.7.D).

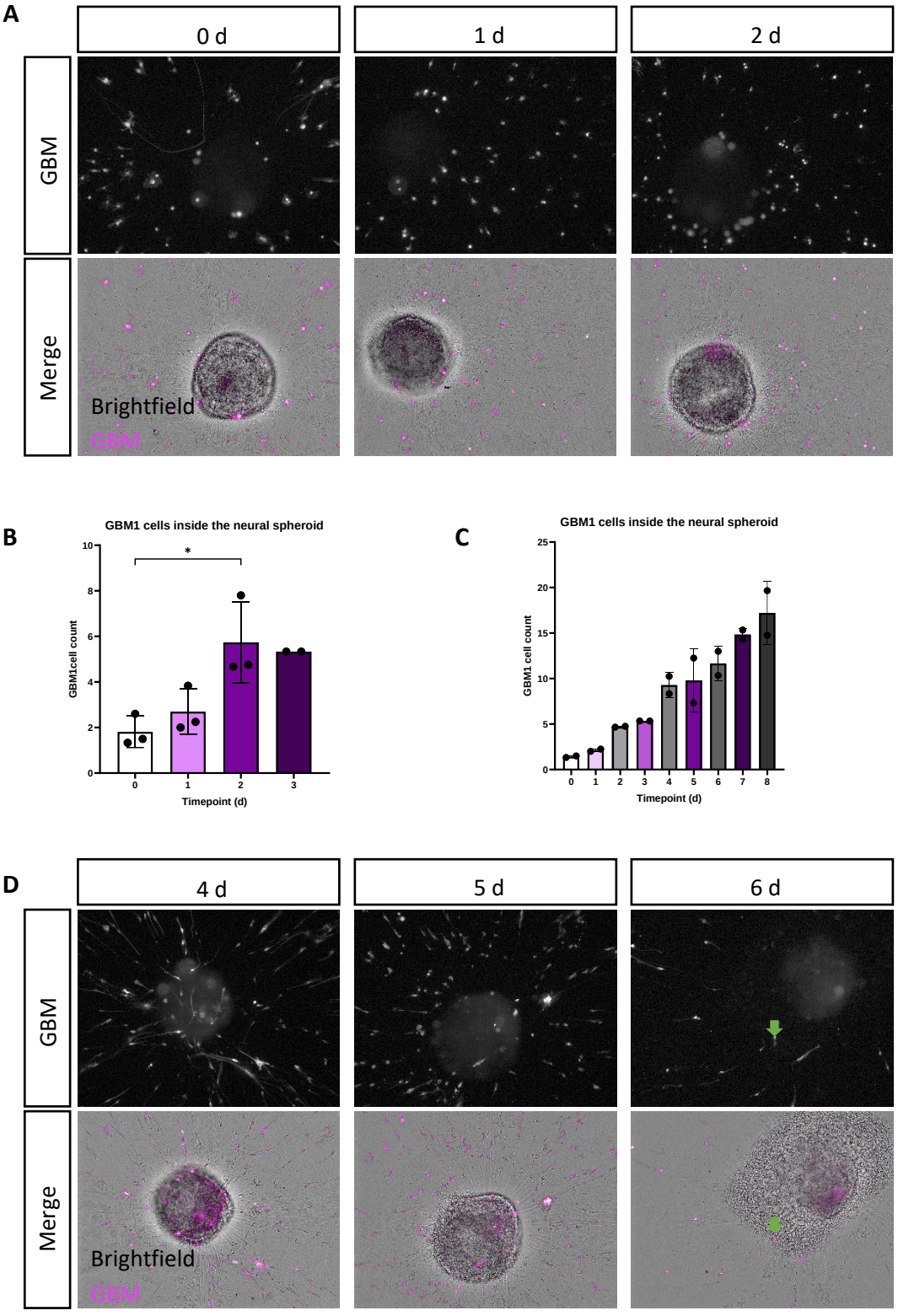

Figure 4.7 Quantification of GBM1 infiltration and migration towards the neural spheroid

A) Images representing co-culture of the neural spheroids and GBM1 from 0 to 2 d acquired on the Operetta Mark 1.

Graphs representing the quantification of GBM1 cell infiltration after 0-3 d N3 **(B)** after 0-8 d N2 **(C)**.
D) Images representing co-culture of neural spheroids and GBM1 from 4 to 5 d acquired on the Operetta Mark 1. The green arrow on day 6 is referring to a GBM1 cell found in the middle of the spread rosettes but outside the neural spheroid initial borders.

4.1.7. There is a higher infiltration with patient-derived GBM1 and GBM20 cell lines compared to NS17 line

Following the successful infiltration of GBM1 cells into neural spheroids, we aimed to compare the infiltration between a healthy control cell line and patient-derived cell lines capturing different phenotypes. We replicated the endpoint assay and co-cultured the neural spheroids with non-cancerous NS17 and patient-derived GBM20 cell lines. The neural spheroid was stained using the lipophilic dye BioTracker 488 localize the ROI using PreciScan as described in the Materials and Methods and at the beginning of this Results chapter (Figure 4.8.A, B, and C). A Z scan of the ROI is available on the CLS which facilitates the segmentation of the cells and further renders the quantification reliable. We found that the number of infiltrating cells increased over time for all cell lines with the lowest infiltration with the NS17 cells and the highest infiltration with GBM1 cells (Figure 4.8.D and E).

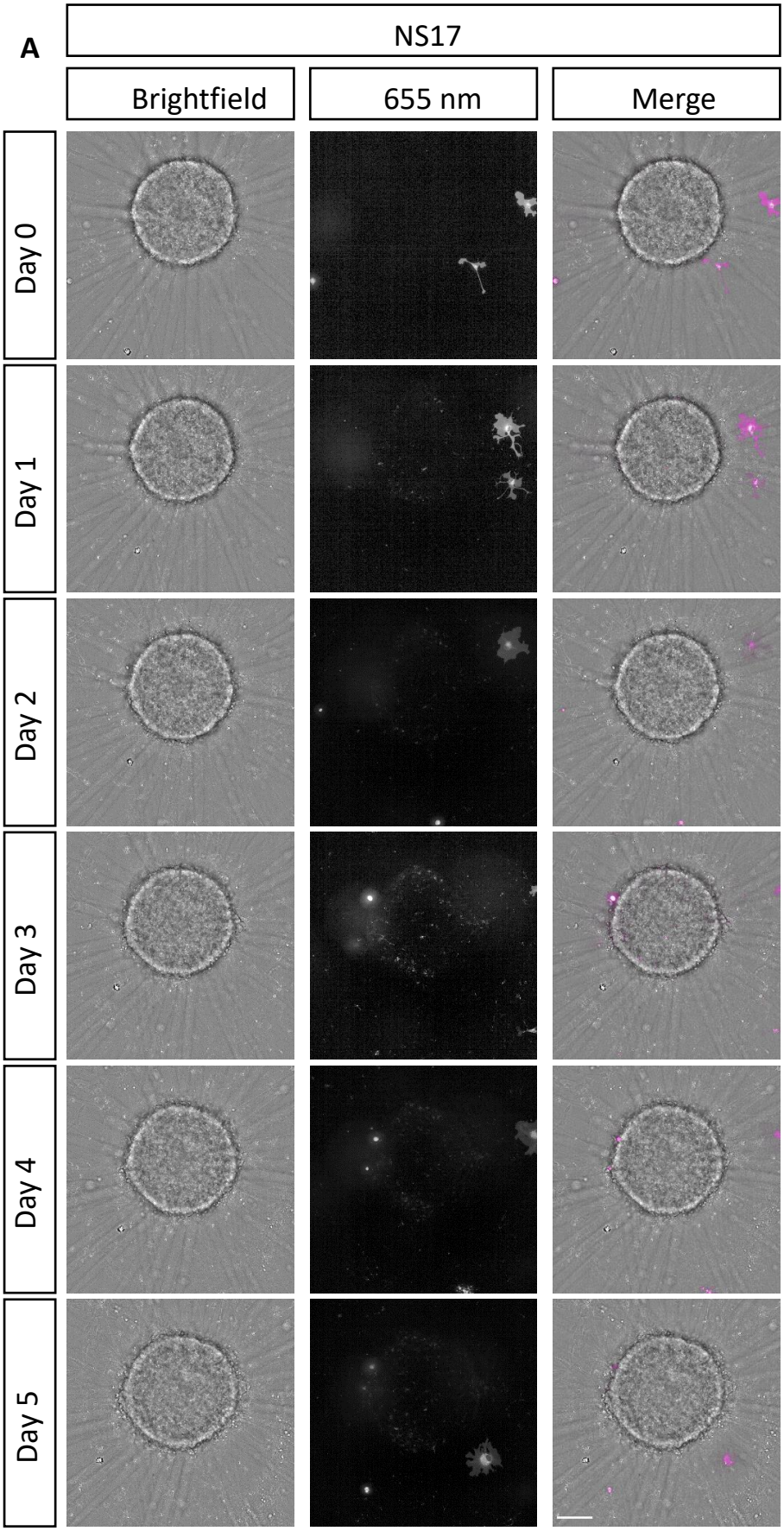
A
NS17
Brightfield
655 nm
Merge
Day 0
Day 1
Day 2
Day 3
Day 4
Day 5

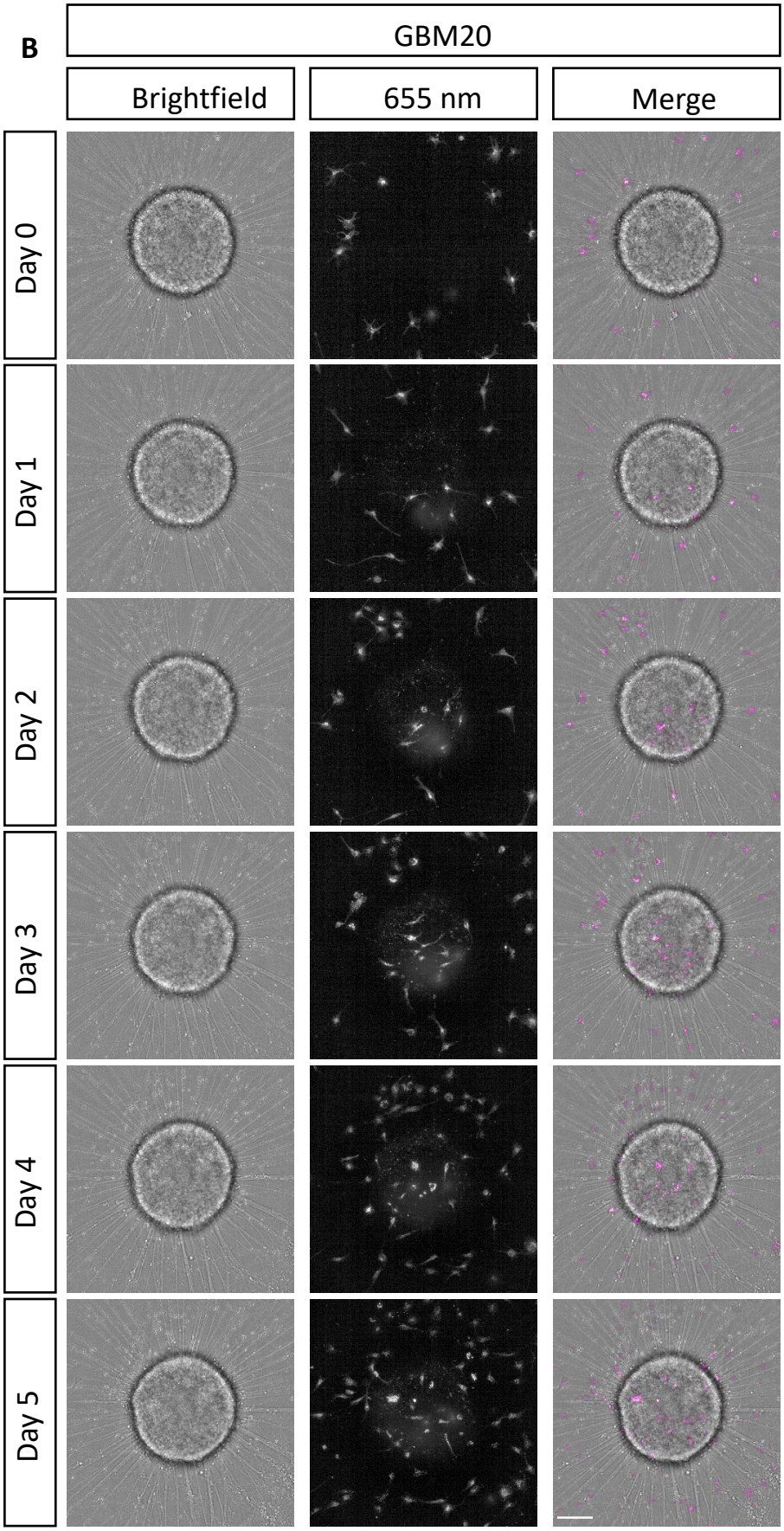
B
GBM20
Brightfield
655 nm
Merge
Day 0
Day 1
Day 2
Day 3
Day 4
Day 5

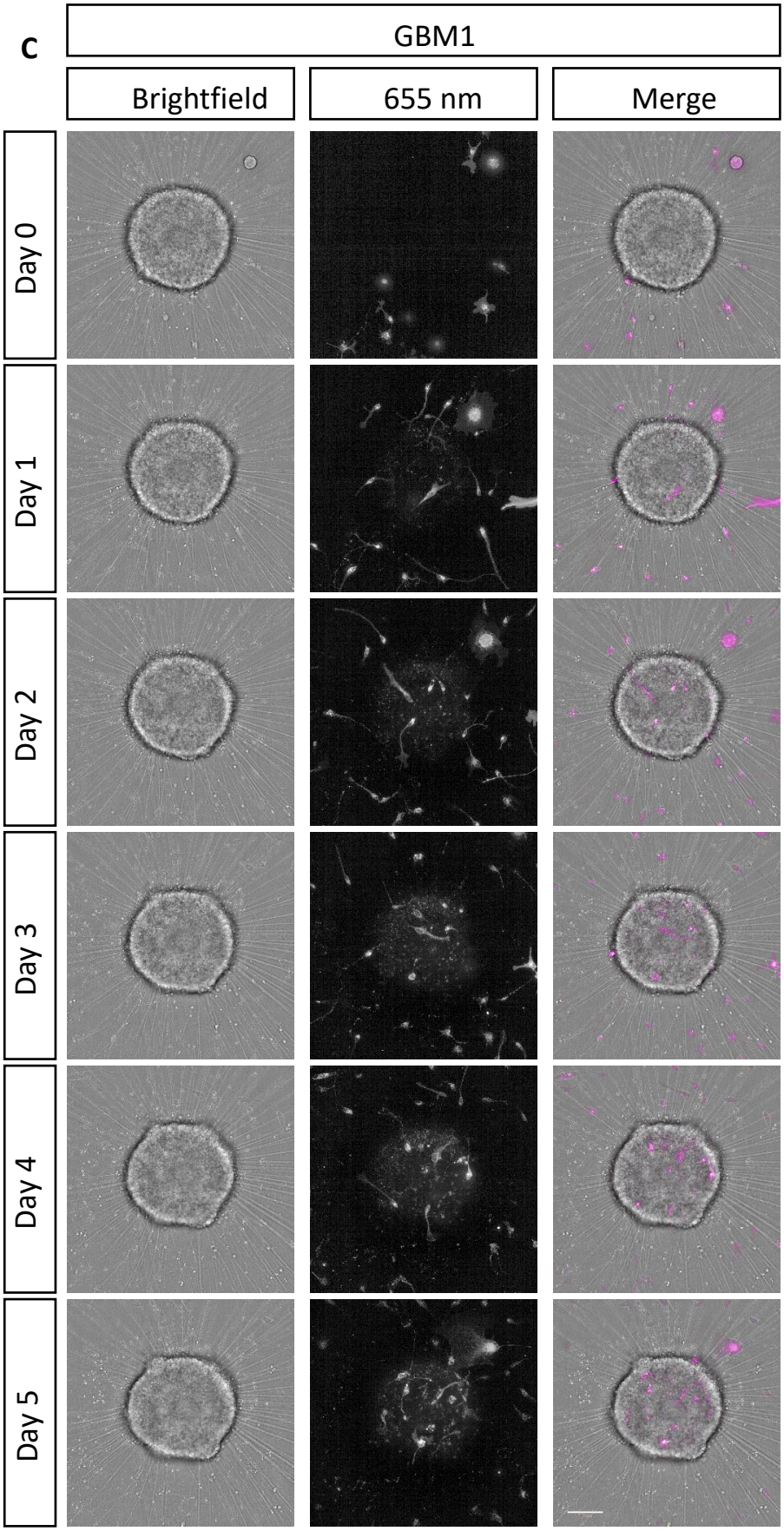
c
GBM1
Brightfield
655 nm
Merge
Day 0
Day 1
Day 2
Day 3
Day 4
Day 5

D

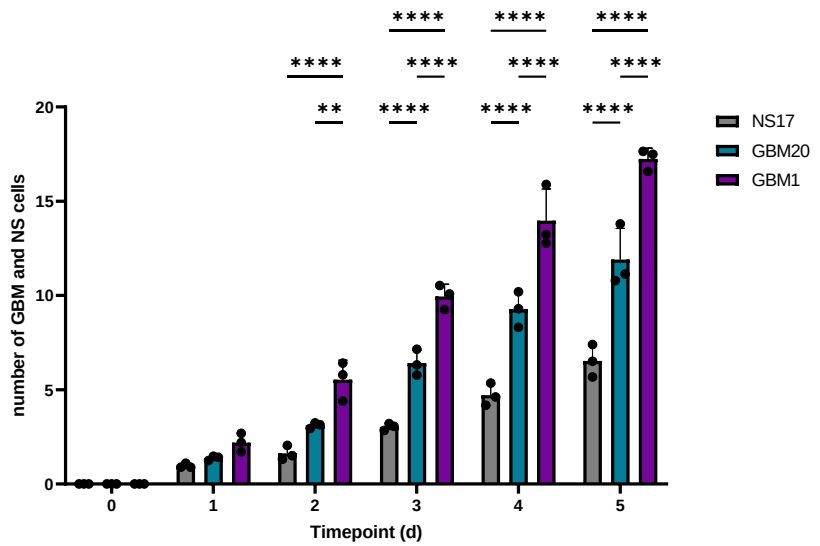

E

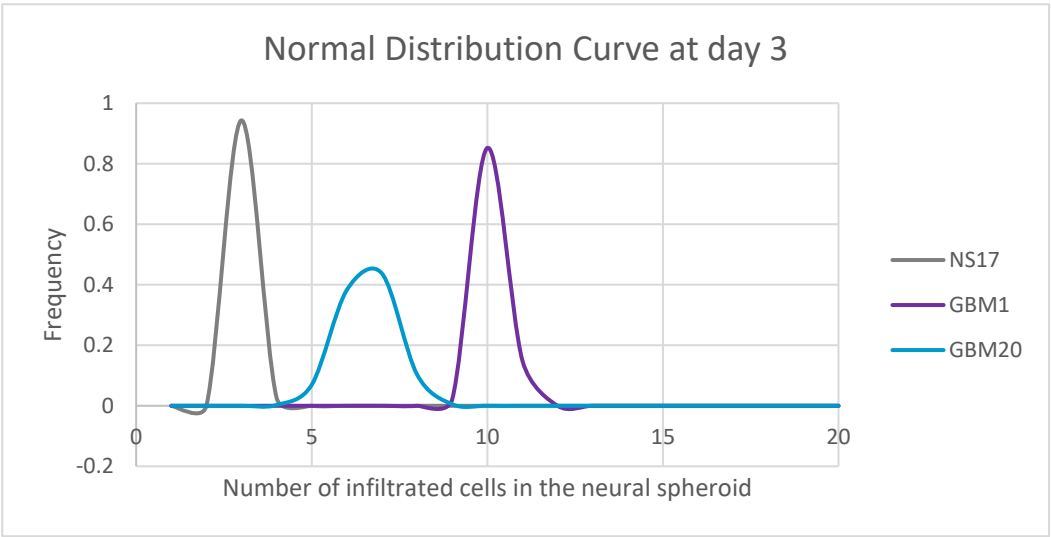

Figure 4.8 Endpoint assays of neural spheroids co-cultured with GBM1, GBM20, and NS17 cells

Images of co-culture of the neural spheroids with **(A)** NS17, **(B)** GBM20, and **(C)** GBM1 cells from day 0 to 5 were acquired on the Operetta CLS. Scale bar = 100 µm.

D) Quantification of the neural spheroids infiltration after days 0-5. Each point represents the mean of technical triplicates for 3 independent biological replicates (N = 3). The error bars represent the mean ± SD. **** p-value <0.0001, ** p-value = 0.0011.

E) Normal distribution curves for NS17, GBM20, and GBM1 cell infiltration were calculated from the means and standard deviation. Z-factor = 0.701246093.

4.2. Discussion

We developed an *in vitro* model mimicking the GBM microenvironment by co-culturing patient-derived GBM cells and hiPSC-derived cortical neural spheroid with radiating axons. To the best of our knowledge, no previous work has been performed that measures single-cell GBM migration on axon bundles towards an hiPSC-derived neural spheroid.

4.2.1. Optimisation of the endpoint and live assays

As I have reported in the previous chapter, tracking of the labelled patient-derived GBM1 cells was not accurate and suboptimal with the Harmony software and Trackmate, therefore we modified our pipelines to develop separate endpoint and live assays. For endpoint assays, we imaged the cells on the Operetta CLS but introduced lipophilic dyes to localise the neural spheroid using PreciScan and for better segmentation of the infiltrated GBM cells of the neural spheroid. The lipophilic dyes were reported to not appreciably affect cell viability, nor transfer between cells with intact membranes. This allows cell migration and tracking studies in mixed populations.

For live assays, we were able to use the Phasefocus Livecyte for our co-culture and image the GBM cell migration on axons. Likewise, Zepecki et al. performed a live-cell assay using phase-contrast microscopy to image human glioma cells every 10 min on parallel myelinated axons (Zepecki *et al.*, 2019). They showed the active formation and retraction of multiple pseudopodia. Moreover, phase-contrast microscopy has previously been used to monitor the growth of GBM spheroids (Bayat *et al.*, 2018; Gudbergsson *et al.*, 2019). These examples further confirm that phase contrast is a robust imaging approach for the long-term imaging and tracking of glioma cells. However, phase-contrast microscopy does not allow the imaging of the neural spheroid due to its density. Therefore, it was not possible to image the real-time infiltration of the neural spheroid with the Phasefocus Livecyte.

4.2.2. Comparison of the extrinsic factor-driven and transcription factor-driven differentiation

The neural spheroids were initially generated using extrinsic factor-driven differentiation and we also tested the transcription factor-driven differentiation. The aggregation of the cortical neurons was successful for both but there were reproducibility issues with the extrinsic-factor-driven differentiation. Extrinsic factor-driven differentiation of iPSCs into neuronal lineages relies on a combination of pathway inhibitors to derive neural progenitor cells, which are then differentiated further with different small molecules and growth factors to obtain the desired neurons. It comprises multiple challenges which include poor efficiency, variable cell types, and lengthy, complicated, and expensive protocols (Fernandopulle *et al.*, 2018)

Even though 10,000 cells were aggregated together for both inductions, the neural spheroids displayed different morphology. The cortical neurons obtained from transcription factor-driven differentiation will remain inside the spheroid, whereas the ones in the extrinsic factor-driven differentiation will spread out more and the spheroid will flatten (Figure 3.2.B and 3.8.B). The images show a round spheroid with clear outlines (transcription factor method) or one with irregular borders (extrinsic factor method). The axons growing out from extrinsic factor-based spheroids were more scarce and shorter than with the transcription factor-driven differentiation.

The small molecules in the extrinsic factor method are not highly efficient and may have led to a mixed population of neural progenitor cells and various neural and glial cell types instead of a homogenous population of cortical neurons (Fernandopulle *et al.*, 2018). In long-term cultures, the proliferative cells may outcompete the cortical neurons of interest and cause the irregular neural spheroid border and the lack of long-developing axons.

As the first protocol was not consistent, lengthy, and complex, we overcame those challenges by using the transcription factor-driven differentiation of cortical neurons and optimised our imaging pipelines with it. Using transcription factor-driven

differentiation allows the generation of cortical neurons in a simplified, rapid, efficient, and scalable manner (C. Wang *et al.*, 2017). In a study in 2013, Zhang et al. initially demonstrated that overexpression of neurogenin-2 rapidly directs iPSCs into functional neurons in a single step (Zhang *et al.*, 2013). Similarly, Busskamp et al. inducibly expressed neurogenin-2 in iPSCs and obtained neurons with a purity greater than 90% (Busskamp *et al.*, 2014). The studies both confirmed that neurogenin-2 overexpression is an appealing method for extrinsic factor-driven differentiation. Indeed, transcription factor-driven differentiation has been reported for iPSC-derived spinal motor neurons, oligodendrocytes, and even pancreatic β cells (Goto *et al.*, 2017; Major, Powers and Tabar, 2017; Zhu *et al.*, 2017)

4.2.3. Co-culture model and axon interaction

As described in the Introduction chapter, studies involving patient-derived GBM cells have previously been performed on laminin-coated surfaces, astrocytes, hydrogels, and electrospun nanofibers surface (Galli *et al.*, 2004; Singh *et al.*, 2004; Aubert *et al.*, 2008; Johnson *et al.*, 2009; Pollard *et al.*, 2009; Rao *et al.*, 2013; Haji Mansor *et al.*, 2018). Although those studies have provided information on the migratory behaviours of patient-derived GBM cells, the real-time interaction between patient-derived GBM cells and hiPSC-derived axons has not been reported.

We developed a co-culture model with patient-derived GBM cells and hiPSC-derived cortical neural spheroid with radiating axons. Using HCI, we developed robust pipelines to quantify the migratory behaviours of patient-derived GBM1 and GBM20 cells and NS17 cells in our co-culture system. In the endpoint assays, we investigated the cell morphology to define that a cell is interacting and engaging on an axon, we looked at the morphological properties. The cells were more elongated on the axons as they settled faster with the axonal structure underneath compared to a laminin-coated glass surface. However, after 2 days, the cell area difference was reduced as the GBM1 cells settled and stretched in empty wells as well as on axons and they reach similar levels in terms of cell elongation too.

Similarly, Zepecki et al. developed a co-culture of human glioma cells with rat dorsal root ganglion axon to study the migration of human glioma cells (Zepecki *et al.*, 2019). The axons were myelinated with the addition of oligodendrocytes in the culture. They demonstrated that the human glioma cells migrated along non-myelinated and myelinated axonal tracks through the formation of pseudopodia. They further investigated the proteins involved in the regulation of pseudopodia which could be applied in our model to further understand the interaction between our patient-derived GBM cells and axons.

4.2.4. Migratory behaviours of patient-derived GBM1 and GBM20 cells and NS17 cells

In the live assays from the Livecyte, we saw differences in the displacement and directionality of the cells when seeded on empty wells compared to when on axons. The cells aligned and followed the structure underneath to migrate. As observed in the directionality data, there was a stronger migration in the direction of the neural spheroid for all cell lines: patient-derived GBM1 and GBM20 and non-cancer NS17 cells.

Because all the cell lines were moving in the direction of the neural spheroid, we wanted to quantify the number of cells infiltrated in the neural spheroid in endpoint assays, as an indicator of invasiveness. We demonstrated a higher infiltration of the neural spheroid with patient-derived GBM1 and GBM20 cells compared to NS17 cells. This meant that despite the NS17 cells migrating in the direction of the neural spheroid in our live assays, the NS17 cells do not infiltrate it. We believe that NS17 cells are attracted to the neural spheroid but do not have the mechanisms to infiltrate like the patient-derived GBM1 and GBM20 cells. Similarly, da Silva et al. demonstrated increased infiltration of their cerebral organoid model with the patient-derived GBM1 spheroids compared to the neural progenitors (da Silva *et al.*, 2018). Those mechanisms may be the cell-surface proteins or the ability to undergo an EMT as explained in the Introduction chapter.

Finally, we compared the migratory behaviours of classical/proneural to mesenchymal subtypes. GBM1 is derived from a non-treated classical/proneural subtype and GBM20 is from a recurrent mesenchymal tumour previously treated. GBM20 is more migratory and invasive than GBM1 by our collaborators from the Wurdak laboratory (data not published). However, in our model, we saw a higher infiltration of the neural spheroid with GBM1 than with GBM20. As the GBM20 is derived from a pre-treated recurrent tumour, a reason for its reduced invasion may be a change in its phenotype. The Parinello laboratory has also reported that tumour cells which spread into the brain's white matter became less aggressive. They explained that this response is caused by the damage in the white matter caused by the tumour. This in turn results in the tumour cells attempting to repair the wound-like environment. Hence, the tumour cells mature into cells resembling the normal brain cells in the white matter and become less able to grow and spread (Brooks *et al.*, 2020).

In terms of other migratory properties, the results showed a large spread of the data and we observed that GBM cells displayed different morphologies. We believe that there are subpopulations of slow and fast-migrating cells causing the spread of the data and that a subpopulation of cells migrating towards the neural spheroid may have a higher persistence and speed. As mentioned in the Introduction, GBMs comprise intra-heterogenous populations and specific driver mutations may cause a subset of cells to migrate (Claes, Idema and Wesseling, 2007; Aubry *et al.*, 2015). Consequently, further investigation will delineate the subpopulations of each cell line and the relevant cells to target to inhibit migration.

5. RESULTS CHAPTER 3 - INVESTIGATE THE MIGRATORY CUES INVOLVED IN THE GBM MIGRATION ON AXON BUNDLES

As described in the Introduction, GBM depends on several mechanisms to migrate (Armento *et al.*, 2017; Liu *et al.*, 2021). Indeed, cellular and environmental conditions can drive a migrating phenotype and lead the GSCs away from the tumour niche (Armento *et al.*, 2017; Nishikawa *et al.*, 2018; Robertson *et al.*, 2019). Therefore, several motility and invasion inhibitors have been in a clinical trials such as inhibitors to integrin, TGF-β receptor, or to the PI3K pathway (Bogdahn *et al.*, 2011; Stupp *et al.*, 2014; Pitz *et al.*, 2015; Wen *et al.*, 2019; Wick *et al.*, 2020). This chapter will investigate the different mechanisms involved in the migration of patient-derived GBM1 and GBM20 cells using our model as a drug screening platform and bulk RNA sequencing. Firstly, I will summarise the various pathways we sought to target using inhibitors. I selected and tested a panel of inhibitors to proteins such as the cytoskeleton, kinases and axonal guidance molecules involved in the motility and invasion of GBM (summarized in Table 5.1).

As positive controls, I selected inhibitors which interfere with the cytoskeleton. The small molecule compounds, Blebbistatin and Latrunculin B interfere with the cytoskeleton by inhibiting myosin II ATPase activity and actin polymerization, respectively. By dysregulating the cytoskeleton formation, they are commonly used inhibitors which decrease the motility of the cell and I expect them to have the same effect on the patient-derived GBM cells and NS17 cells. Another common motility inhibitor is Y-27632 dihydrochloride, which is a selective ROCK1 (p160 ROCK) and ROCK2 inhibitor.

In GBM, pathways involved in the motility of the cell have been inhibited to explore if the prevention of GBM migration could be used as an anti-cancer therapy. Examples of it are inhibitors to the canonical pathway linked to the migration and survival of GBM cells. Those are inhibitors to TGF-β Receptors such as SB 431542 or to the Akt/PKB signalling such as LY294002 or API-2 (Ströbele *et al.*, 2015; Djuzenova *et al.*, 2019). TGF-

β1 was shown to promote the motility and invasiveness of glioma cells through activation of ADAM17 (Lu *et al.*, 2011) and inhibitors to the Akt/PKB signalling affect the migration and radiation sensitivity of GBM cells differentially (Djuzenova *et al.*, 2019). As previously mentioned, drugs inhibiting the TGF-β receptor I, LY2157299 (galunisertib), or TGF-β2, AP-12009 (trabedersen) have been in clinical trials in Phase 1b/2a and Phase 3 respectively (Bogdahn *et al.*, 2011; Wick *et al.*, 2020). The PI3K is also a promising pathway to target with the inhibitors PX-866 in Phase 2, NVP-BKM120 (buparlisib) in Phase 2 and SAR245409 (voxtalisib) inhibiting PI3K/mTOR in Phase 1 (Pitz *et al.*, 2015; Wen *et al.*, 2015, 2019).

Other inhibitors are involved in non-canonical pathways such as HPI 1 which inhibits Sonic Hedgehog signalling (Hung *et al.*, 2020) and IWP 2 (PORCN inhibitor) which inhibits Wnt processing and secretion (Lee *et al.*, 2015). Those pathways activate diverse signalling cascades involved in the regulation of cell growth, differentiation, but also motility.

Additional inhibitors which can affect GBM cell migration are inhibitors to FAK, FGFR, and integrins such as PF 573228, PD 173074, and Cilengitide/EMD121974, respectively. The integrin inhibitor is a potent and selective inhibitor of integrins αvβ3 and αvβ5 and is currently in Phase 3 of a clinical trial Those small-molecule inhibitors of FAK, FGFR, and integrins work in combination by selectively decreasing GBM cell motility and proliferation specifically when stimulated with L1 cell adhesion molecule (L1CAM) (Anderson and Galileo, 2016). FAK may act as a downstream molecule in the pathway between the integrin and FGFR signalling pathways stimulated by L1 in the established GBM cell lines, T98G and U-118 MG (Anderson and Galileo, 2016).

I also considered inhibitors to growth factor receptors such as PDGFR or EGFR; these two receptors mediate the migration of GBM cells. Through the ERK and ROCK pathways, PDGFR inhibition affects migration as well as growth (Singh, Sharma and Pillai, 2018). As previously mentioned, amplification of the EGFR genes is common in GBM. Gefitinib selectively inhibits tumour cell migration in EGFR-amplified human GBM

(Parker *et al.*, 2013). Targeting Protein Kinase C with GF 109203X in GBM Treatment has also been shown to be effective (Geribaldi-Doldán *et al.*, 2021).

As previously explained, GBM cell movement can occur along the axons of myelinated neurons of the white matter tract. Those molecules are receptors found on the axons or the GBM cell which are involved in the attachment of the GBM cell to the axon as well as the directionality of the GBM cell movement. They act as attractants or repellents and "Go or Grow" regulators of GBM (Armento *et al.*, 2017). Therefore, I expect the most promising candidate compounds to be inhibitors to axonal guidance molecules, in alignment with the key hypothesis guiding this project.

Ephrins and their Eph receptors play a key role in the cell-surface-bound axon guidance cues (Armento *et al.*, 2017). They are involved in the development of the central nervous system as well as the regulation of cancer cell migration and invasion (Makarov *et al.*, 2013). Hence, the Eph family tyrosine kinase inhibitor that targets Eph receptors is a common and viable option to inhibit migration. Examples include Ehp-inhibitor inhibiting EphB2 kinase, EphB4 kinase, and related Eph kinases; ALW II-41-27 (compound 7) inhibiting EphA2; and NVP-BHG712 S2 inhibiting EphB4. These inhibitors of Eph receptor tyrosine kinases work by inhibiting the cell growth, stemness, and migration of GSCs (Affinito *et al.*, 2020). Specifically, EphB4 overexpression was shown to mediate the resistance in experimental glioma to anti-angiogenic therapy by altering vascular morphogenesis, pericyte coverage, and cellular proliferation/apoptosis in SF126 glioma cells (C *et al.*, 2018).

As mentioned in the Introduction, hypoxia and nutrient starvation around the centre of GBM activate the migratory processes such as CXCRA which mediates CXCL12-glioma cell migration. Motixafortide (BL-8040) is an inhibitor of CXCR4 and targeting CXCL12/CXCR4 Axis was shown to be effective in immunotherapy (Zhou *et al.*, 2019).

Finally, another potential strategy for GBM could be to repurpose existing drugs which have already passed clinical trials and are currently used to treat other conditions. This will reduce the time researching a drug and for clinical trials. Indeed, in a pre-clinical

mouse model, the Parinello lab has shown that the asthma drug ONO 1078 (Pranlukast) which is a selective CysLT1 inhibitor can suppress the growth by impacting the white matter tracts where the cancer cells spread (Brooks *et al.*, 2020).

This chapter aimed to validate our model as a tool for screening inhibitors which can decrease the GBM1 or GBM20 infiltration of the neural spheroid. The patient-derived GBM1 and GBM20 cell lines were sent for bulk RNA sequencing and I used this data to correlate the gene expression to the drug response. In the future, primary hits will then be further investigated using live imaging to see how the inhibitor affects the migratory properties of the GBM cells.

To investigate the migratory cues involved in the GBM migration on axon bundles, this chapter involved the following objectives: (1) screen inhibitors which can decrease the neural spheroid infiltration and (2) correlate the drug response to gene expression profiles of the patient-derived GBM1 and GBM20 cells from bulk RNA sequencing data.

Table 5.1 Inhibitors used in our model including the compound name, the pharmacological target, the catalogue number, and the provider

Compound name	Pharmacological Target	IC50 in nM	Company	Catalogue number
API-2	Akt	50	Tocris	2151
PF 573228	FAK	4	Tocris	3239
ONO 1078 (Pranlukast)	CysLT1	4	Tocris	3026/50
Blebbistatin	myosin II ATPase	2000	Tocris	1760
Latrunculin B	actin polymerization	60	Tocris	3974
Y-27632	ROCK	140	Tocris	1254
PD 173074	FGFR	5	Tocris	3044
HPI 1	Sonic Hedgehog	150	Tocris	3839

IWP 2	Wnt	27	Tocris	3533
ALW II-41-27 (Compound 7)	EphA2	12	Selleck Chem	S6515
NVP-BHG712 S2202	EphB4	25	Selleck Chem	S2202
Ehp-inhibitor-1	Ephrin receptors (EphB2 kinase, EphB4 kinase and related Eph kinases)	10	Selleck Chem	S0256
Cilengitide (EMD121974)	integrins αvβ3 and αvβ5	4.1	Tocris	5870
Motixafortide (BL-8040)	stromal derived factor 1 (SDF-1, CXCL12)	1	Selleck	S9665
GF 109203X	Protein Kinase C	8.4	Tocris	0741
SB 431542	TGF-beta Receptors	94	Tocris	1614
AC 710	PDGFR	1.2	Tocris	5013
Iressa	EGFR	23	Tocris	3000

5.1. Results

5.1.1. The screen identified inhibitors which significantly decreased GBM20 and GBM1 infiltration of the NS at day 3

I used our previous pipeline with the endpoint assay to see if those inhibitors have an effect on the infiltration and the migratory behaviour of the non-cancer NS17 cells and patient-derived GBM1 and GBM20 cells (Figure 5.1). As this is an initial drug screening, all the inhibitors were used at 1 µM to identify the drugs of interest. On day 0, I stained the neural spheroid and the cells and seeded the cells for co-culture. On day 1, the co-cultures were treated with the inhibitors and imaged after 6 h of inhibitor incubation on the Operetta CLS. This was repeated over the next 2 days. The quantification was performed using the Harmony software and the data was normalized to day 0.

For the patient-derived GBM1 and GBM20 cell lines, the number of infiltrated cells increased with days similar to the non-treated co-cultures. I investigated whether the spheroid was affected by the inhibitor by examining the morphology of the neural spheroids which stayed circular with clear borders following the inhibitor treatment for 3 days. The images show a visible increase of the GBM1 cells inside and around the neural spheroid from 1 to 3 days.

The differences in infiltration were seen on day 3 (Figure 5.3) apart from the increase of GBM1 infiltration on day 2 after the IWP 2 treatment. Overall, GBM20 was more susceptible to the range of inhibitors compared to GBM1 with four inhibitors which significantly decreased GBM20 infiltration of the neural spheroid at day 3 compared to only two inhibitors for GBM1. For the GBM1 cells, there was a significant decrease with Latrunculin B (p value=*) and Motixafortide (p value=*). For the GBM20 cells, there was a significant decrease with PF 573228 (p value=**), Cilengitide, GF 109203X, and SB 431542 (p value=*).

Based on our results, the inhibitors did not affect the NS17 cell lines. There was no significant difference in the NS17 infiltration of the neural spheroid which remained low as the control also has few NS17 infiltrated in the neural spheroid.

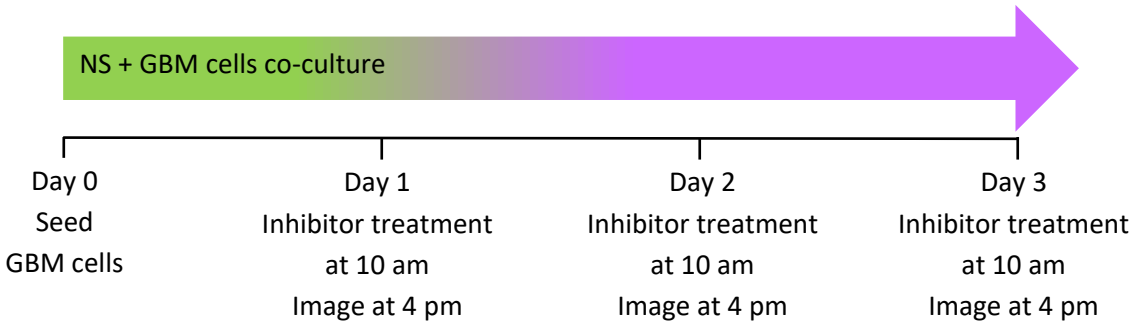

Figure 5.1 Timeline for treating the neural spheroid and GBM/NSC cells co-culture with inhibitors and acquiring images

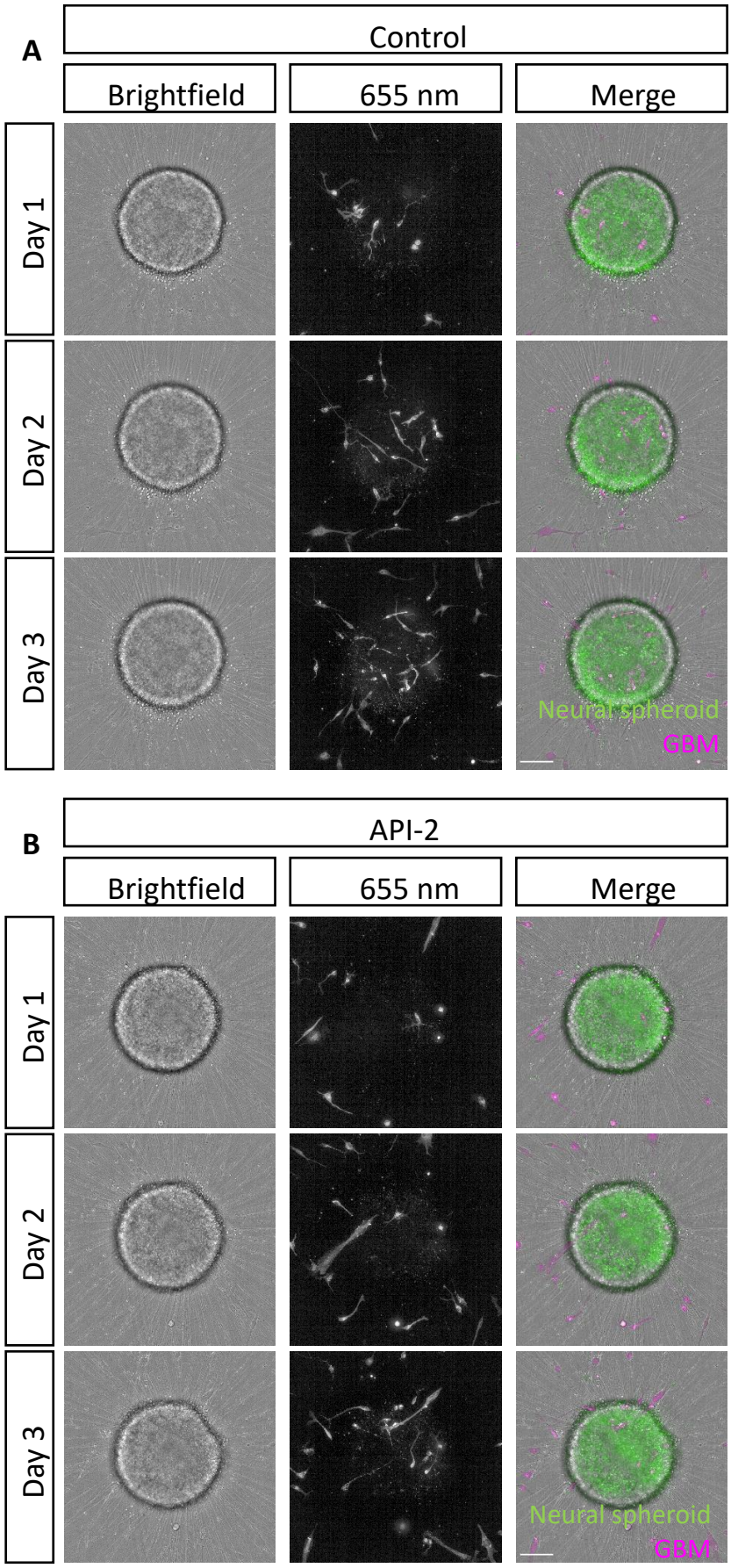
A
Control
Brightfield
655 nm
Merge
Day 1
Day 2
Day 3
Neural spheroid
GBM
B
API-2
Brightfield
655 nm
Merge
Day 1
Day 2
Day 3
Neural spheroid
GBM

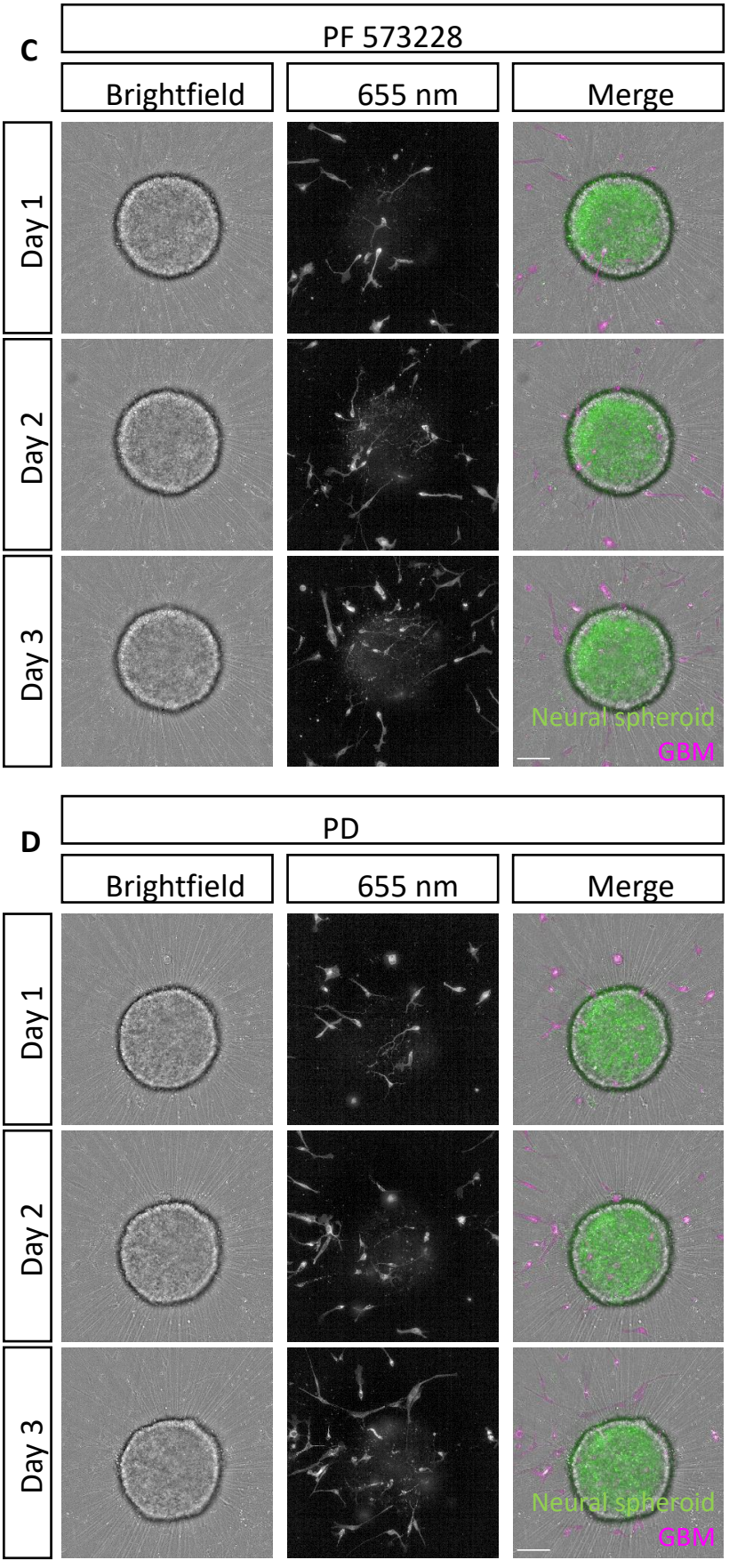
C
PF 573228
Brightfield
655 nm
Merge
Day 1
Day 2
Day 3
Neural spheroid
GBM
D
PD
Brightfield
655 nm
Merge
Day 1
Day 2
Day 3
Neural spheroid
GBM

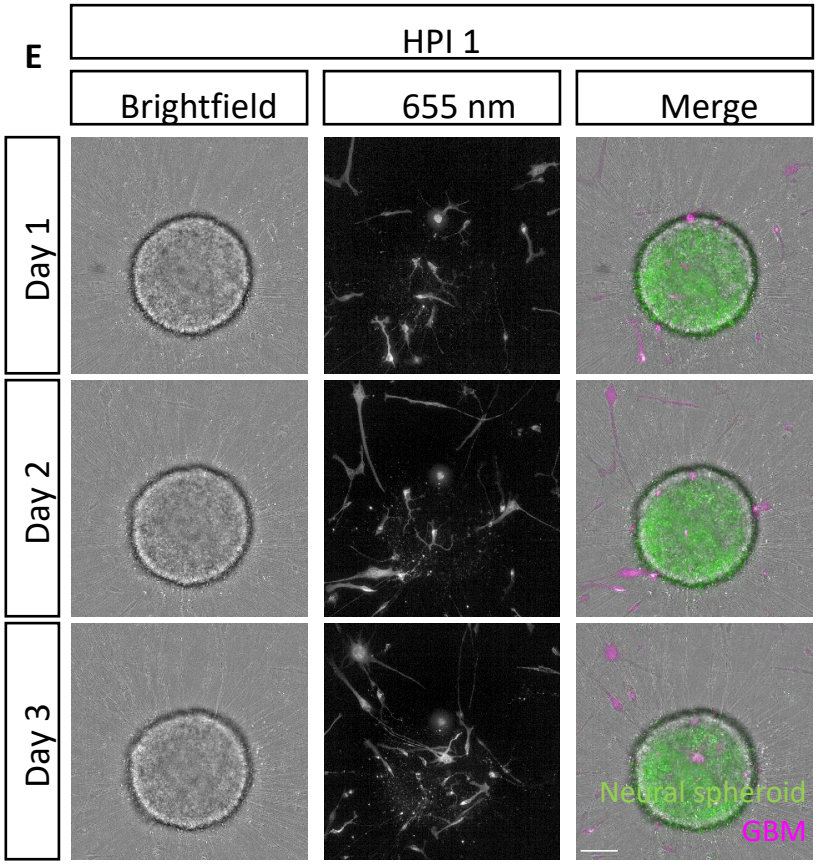
E
HPI 1
Brightfield
655 nm
Merge
Day 1
Day 2
Day 3
Neural spheroid
G8M

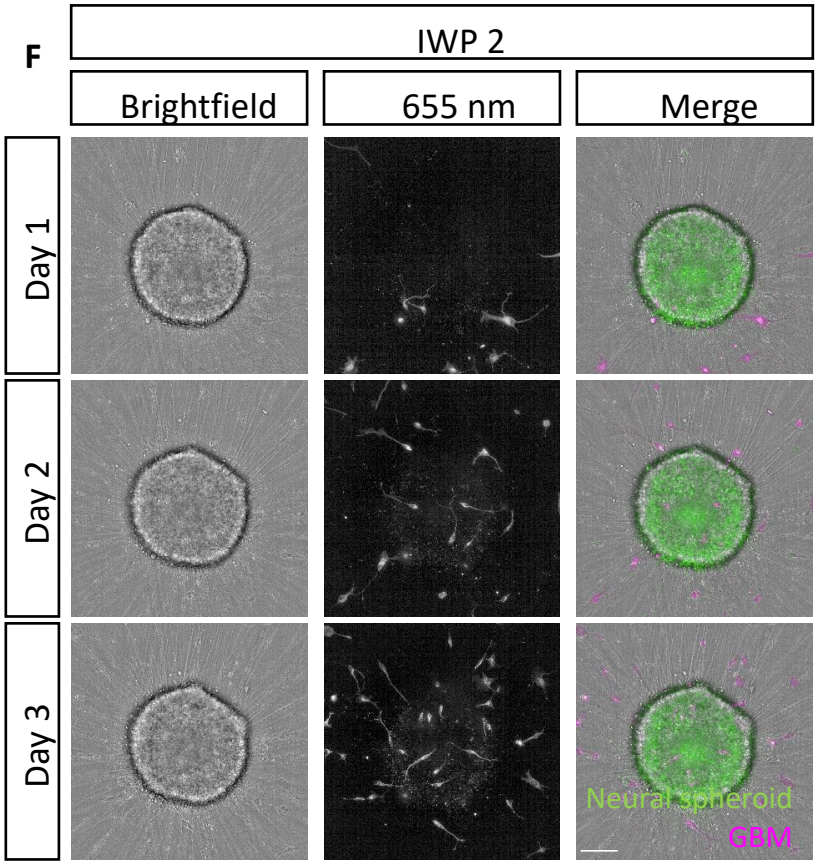
F
IWP 2
Brightfield
655 nm
Merge
Day 1
Day 2
Day 3
Neural spheroid
G8M

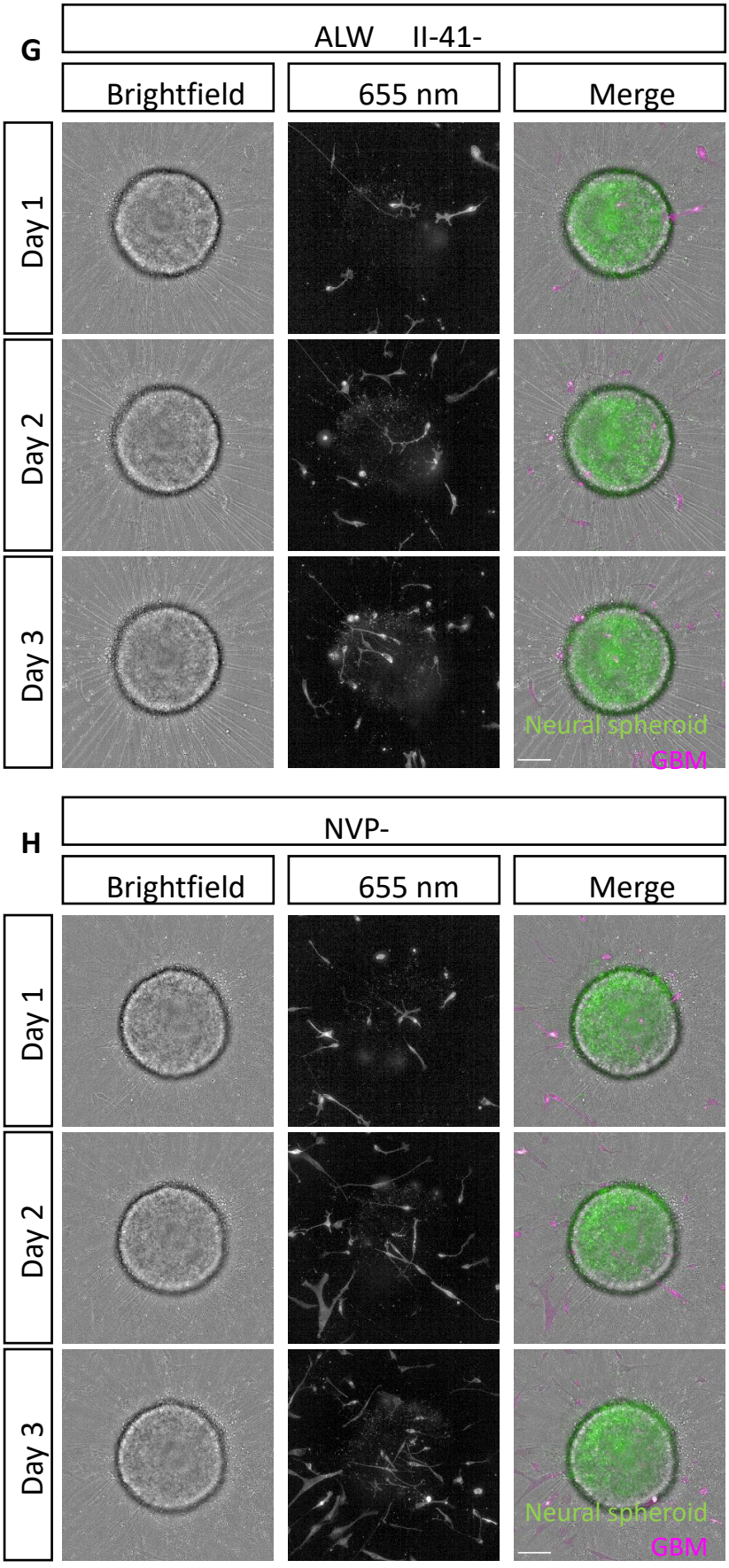
G
ALW II-41-
Brightfield
655 nm
Merge
Day 1
Day 2
Day 3
Neural spheroid
GBM
H
NVP-
Brightfield
655 nm
Merge
Day 1
Day 2
Day 3
Neural spheroid
GBM

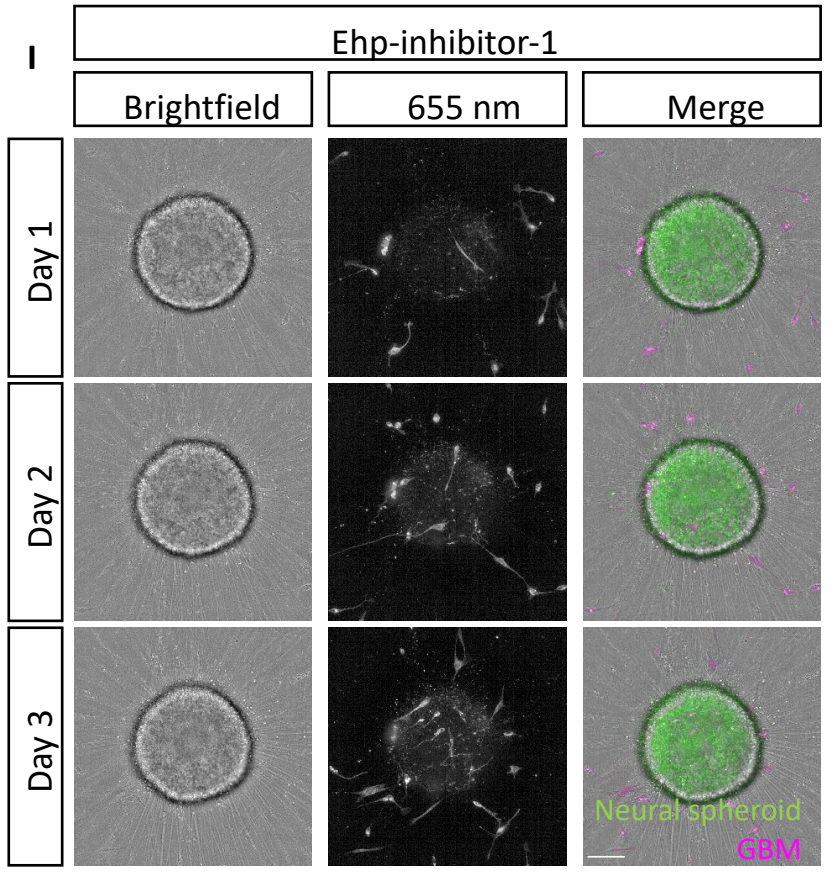
I
Ehp-inhibitor-1
Brightfield
655 nm
Merge
Day 1
Day 2
Day 3
Neural spheroid
GBM

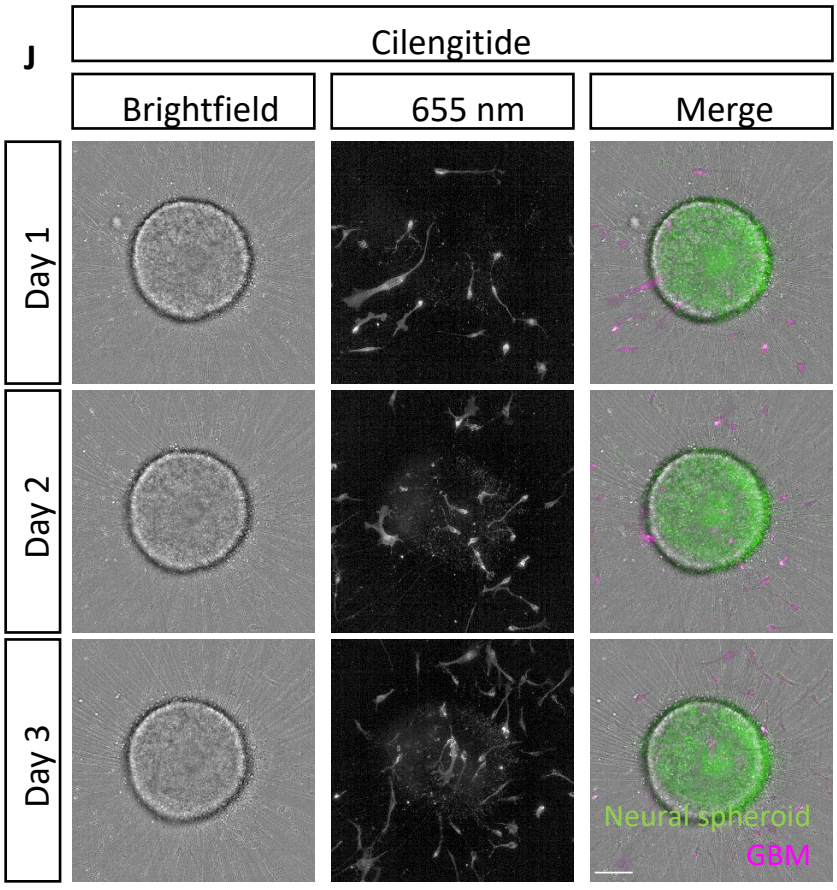
J
Cilengitide
Brightfield
655 nm
Merge
Day 1
Day 2
Day 3
Neural spheroid
GBM

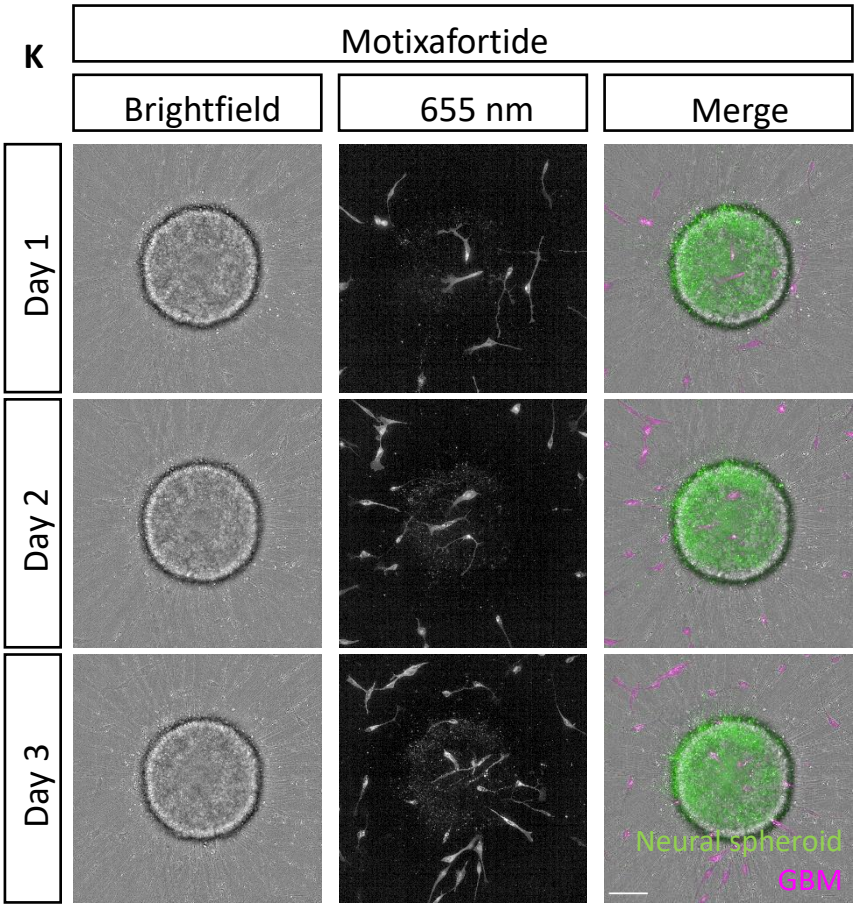

Figure 5.2 Co-culture of neural spheroids with GBM1 and the inhibitors

Example images of neural spheroids co-culture with GBM1 cells from day 1-3 acquired on the Operetta CLS device showing the **(A)** control condition and the following inhibitors: **(B)** API-2, **(C)** PF 573228, **(D)** PD 173074, **(E)** HPI 1, **(F)** IWP 2, **(G)** ALW II-41-27, **(H)** NVP-BHG712, **(I)** Ehp-inhibitor-1, **(J)** Cilengitide, and **(K)** Motixafortide. Merge images of the brightfield, GBM1 (magenta), and neural spheroids (green). Scale bars = 100 µm.

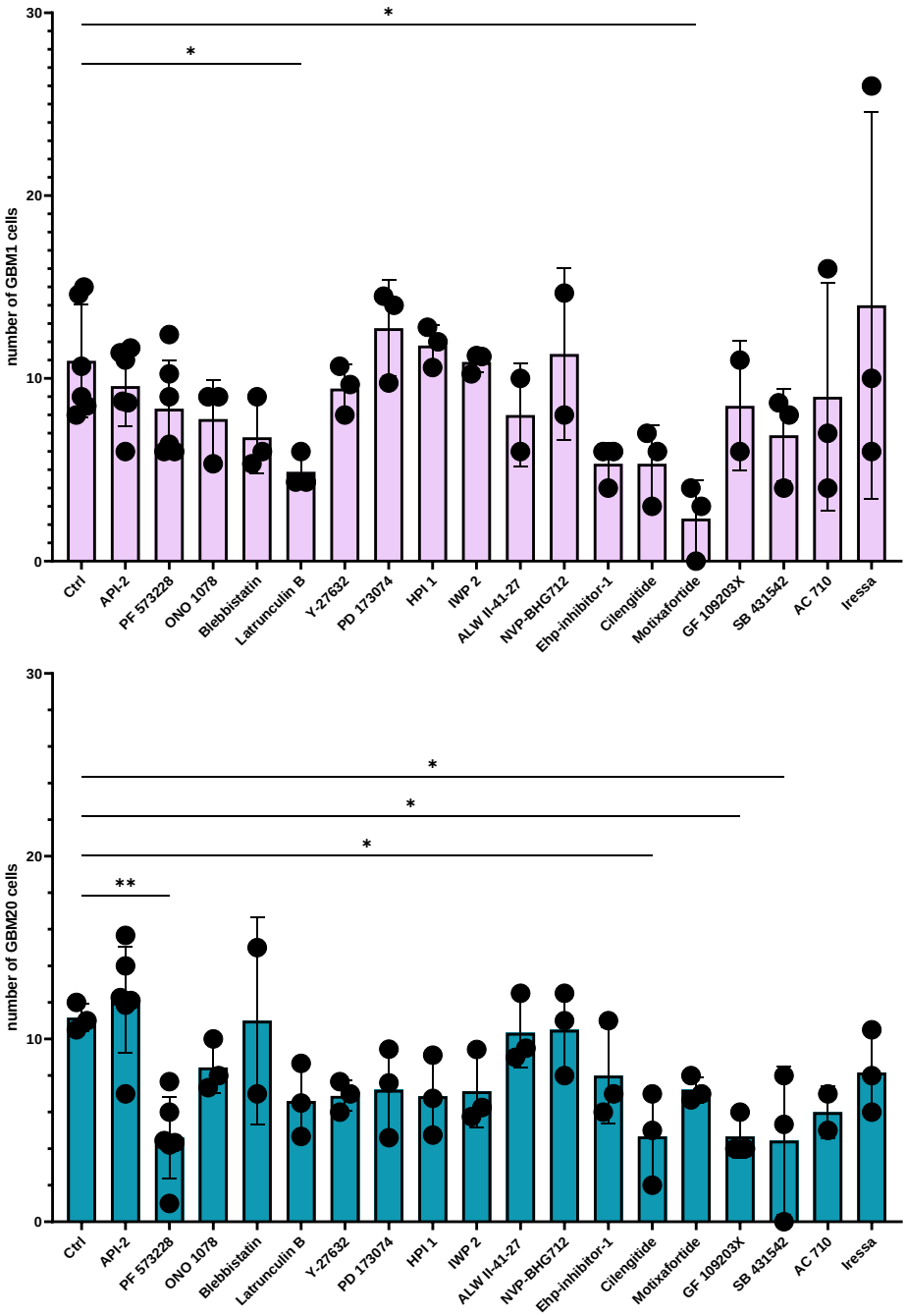

Figure 5.3 Quantification of the GBM1 and GBM20 infiltration of the neural spheroid treated with the inhibitors

Graphs representing the quantification of GBM1 and GBM20 cell infiltration after day 3 following the inhibitors treatments. All cells were treated with the antagonists at 1 µM. Each point represents the mean of technical triplicates for 3-5 independent biological replicates (N = 3-5). The error bars represent the mean ± SD. * p-value <0.1, ** p-value <0.01.

5.1.2. Correlate gene expression to drug response

As we mentioned in the Introduction, GBM can harbour chromosomal rearrangements, such as translocations or inversions, which can disrupt the karyotypes. These rearrangements can affect the spatial organization of the genome and alter the gene expression profiles of GBM cells (Turner et al., 2017; Robertson et al., 2019). To gain insight into the gene expression profile and heterogeneity between GBM1 and GBM20, the cell lines were submitted to Eurofins Genomics for bulk RNA sequencing. In doing so, we were aiming to correlate their gene expression to the drug response. As described in the methods, the raw sequencing data were pre-processed by Eurofins Genomics and included the quality control, the mapping to Reference Genome, the transcript quantification, and the differential gene expression (Figure 2.5). Using the data of differential gene expression, I further analysed on R studio using the ggplot2 package (Figure 2.6). I generated a volcano plot using the sample-wise comparison of foldchange and significant foldchange values (Figure 5.4). Finally, I highlighted the differential expression of the genes involved in the migratory pathways targeted by our panel of inhibitor screens. Genes enriched in GBM1 included WNT2, MYO16, ACTL10, CXCL12, MYO7A, ITGB4, EPHA7, and TGFBI whereas genes enriched in GBM20 included PRKCB, ITGBL1, WNT9A, MYO1B, MYH14, ITGB3, EPHX4, ITGA10, WNT5A, and ITGA11.

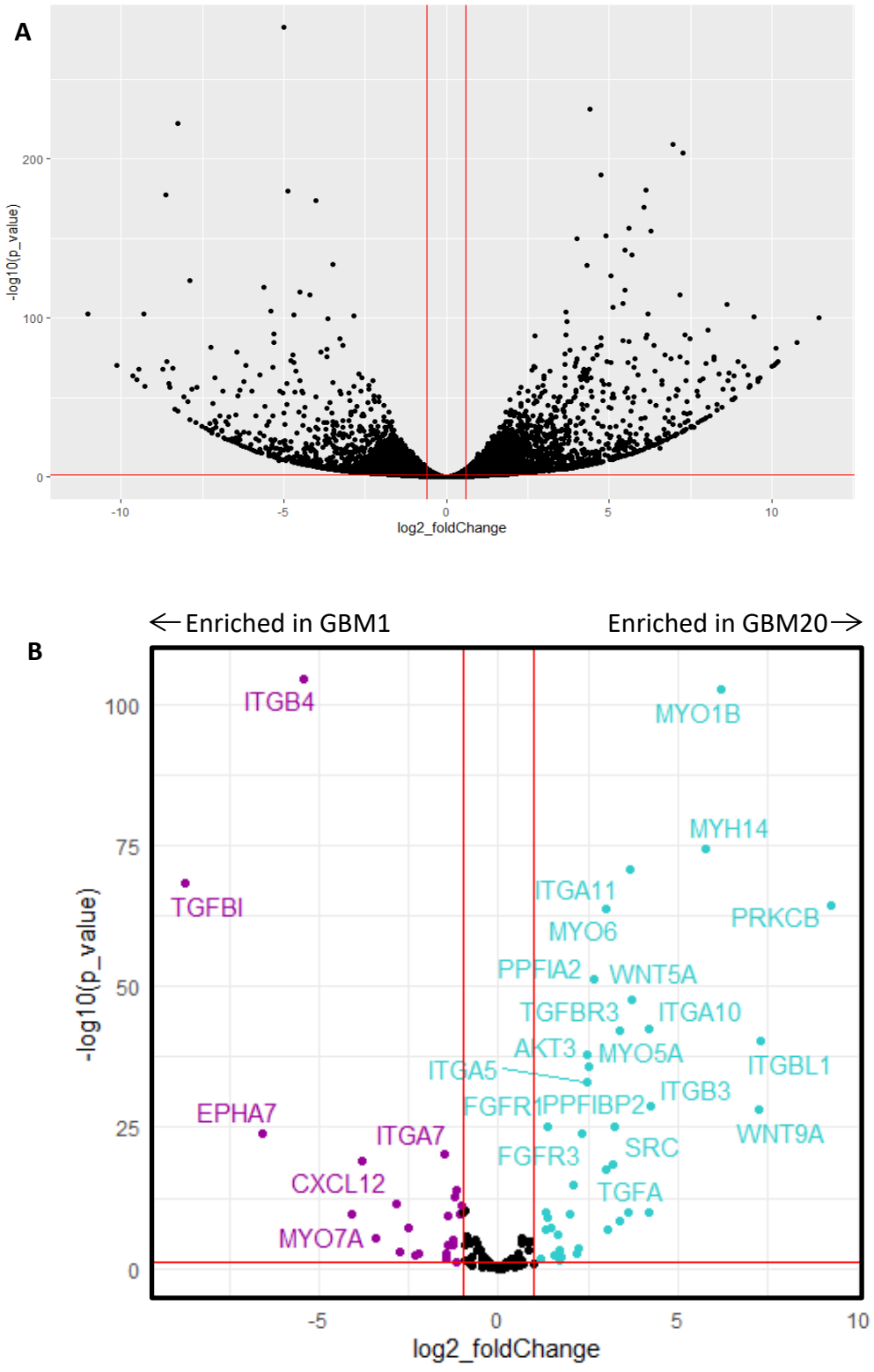

Figure 5.4 Differential gene expression of the GBM1 and GBM20 cell lines

Volcano plots representing the differential gene expression of GBM20 versus GBM1 **(A)** and with the genes involved in the inhibitor screen highlighted **(B)**.

5.2. Discussion

In this chapter, I reported the effects of several inhibitors on the infiltration of the neural spheroids in the co-culture model I developed.

5.2.1. Drugs which decreased GBM1 and GBM20 cells infiltration of the neural spheroid

Importantly, the drug effect was different between the two patient-derived GBM cell lines. I saw a significant decrease at day 3 in the GBM20 cells infiltration of the neural spheroid when treated with PF 573228 inhibiting FAK inhibitor, Cilengitide inhibiting integrins αvβ3 and αvβ5, GF 109203X inhibiting Protein Kinase C, and SB 431542 inhibiting TGF-β receptors. On the other hand, Motixafortide which inhibits CXCL12 and Latrunculin B significantly decreased GBM1 infiltration of the neural spheroid. The difference in the drug effect in the two patient-derived cell lines suggests that different migration-related pathways are active in GBM1 and GBM20 cells. This further emphasizes the importance of the heterogeneity between tumours and the need for personalized medicine.

The inhibitors which mainly affected the GBM20 cell line derived from a recurrent tumour, are involved in the mechanism of the migratory pathways downstream of Protein Kinase C, and TGF-β receptors. As mentioned earlier in the chapter, Geribaldi-Doldan et al. reported that targeting Protein Kinase C with GF 109203X was effective to treat (Geribaldi-Doldán *et al.*, 2021) and several drugs inhibiting the TGF-β receptor I, LY2157299 (galunisertib), or TGF-β2, AP-12009 (trabedersen) have been in clinical trials (Bogdahn *et al.*, 2011; Wick *et al.*, 2020). Therefore, our results are in line with these studies. Other drugs which decreased the infiltration of GBM20 cells in the neural spheroid included cilengitide which inhibits integrins αvβ3 and αvβ5 and PF 573228 which inhibits FAK. This was also demonstrated by Anderson and Galileo to reduce the migration of established GBM cell lines, T98G and U-118 MG (Anderson and Galileo, 2016).

As previously mentioned in the discussion of Results Chapter 2, Zepecki developed a co-culture of axon-oligodendrocyte and human glioma cells (Zepecki *et al.*, 2019). Interestingly, they used an inhibitor, A770041, which targets Lck, a downstream effector of the integrin signalling pathway and involved in the pseudopodia formation. They showed that treatment of human GSCs with Lck-I resulted in significant inhibition of self-renewal and tumour-sphere formation. They also revealed that A770041 is more specific than cilengitide in the cytoskeletal changes involved in GBM cell migration and also more selective as phosphor-Lck is expressed in GSCs in particular.

As mentioned earlier in this chapter, Motixafortide (BL-8040) is an inhibitor of CXCR4. As it only decreased the GBM1 cells infiltration of the neural spheroid and not GBM20, it can suggest that GBM1 relies on CXCL12/CXCR4 axis for migration and that targeting it could have potential in GBM immunotherapy of the classical/proneural subtype (Zhou *et al.*, 2019).

5.2.1. Differential gene expression explains the different drug response between GBM1 and GBM20

The gene expression was compared between the GBM1 and GBM20 cell lines rather than with the NS17 control cells which have been derived from a different laboratory at another time. As we have seen, the response to the inhibitors was different from GBM1 and GBM20. To correlate the drug response to the gene expression, we analyse the data from bulk RNA sequencing with a focus on the genes involved in the migratory pathways targeted by our panel of inhibitors.

One of the only inhibitors which decreased the GBM1 cell infiltration of the neural spheroid is Motixafortide and this correlates with the gene expression. Indeed, Motixafortide targets CXCL12 and its expression is enriched in GBM1 compared to GBM20 as seen from the volcano plot. This could explain why Motixafortide has decreased the GBM1 cell infiltration but not GBM20.

On the other hand, GBM20 cells showed a significant decrease in the infiltration of the neural spheroid when treated with PF 573228, Cilengitide, GF 109203X, and SB 431542.

The main inhibitor which decreased the GBM20 infiltration is PF 573228. This inhibitor targets the FAK pathway and we found that GBM20 is enriched in various genes related to the FAK pathway such as SRC, SRCIN1, PPFIA1, PPFIA4, and PPFIBP2. Similarly, the expression of several integrins was enriched such as ITGA5, ITGB3, and ITGBL1, supporting that cilengitide decreased the infiltration by targeting integrins αvβ3 and αvβ5. Finally, GBM20 is also enriched in PRKCB related to Protein Kinase C which we targeted using GF 109203X and showed a GBM20 infiltration decrease.

Interestingly, the TGF-β Receptors inhibitor, SB 431542, has only decreased the GBM20 infiltration whereas the actin polymerization dysregulation, Latrunculin B, has only decreased the GBM1 infiltration. Although, the differential expression showed that both GBM1 and GBM20 are enriched in various genes related to TGF- β and actin. As such, GBM1 is in particular highly enriched in ACTL10 and TGFBI while GBM20 is enriched in ACTG2, TGFA, and TGFBR3.

Furthermore, GBM1 and GBM20 are enriched in genes involved in pathways we had targeted using our inhibitors but the inhibitors did not have any effect. For example, AKT3 is enriched in GBM20 but our inhibitor to the AKT pathway, API-2, showed no effect.

5.2.2. Drugs expected to inhibit migration did not decreased of GBM1 and GBM20 cells infiltration of the neural spheroid

Nevertheless, it is surprising that many other inhibitors had no effect on GBM1 and that one drug, IWP2 which inhibits Wnt, even increased the neural spheroid infiltration. Although the panel of inhibitors were selected based on the literature, several did not affect our co-culture. One of the reasons could be the differences in the cell model and cell line between my project and other studies. As we have also shown, inhibitors affect cell lines differently as they migrate using varied means. Another reason could be that a combination of inhibitors is required to inhibit a specific pathway. For example, the PDGFR and PKA pathways have been reported to work synergistically (Feng *et al.*, 2015). To our surprise, other cytoskeleton dysregulation we included such as Blebbistatin

inhibiting myosin II ATPase activity or Y-27632 dihydrochloride, which is a selective ROCK1 (p160 ROCK) and ROCK2 inhibitor showed no decrease of GBM1 and GBM20 infiltration of the neural spheroid. This contradicts previous findings where these inhibitors decreased the motility of the cell. However, da Silva treated the patient-derived GBM1 and GBM20 cell lines with chemical ROCK inhibition and revealed a significant elongation of cellular projections compared to the non-treated cells (da Silva *et al.*, 2019). The lack of drug response in the patient-derived cell lines may suggest that the cells have a mechanism to counteract the pathway inhibit to migration.

5.2.3. Drugs effect on the neural spheroid

Finally, the inhibitors did not affect the neural spheroids as shown in the images. The morphology of the neural spheroid remained unchanged, circular and with clear borders. This reinforces the proof of concept that the neural spheroid model will enable the screening and identification of compounds specifically affecting the migration of GBM cells.

6. DISCUSSION

6.1. Future directions

As we have identified several inhibitors which decreased the GBM cell infiltration of the neural spheroid, the immediate following experiments I wanted to perform involved live assays of the co-culture treated with the identified inhibitors. This would allow a study of the effect on the migratory behaviours of the cells including the speed, directionality, displacement, and persistence. Also, it would have been interesting to evaluate the drug concentration needed to see an effect in the migration inhibition with less dose-dependent toxicity and effect on the cell viability. Furthermore, more inhibitors targeting the axonal guidance molecules should be tested. Indeed, we covered the ephrin molecules but I would have liked to investigate inhibitors to netrins, robo receptors, and semaphorins.

As we have different patient-derived GBM cell lines, we could combine the individual metrics of migratory behaviours with morphology features to delineate the sub-populations. This could reveal distinct migratory phenotypes of different sizes and shapes within the same cell line and further investigate the intra-heterogeneity. Arguably, the introduction of other patient-derived GBM cell lines will be valuable to cover all subtypes of GBM.

A possible future direction for our in vitro model is the addition of myelin which would be a more appropriate environment to study the migration of GBM on axons. Similar to the study by Zepecki et al. who developed a culture of human glioma cells with myelinated or non-myelinated tracks using oligodendrocyte myelination, our culture will benefit from having oligodendrocyte myelination for the study of GBM migration on axons (Zepecki et al., 2019).

6.2. Limitations

The main limitation of our co-culture model is the lack of myelin sheath around the axons. Glioma cells migrate on axons but preferentially on myelinated axons (Giese *et al.*, 1996). Indeed, the Parinello group has stressed the role of white matter as a pro-differentiative niche for GBM (Brooks *et al.*, 2020). The brain is composed of grey matter, composed of cell bodies such as neurons, and white matter, composed of the neuronal projections insulated by a myelin sheath. As such, the axons we developed do not accurately represent the central nervous system due to its complexity and various cell types. To be representative of the migration of GBM cells on axons within the brain, our culture should include the fatty membranes from oligodendrocytes which surround the axons.

Furthermore, our study focused on the investigation of two patient-derived cell lines GBM1 and GBM20. However, patient-derived cell lines may harbour genetic variants which could influence the phenotypes and not be representative of the disease. Indeed, we found that GBM1 is more infiltrative than GBM20 although GBM1 is a primary tumour and GBM20 is from a recurrent tumour. We have previously discussed the possible explanations for this in Results Chapter 2.

Another limitation of our model is the endpoint assay. Despite its capability to quantify the number of infiltrated cells within the neural spheroid, the numbers remain low (0-25 cells) which does not leave a large margin for errors and outliers. Although our co-culture model can readily screen for inhibitors, *in vitro* spheroid model for GBM has previously been severely questioned (Paolillo, Comincini and Schinelli, 2021). The drug erlotinib which inhibits EGFR has demonstrated promising results in GSC spheroid but failed in clinical trials (Karpel-Massler *et al.*, 2012; Westphal, Maire and Lamszus, 2017).

6.3. Biological Significance

While extensive studies have focused on glioma growth, much less is known about its migration on prognosis. Given the tumour microenvironment influence on glioma

migration, it is crucial to dissect the migratory mechanisms involved in the tumour microenvironment interactions to develop targeted therapeutic strategies. This has led to a rise in interest in patient-derived 3D organoid models for GBM drug screens. As mentioned in the Introduction, 3D models can better recapitulate the phenotype of the disease and mimic the tumour microenvironment.

The majority of studies have attempted to investigate the GBM infiltration of patient-derived brain organoids as drug screening platforms. Comparable to our model, da Silva et al. investigated the infiltration of patient-derived GBM cells and neural progenitors in a hiPSC-derived organoid (da Silva *et al.*, 2018). However, they cultured patient-derived GBM cells and neural progenitors in spheroids whereas we investigated the single GBM cell infiltration using axons. Another example is the model from Goranci-Buzhala et al., who investigated the invasion of GBM into human brain organoids and used their model for drug screening (Goranci-Buzhala *et al.*, 2020). Indeed, they demonstrated that GI254023X, an inhibitor of ADAM10, slowed the invasion of glioma stem cells into human brain organoids. In unpublished findings, Jermakowicz et al. also discovered that a novel BET (Bromodomain and Extra-terminal Domain) inhibitor, UM-002 reduces GBM cell proliferation in an organoid-GBM model (Rybin *et al.*, 2021). Both Jacob et al. and Abdullah et al. reported that their patient-derived organoid models accurately recapitulated the phenotype of the disease and could potentially support preclinical studies and drug screening (Jacob *et al.*, 2020; Abdullah *et al.*, 2022). Jacob et al. showed that their patient-derived GBM brain organoid models could recapitulate the histological feature, cellular diversity, gene expression and mutation profile of the parental tumours (Jacob *et al.*, 2020). As their model could recapitulate the inter- and intra-tumoral heterogeneity, they reported that their biobanks of GBM brain organoids could benefit personalized therapies and chimeric antigen receptor T cell immunotherapy. Abdullah et al. showed that their patient-derived organoid models of lower-grade glioma with a 91% success rate recapitulated the phenotype and the tumour-stromal composition profile of the tumour specimen it was derived from (Abdullah *et al.*, 2022).

The focus of the previous studies mentioned is to use organoids to accurately represent the phenotype of the disease for the benefit of personalised medicine. Although brain organoids provide powerful drug screening platforms, they may miss the structural integrity of the tissue. A key feature that brain organoids may lack is the representation of GBM migration on the axons of the neurons. To the best of our knowledge, our model is the first composed of patient-derived GBM cells and axons from an hiPSC-derived spheroid used to identify drug-targeting migration. Although our spheroid lacks the complexity of the brain, it generates axons which are important migratory substrates used by GBM to migrate from one hemisphere to the other. Another similar model to ours is the model from Zepecki et. al, (Zepecki *et al.*, 2019) which comprises a culture of human glioma cells with myelinated axons derived from rats and was used to study the infiltration using axons. They also showed that the inhibitor, A770041, targeting Lck, resulted in significant inhibition of self-renewal and tumour-sphere formation. They compared A770041 and cilengitide, which we have tested in our drug screen, and showed that A770041 is more specific and more selective than cilengitide in the cytoskeletal changes involved in GSCs migration. Compared to the model by Zepecki et al., our model lacks the myelin sheath but has the advantage of being entirely derived from humans.

By using patient-derived GBM cells, we were able to recapitulate the phenotype of the disease and facilitated the investigation of GBM migration on axons. By modelling the GBM microenvironment with hiPSC, our model could reduce the use of animal models. Our model based on patient-derived cells and iPSC-based technology could reduce study time and costs to screen for compounds affecting cell migration as well as potentially offer innovative precision-medicine therapies. Therefore, the deliverable of this project is expected to bridge the gap between *in vitro* and *in vivo* drug screening.

6.4. Conclusion

Altogether, we generated a co-culture model of a hiPSC-derived cortical neural spheroid with patient-derived cells. Firstly, we tested several methods to differentiate hiPCSs into

cortical neurons using extrinsic or transcription factor-mediated differentiation and for the generation of neural spheroids. We developed our co-culture model with the transcription factor-mediated differentiation which was more efficient, more reproducible, and shorter. Using HCI, we developed robust pipelines to analyse the engagement of the cells on axons and the infiltration of the neural spheroid in endpoint assays as well as migratory properties such as the speed, displacement, directionality, and persistence in live imaging assays. Images were acquired on the Operetta CLS HCI device and quantified using Harmony software. In live assays, images were acquired with the Phasefocus Livecyte and we characterised the migratory behaviours of the cells with or without the presence of axons. Furthermore, we used clinically relevant distinct cells for our co-culture including the patient-derived GBM1 and GBM20 cells and the non-cancer NS17 cells. We showed that all GBM1, GBM20, and NS17 cells migrated towards the neural spheroid once engaged on axons and that they showed distinct levels of infiltration capability.

Using our model, we were able to test various antagonists to inhibit migration and infiltration and observed distinct patterns of responses to the candidate drugs between the two patient-derived cell lines. This is proof of concept that the neural spheroid model will enable the screening and identification of compounds specifically affecting cell migration in a patient/tumour-specific fashion. Furthermore, the characterisation of the genetic profiles of the patient-derived GBM cell lines complements our drug screen but also provides an essential resource for their future use and the development of personalised medicine.

7. REFERENCE LIST

Abdullah, K. G. *et al.* (2022) 'Establishment of patient-derived organoid models of lower-grade glioma', *Neuro-Oncology*, 24(4), pp. 612–623. doi: 10.1093/neuonc/noab273.

Affinito, A. *et al.* (2020) 'Targeting Ephrin Receptor Tyrosine Kinase A2 with a Selective Aptamer for Glioblastoma Stem Cells', *Molecular therapy. Nucleic acids*. Mol Ther Nucleic Acids, 20, pp. 176–185. doi: 10.1016/J.OMTN.2020.02.005.

Alexander, B. M. and Cloughesy, T. F. (2017) 'Adult glioblastoma', *Journal of Clinical Oncology*. American Society of Clinical Oncology, 35(21), pp. 2402–2409. doi: 10.1200/JCO.2017.73.0119.

Allen, M. *et al.* (2016) 'Origin of the U87MG glioma cell line: Good news and bad news', *Science Translational Medicine*. American Association for the Advancement of Science, 8(354), pp. 354re3-354re3. doi: 10.1126/scitranslmed.aaf6853.

Alsehli, H. *et al.* (2021) 'An integrated pipeline for high-throughput screening and profiling of spheroids using simple live image analysis of frame to frame variations', *Methods (San Diego, Calif.)*. Elsevier, 190, p. 33. doi: 10.1016/J.YMETH.2020.05.017.

Anderson, H. J. and Galileo, D. S. (2016) 'Small-molecule inhibitors of FGFR, integrins and FAK selectively decrease L1CAM-stimulated glioblastoma cell motility and proliferation', *Cellular Oncology*. Cell Oncol (Dordr), 39(3), pp. 229–242. doi: 10.1007/s13402-016-0267-7.

Ansari, A. M. *et al.* (2016) 'Cellular GFP Toxicity and Immunogenicity: Potential Confounders in in Vivo Cell Tracking Experiments', *Stem Cell Reviews*. Springer, 12(5), p. 553. doi: 10.1007/S12015-016-9670-8.

Armento, A. *et al.* (2017) 'Molecular mechanisms of cell motility', in *Cancer and Metastasis Review*. Codon Publications, pp. 73–93. doi: 10.15586/codon.glioblastoma.2017.ch5.

Aubert, M. *et al.* (2008) 'A model for glioma cell migration on collagen and astrocytes', *Journal of the Royal Society Interface*. Royal Society, 5(18), pp. 75–83. doi: 10.1098/rsif.2007.1070.

Aubry, M. *et al.* (2015) '"From the core to beyond the margin": a genomic picture of glioblastoma intratumor heterogeneity', *Oncotarget*. Impact Journals, LLC, 6(14), p. 12094. doi: 10.18632/ONCOTARGET.3297.

Azzarelli, R. (2020) 'Organoid Models of Glioblastoma to Study Brain Tumor Stem Cells', *Frontiers in Cell and Developmental Biology*. Frontiers Media SA, p. 220. doi: 10.3389/fcell.2020.00220.

Bao, S. *et al.* (2006) 'Glioma stem cells promote radioresistance by preferential activation of the DNA damage response', *Nature 2006 444:7120*. Nature Publishing Group, 444(7120), pp. 756–760. doi: 10.1038/nature05236.

Barbero, S. *et al.* (2002) 'Expression of the Chemokine Receptor CXCR4 and Its Ligand Stromal Cell-Derived Factor 1 in Human Brain Tumors and Their Involvement in Glial Proliferation in Vitro', *Annals of the New York Academy of Sciences*. New York Academy of Sciences, 021(1), pp. 60–69. doi: 10.1111/j.1749-6632.2002.tb04607.x.

Bayat, N. *et al.* (2018) 'The anti-angiogenic effect of atorvastatin in glioblastoma spheroids tumor cultured in fibrin gel: In 3D in vitro model', *Asian Pacific Journal of Cancer Prevention*. Asian Pacific Organization for Cancer Prevention, 19(9), pp. 2553–2560. doi: 10.22034/APJCP.2018.19.9.2553.

Beliën, A. T. J., Paganetti, P. A. and Schwab, M. E. (1999) 'Membrane-type 1 Matrix Metalloprotease (MT1-MMP) Enables Invasive Migration of Glioma Cells in Central Nervous System White Matter', *The Journal of Cell Biology*. The Rockefeller University Press, 144(2), p. 373. doi: 10.1083/JCB.144.2.373.

Bellail, A. C. *et al.* (2004) *Microregional extracellular matrix heterogeneity in brain modulates glioma cell invasion*, *International Journal of Biochemistry and Cell Biology*. Pergamon. doi: 10.1016/j.biocel.2004.01.013.

Bello, L. *et al.* (2001) 'αvβ3 and αvβ5 integrin expression in glioma periphery', *Neurosurgery*. Lippincott Williams and Wilkins, 49(2), pp. 380–390. doi: 10.1097/00006123-200108000-00022.

Belousov, A. *et al.* (2019) 'The Extracellular Matrix and Biocompatible Materials in Glioblastoma Treatment', *Frontiers in Bioengineering and Biotechnology*. Frontiers Media S.A., p. 341. doi: 10.3389/fbioe.2019.00341.

Bhaduri, A. *et al.* (2020) 'Outer Radial Glia-like Cancer Stem Cells Contribute to Heterogeneity of Glioblastoma', *Cell Stem Cell*. Cell Press, 26(1), pp. 48-63.e6. doi: 10.1016/j.stem.2019.11.015.

Bian, S. *et al.* (2018) 'Genetically engineered cerebral organoids model brain tumor formation', *Nature Methods*. Nature Publishing Group, 15(8), pp. 631–639. doi: 10.1038/s41592-018-0070-7.

Bogdahn, U. *et al.* (2011) 'Targeted therapy for high-grade glioma with the TGF-β2 inhibitor trabedersen: results of a randomized and controlled phase IIb study', *Neuro-Oncology*. Oxford University Press, 13(1), p. 132. doi: 10.1093/NEUONC/NOQ142.

Bon, C., Si, Y. and Arimondo, P. B. (2020) 'Targeting DOT1L for mixed-lineage rearranged leukemia', *Histone Modifications in Therapy*. Academic Press, pp. 81–99. doi: 10.1016/B978-0-12-816422-8.00005-2.

Boquet-Pujadas, A., Olivo-Marin, J. C. and Guillén, N. (2021) *Bioimage Analysis and Cell Motility*, *Patterns*. Cell Press. doi: 10.1016/j.patter.2020.100170.

Brennan, C. W. *et al.* (2013) 'The somatic genomic landscape of glioblastoma', *Cell*. Elsevier B.V., 155(2), p. 462. Available at: http://www.cell.com/article/S0092867413012087/fulltext (Accessed: 4 August 2022).

Brooks, L. J. *et al.* (2020) 'The white matter is a pro-differentiative microenvironment for glioblastoma', *Journal of Chemical Information and Modeling*, 01(01), pp. 1689–1699.

Brösicke, N. and Faissner, A. (2015) 'Role of tenascins in the ECM of gliomas', *Cell Adhesion and Migration*. Taylor and Francis Inc., pp. 131–140. doi: 10.1080/19336918.2014.1000071.

Brown, M. C. *et al.* (2008) 'Regulatory effect of nerve growth factor in alpha9beta1 integrin-dependent progression of glioblastoma', *Neuro-oncology*. Neuro Oncol, 10(6), pp. 968–980. doi: 10.1215/15228517-2008-047.

Bulstrode, H. *et al.* (2017) 'Elevated FOXG1 and SOX2 in glioblastoma enforces neural stem cell identity through transcriptional control of cell cycle and epigenetic regulators', *Genes & Development*. Cold Spring Harbor Laboratory Press, 31(8), pp. 757–773. doi: 10.1101/GAD.293027.116.

Busskamp, V. *et al.* (2014) 'Rapid neurogenesis through transcriptional activation in human stem cells', *Molecular systems biology*. Mol Syst Biol, 10(11), p. 760. doi: 10.15252/MSB.20145508.

C, U. *et al.* (2018) 'EphB4 mediates resistance to antiangiogenic therapy in experimental glioma', *Angiogenesis*. Angiogenesis, 21(4), pp. 873–881. doi: 10.1007/S10456-018-9633-6.

Carrano, A. *et al.* (2021) 'Sex-Specific Differences in Glioblastoma', *Cells*. Multidisciplinary Digital Publishing Institute (MDPI), 10(7). doi: 10.3390/CELLS10071783.

Ceccarelli, M. *et al.* (2016) 'Molecular Profiling Reveals Biologically Discrete Subsets and Pathways of Progression in Diffuse Glioma', *Cell*. Cell Press, 164(3), pp. 550–563. doi: 10.1016/j.cell.2015.12.028.

Cha, J., Kang, S. G. and Kim, P. (2016) 'Strategies of Mesenchymal Invasion of Patient-derived Brain Tumors: Microenvironmental Adaptation', *Scientific Reports*. Nature Publishing Group, 6. doi: 10.1038/srep24912.

Cha, J. and Kim, P. (2017) 'Biomimetic strategies for the glioblastoma

microenvironment', *Frontiers in Materials*. Frontiers Media S.A. doi: 10.3389/fmats.2017.00045.

Chédotal, A., Kerjan, G. and Moreau-Fauvarque, C. (2005) 'The brain within the tumor: New roles for axon guidance molecules in cancers', *Cell Death and Differentiation*, pp. 1044–1056. doi: 10.1038/sj.cdd.4401707.

Chen, J. W. E. *et al.* (2018) 'Influence of hyaluronic acid transitions in tumor microenvironment on glioblastoma malignancy and invasive behavior', *Frontiers in Materials*. Frontiers Media S.A., 5, p. 39. doi: 10.3389/fmats.2018.00039.

Chen, S. *et al.* (2018) 'fastp: an ultra-fast all-in-one FASTQ preprocessor', *Bioinformatics*. Oxford Academic, 34(17), pp. i884–i890. doi: 10.1093/BIOINFORMATICS/BTY560.

Claes, A., Idema, A. J. and Wesseling, P. (2007) 'Diffuse glioma growth: A guerilla war', *Acta Neuropathologica*, pp. 443–458. doi: 10.1007/s00401-007-0293-7.

Conti, L. *et al.* (2005) 'Niche-Independent Symmetrical Self-Renewal of a Mammalian Tissue Stem Cell', *PLOS Biology*. Public Library of Science, 3(9), p. e283. doi: 10.1371/JOURNAL.PBIO.0030283.

Cuddapah, V. A. *et al.* (2014) 'A neurocentric perspective on glioma invasion', *Nature Reviews Neuroscience*. Nature Publishing Group, pp. 455–465. doi: 10.1038/nrn3765.

Danovi, D. *et al.* (2013) 'A high-content small molecule screen identifies sensitivity of glioblastoma stem cells to inhibition of polo-like kinase 1.', *PloS one*, 8(10), p. 77053. doi: 10.1371/journal.pone.0077053.

Darmanis, S. *et al.* (2017) 'Single-Cell RNA-Seq Analysis of Infiltrating Neoplastic Cells at the Migrating Front of Human Glioblastoma', *Cell Reports*. Elsevier B.V., 21(5), pp. 1399–1410. doi: 10.1016/j.celrep.2017.10.030.

Das, K. K. and Kumar, R. (2017) 'Pediatric Glioblastoma', *Glioblastoma*. Codon Publications, pp. 297–312. doi: 10.15586/CODON.GLIOBLASTOMA.2017.CH15.

Delamarre, E. *et al.* (2009) 'Expression of integrin α6β1 enhances tumorigenesis in glioma cells', *American Journal of Pathology*. American Society for Investigative Pathology Inc., 175(2), pp. 844–855. doi: 10.2353/ajpath.2009.080920.

Demuth, T. *et al.* (2001) *Migratory activity of human glioma cell lines in vitro assessed by continuous single cell observation*, *Clinical & Experimental Metastasis*.

Diao, W. *et al.* (2019) 'Behaviors of Glioblastoma Cells in in Vitro Microenvironments', *Scientific Reports*. Nature Publishing Group, 9(1). doi: 10.1038/s41598-018-36347-7.

Djuzenova, C. S. *et al.* (2019) 'Differential effects of the Akt inhibitor MK-2206 on migration and radiation sensitivity of glioblastoma cells', *BMC Cancer 2019 19:1*. BioMed Central, 19(1), pp. 1–18. doi: 10.1186/S12885-019-5517-4.

Dobin, A. *et al.* (2013) 'STAR: ultrafast universal RNA-seq aligner', *Bioinformatics*. Oxford Academic, 29(1), pp. 15–21. doi: 10.1093/BIOINFORMATICS/BTS635.

Eckel-Passow, J. E. *et al.* (2015) ' Glioma Groups Based on 1p/19q, IDH , and TERT Promoter Mutations in Tumors ', *New England Journal of Medicine*. Massachusetts Medical Society, 372(26), pp. 2499–2508. doi: 10.1056/NEJMOA1407279/SUPPL_FILE/NEJMOA1407279_DISCLOSURES.PDF.

Ellert-Miklaszewska, A. *et al.* (2020) 'Integrin signaling in glioma pathogenesis: From biology to therapy', *International Journal of Molecular Sciences*. MDPI AG. doi: 10.3390/ijms21030888.

Fedele, M. *et al.* (2019) 'Proneural-Mesenchymal Transition: Phenotypic Plasticity to Acquire Multitherapy Resistance in Glioblastoma', *International Journal of Molecular Sciences*. Multidisciplinary Digital Publishing Institute (MDPI), 20(11). doi: 10.3390/IJMS20112746.

Feng, H. *et al.* (2015) 'Protein kinase A–dependent phosphorylation of Dock180 at serine residue 1250 is important for glioma growth and invasion stimulated by platelet derived-growth factor receptor α', *Neuro-Oncology*. Oxford Academic, 17(6), pp. 832–842. doi:

10.1093/NEUONC/NOU323.

Fernandopulle, M. S. *et al.* (2018) 'Transcription Factor–Mediated Differentiation of Human iPSCs into Neurons', *Current Protocols in Cell Biology*. John Wiley and Sons Inc., 79(1), p. e51. doi: 10.1002/cpcb.51.

Fortin Ensign, S. P. *et al.* (2013) 'Implications of Rho GTPase Signaling in Glioma Cell Invasion and Tumor Progression', *Frontiers in Oncology*. Frontiers Media SA, 3. doi: 10.3389/FONC.2013.00241.

Fujikawa, A. *et al.* (2017) 'Targeting PTPRZ inhibits stem cell-like properties and tumorigenicity in glioblastoma cells', *Scientific reports*. Sci Rep, 7(1). doi: 10.1038/S41598-017-05931-8.

Furnari, F. B. *et al.* (2015) 'Heterogeneity of epidermal growth factor receptor signalling networks in glioblastoma', *Nature Reviews Cancer 2015 15:5*. Nature Publishing Group, 15(5), pp. 302–310. doi: 10.1038/nrc3918.

Gaillard, F. (2021) 'Diffuse glioma classification (WHO 5th Edition, 2021)', in *Radiopaedia.org*. doi: 10.53347/rid-94212.

Galli, R. *et al.* (2004) 'Isolation and characterization of tumorigenic, stem-like neural precursors from human glioblastoma', *Cancer Research*. American Association for Cancer Research, 64(19), pp. 7011–7021. doi: 10.1158/0008-5472.CAN-04-1364.

Garnier, D. *et al.* (2019) 'Glioblastoma stem-like cells, Metabolic strategy to kill a challenging target', *Frontiers in Oncology*. Frontiers Media S.A., p. 118. doi: 10.3389/fonc.2019.00118.

Garrett, A. M., Lastakchi, S. and McConville, C. (2020) 'The Personalisation of Glioblastoma Treatment Using Whole Exome Sequencing: A Pilot Study', *Genes*. Multidisciplinary Digital Publishing Institute (MDPI), 11(2). doi: 10.3390/GENES11020173.

Geribaldi-Doldán, N. *et al.* (2021) 'Targeting Protein Kinase C in Glioblastoma Treatment', *Biomedicines*. Multidisciplinary Digital Publishing Institute (MDPI), 9(4). doi: 10.3390/BIOMEDICINES9040381.

Giandomenico, S. L. *et al.* (2019) 'Cerebral organoids at the air–liquid interface generate diverse nerve tracts with functional output', *Nature Neuroscience*. Nature Publishing Group, 22(4), pp. 669–679. doi: 10.1038/s41593-019-0350-2.

Giese, A. *et al.* (1996) *Migration of Human Glioma Cells on Myelin : Neurosurgery*, *Neurosurgery*. Available at: https://journals.lww.com/neurosurgery/Abstract/1996/04000/Migration_of_Human_Glioma_Cells_on_Myelin.26.aspx (Accessed: 8 November 2022).

Gilbertson, R. J. and Rich, J. N. (2007) 'Making a tumour's bed: glioblastoma stem cells and the vascular niche', *Nature reviews. Cancer*. Nat Rev Cancer, 7(10), pp. 733–736. doi: 10.1038/NRC2246.

Gill, B. J. *et al.* (2014) 'MRI-localized biopsies reveal subtype-specific differences in molecular and cellular composition at the margins of glioblastoma', *Proceedings of the National Academy of Sciences of the United States of America*. National Academy of Sciences, 111(34), pp. 12550–12555. doi: 10.1073/PNAS.1405839111/-/DCSUPPLEMENTAL.

Gimple, R. C. *et al.* (2019) 'Glioblastoma stem cells: lessons from the tumor hierarchy in a lethal cancer', *Genes & development*. Genes Dev, 33(11–12), pp. 591–609. doi: 10.1101/GAD.324301.119.

de Gooijer, M. C. *et al.* (2018) 'An Experimenter's Guide to Glioblastoma Invasion Pathways', *Trends in Molecular Medicine*. Elsevier Ltd, pp. 763–780. doi: 10.1016/j.molmed.2018.07.003.

Goranci-Buzhala, G. *et al.* (2020) 'Rapid and Efficient Invasion Assay of Glioblastoma in Human Brain Organoids', *Cell Reports*. ElsevierCompany., 31(10), p. 107738. doi: 10.1016/j.celrep.2020.107738.

Goto, K. *et al.* (2017) 'Simple Derivation of Spinal Motor Neurons from ESCs/iPSCs Using Sendai Virus Vectors', *Molecular Therapy. Methods & Clinical Development*. American Society of Gene & Cell Therapy, 4, p. 115. doi: 10.1016/J.OMTM.2016.12.007.

Gudbergsson, J. M. *et al.* (2019) 'A tumorsphere model of glioblastoma multiforme with intratumoral heterogeneity for quantitative analysis of cellular migration and drug response', *Experimental Cell Research*. Elsevier Inc., 379(1), pp. 73–82. doi: 10.1016/j.yexcr.2019.03.031.

Guo, W. and Giancotti, F. G. (2004) 'Integrin signalling during tumour progression', *Nature Reviews Molecular Cell Biology*. Nature Publishing Group, pp. 816–826. doi: 10.1038/nrm1490.

Gutiérrez-Caballero, C. *et al.* (2015) 'TACC3-ch-TOG track the growing tips of microtubules independently of clathrin and Aurora-A phosphorylation', *Biology Open*. Company of Biologists Ltd, 4(2), pp. 170–179. doi: 10.1242/bio.201410843.

Haji Mansor, M. *et al.* (2018) 'Development of a non-toxic and non-denaturing formulation process for encapsulation of SDF-1α into PLGA/PEG-PLGA nanoparticles to achieve sustained release', *European Journal of Pharmaceutics and Biopharmaceutics*. Elsevier, 125, pp. 38–50. doi: 10.1016/J.EJPB.2017.12.020.

Hambardzumyan, D. and Bergers, G. (2015) 'Glioblastoma: Defining Tumor Niches', *Trends in cancer*. Trends Cancer, 1(4), pp. 252–265. doi: 10.1016/J.TRECAN.2015.10.009.

Hegi, M. E. *et al.* (2005) 'MGMT gene silencing and benefit from temozolomide in glioblastoma', *The New England journal of medicine*. N Engl J Med, 352(10), pp. 997–1003. doi: 10.1056/NEJMOA043331.

Hegi, M. E. and Stupp, R. (2015) 'Withholding temozolomide in glioblastoma patients with unmethylated MGMT promoter—still a dilemma?', *Neuro-Oncology*. Oxford University Press, 17(11), p. 1425. doi: 10.1093/NEUONC/NOV198.

Hirata, E. *et al.* (2012) 'In vivo fluorescence resonance energy transfer imaging reveals

differential activation of Rho-family GTPases in glioblastoma cell invasion', *Journal of cell science*. J Cell Sci, 125(Pt 4), pp. 858–868. doi: 10.1242/JCS.089995.

Hoang-Minh, L. B. *et al.* (2018) 'Infiltrative and drug-resistant slow-cycling cells support metabolic heterogeneity in glioblastoma', *The EMBO Journal*. EMBO, 37(23), pp. 1–21. doi: 10.15252/embj.201798772.

Hoelzinger, D. B., Demuth, T. and Berens, M. E. (2007) 'Autocrine factors that sustain glioma invasion and paracrine biology in the brain microenvironment', *Journal of the National Cancer Institute*, pp. 1583–1593. doi: 10.1093/jnci/djm187.

Holland, E. C. (2000) 'Glioblastoma multiforme: The terminator', *Proceedings of the National Academy of Sciences of the United States of America*. National Academy of Sciences, pp. 6242–6244. doi: 10.1073/pnas.97.12.6242.

Hu, B. *et al.* (2003) 'Angiopoietin-2 induces human glioma invasion through the activation of matrix metalloprotease-2.', *Proceedings of the National Academy of Sciences of the United States of America*, 100(15), pp. 8904–8909. doi: 10.1073/PNAS.1533394100.

Hu, B. *et al.* (2008) 'The proteoglycan brevican binds to fibronectin after proteolytic cleavage and promotes glioma cell motility', *Journal of Biological Chemistry*. American Society for Biochemistry and Molecular Biology, 283(36), pp. 24848–24859. doi: 10.1074/jbc.M801433200.

Hung, H. C. *et al.* (2020) 'Inhibition of Sonic Hedgehog Signaling Suppresses Glioma Stem-Like Cells Likely Through Inducing Autophagic Cell Death', *Frontiers in Oncology*. Frontiers Media S.A., 10, p. 1233. doi: 10.3389/FONC.2020.01233/BIBTEX.

Jacob, F. *et al.* (2020) 'A Patient-Derived Glioblastoma Organoid Model and Biobank Recapitulates Inter- and Intra-tumoral Heterogeneity', *Cell*. Cell Press, 180(1), pp. 188-204.e22. doi: 10.1016/j.cell.2019.11.036.

Jiang, K. *et al.* (2020) 'MOB2 suppresses GBM cell migration and invasion via regulation

of FAK/Akt and cAMP/PKA signaling', *Cell Death & Disease 2020 11:4*. Nature Publishing Group, 11(4), pp. 1–14. doi: 10.1038/s41419-020-2381-8.

Johnson, J. *et al.* (2009) 'Quantitative analysis of complex glioma cell migration on electrospun polycaprolactone using time-lapse microscopy', *Tissue Engineering - Part C: Methods*, 15(4), pp. 531–540. doi: 10.1089/ten.tec.2008.0486.

Kantor, D. B. *et al.* (2004) 'Semaphorin 5A is a bifunctional axon guidance cue regulated by heparan and chondroitin sulfate proteoglycans', *Neuron*. Elsevier, 44(6), pp. 961–975. doi: 10.1016/j.neuron.2004.12.002.

Karpel-Massler, G. *et al.* (2012) 'Erlotinib in Glioblastoma - Lost in Translation?', *Anti-Cancer Agents in Medicinal Chemistry*. Bentham Science Publishers Ltd., 11(8), pp. 748–755. doi: 10.2174/187152011797378788.

Kasprowicz, R., Suman, R. and O'Toole, P. (2017) 'Characterising live cell behaviour: Traditional label-free and quantitative phase imaging approaches', *International Journal of Biochemistry and Cell Biology*. Elsevier Ltd, pp. 89–95. doi: 10.1016/j.biocel.2017.01.004.

Katakowski, M. *et al.* (2016) 'Density-Dependent Regulation of Glioma Cell Proliferation and Invasion Mediated by miR-9', *Cancer Microenvironment*. Springer New York LLC, 9(2–3), pp. 149–159. doi: 10.1007/s12307-016-0190-5.

Kawataki, T. *et al.* (2007) 'Laminin isoforms and their integrin receptors in glioma cell migration and invasiveness: Evidence for a role of α5-laminin(s) and α3β1 integrin', *Experimental Cell Research*. Academic Press Inc., 313(18), pp. 3819–3831. doi: 10.1016/j.yexcr.2007.07.038.

Kerrisk, M. E., Cingolani, L. A. and Koleske, A. J. (2014) 'ECM receptors in neuronal structure, synaptic plasticity, and behavior', in *Progress in Brain Research*. Elsevier B.V., pp. 101–131. doi: 10.1016/B978-0-444-63486-3.00005-0.

Kim, S. S. *et al.* (2015) 'Effective treatment of glioblastoma requires crossing the blood-

brain barrier and targeting tumors including cancer stem cells: The promise of nanomedicine', *Biochemical and Biophysical Research Communications*. Academic Press Inc., pp. 485–489. doi: 10.1016/j.bbrc.2015.06.137.

Koh, I. *et al.* (2018) 'The mode and dynamics of glioblastoma cell invasion into a decellularized tissue-derived extracellular matrix-based three-dimensional tumor model.', *Scientific Reports*. Nature Publishing Group, 8(1), pp. 4608–4608. doi: 10.1038/S41598-018-22681-3.

Könnecke, H. and Bechmann, I. (2013) 'The Role of Microglia and Matrix Metalloproteinases Involvement in Neuroinflammation and Gliomas', *Clinical and Developmental Immunology*. Hindawi Limited, 2013. doi: 10.1155/2013/914104.

Koochekpour, S., Pilkington, G. J. and Merzak, A. (1995) 'Hyaluronic acid/CD44H interaction induces cell detachment and stimulates migration and invasion of human glioma cells in vitro', *International Journal of Cancer*. John Wiley & Sons, Ltd, 63(3), pp. 450–454. doi: 10.1002/ijc.2910630325.

Kouam, P. N. *et al.* (2018) 'Robo1 and vimentin regulate radiation-induced motility of human glioblastoma cells', *PLoS ONE*. Public Library of Science, 13(6). doi: 10.1371/JOURNAL.PONE.0198508.

Lathia, J. D. *et al.* (2015) 'Cancer stem cells in glioblastoma', *Genes & Development*. Cold Spring Harbor Laboratory Press, 29(12), p. 1203. doi: 10.1101/GAD.261982.115.

Lau, J. *et al.* (2015) 'STAT3 blockade inhibits a radiation-induced proneural-to-mesenchymal transition in glioma', *Cancer research*. NIH Public Access, 75(20), p. 4302. doi: 10.1158/0008-5472.CAN-14-3331.

Lee, H. K. *et al.* (2008) 'Netrin-1 Specifically Enhances Cell Spreading on Fibronectin in Human Glioblastoma Cells', *The Korean Journal of Physiology & Pharmacology : Official Journal of the Korean Physiological Society and the Korean Society of Pharmacology*. Korean Physiological Society and Korean Society of Pharmacology, 12(5), p. 225. doi: 10.4196/KJPP.2008.12.5.225.

Lee, J. *et al.* (2006) 'Tumor stem cells derived from glioblastomas cultured in bFGF and EGF more closely mirror the phenotype and genotype of primary tumors than do serum-cultured cell lines', *Cancer Cell*. Elsevier, 9(5), pp. 391–403. doi: 10.1016/j.ccr.2006.03.030.

Lee, S. *et al.* (2022) 'Targeting tumour-intrinsic neural vulnerabilities of glioblastoma', *bioRxiv*. Cold Spring Harbor Laboratory, p. 2022.10.07.511321. doi: 10.1101/2022.10.07.511321.

Lee, Y. *et al.* (2015) 'WNT signaling in glioblastoma and therapeutic opportunities', *Laboratory Investigation 2016 96:2*. Nature Publishing Group, 96(2), pp. 137–150. doi: 10.1038/labinvest.2015.140.

Leite, D. M. *et al.* (2020) 'A human co-culture cell model incorporating microglia supports glioblastoma growth and migration, and confers resistance to cytotoxics', *FASEB Journal*. John Wiley and Sons Inc., 34(1), pp. 1710–1727. doi: 10.1096/fj.201901858RR.

Li, B. and Dewey, C. N. (2011) 'RSEM: Accurate transcript quantification from RNA-Seq data with or without a reference genome', *BMC Bioinformatics*. BioMed Central, 12(1), pp. 1–16. doi: 10.1186/1471-2105-12-323/TABLES/6.

Li, X., Law, J. W. S. and Lee, A. Y. W. (2011) 'Semaphorin 5A and plexin-B3 regulate human glioma cell motility and morphology through Rac1 and the actin cytoskeleton', *Oncogene 2012 31:5*. Nature Publishing Group, 31(5), pp. 595–610. doi: 10.1038/onc.2011.256.

Li, X. and Lee, A. Y. W. (2010) 'Semaphorin 5A and Plexin-B3 Inhibit Human Glioma Cell Motility through RhoGDIα-mediated Inactivation of Rac1 GTPase', *The Journal of Biological Chemistry*. American Society for Biochemistry and Molecular Biology, 285(42), p. 32436. doi: 10.1074/JBC.M110.120451.

van Linde, M. E. *et al.* (2017) 'Treatment outcome of patients with recurrent glioblastoma multiforme: a retrospective multicenter analysis', *Journal of Neuro-Oncology*. Springer New York LLC, 135(1), pp. 183–192. doi: 10.1007/s11060-017-2564-

z.

Liu, A. *et al.* (2016) 'Genetics and epigenetics of glioblastoma: Applications and Overall Incidence of IDH1 Mutation', *Frontiers in Oncology*. Frontiers Media S.A., 6(JAN), p. 16. doi: 10.3389/FONC.2016.00016/BIBTEX.

Liu, C. A. *et al.* (2018) 'Migration/invasion of malignant gliomas and implications for treatment', *International Journal of Molecular Sciences*. MDPI AG. doi: 10.3390/ijms19041115.

Liu, E. and Nolan, J. P. (2014) 'Surface Enhanced Raman Scattering (SERS) Image Cytometry for High-Content Screening', *Fluorescence Microscopy: Super-Resolution and other Novel Techniques*. Academic Press, pp. 93–108. doi: 10.1016/B978-0-12-409513-7.00007-5.

Liu, X. *et al.* (2021) 'Overview of the molecular mechanisms of migration and invasion in glioblastoma multiforme', *Journal of the Chinese Medical Association*, 84(7), pp. 669–677. doi: 10.1097/JCMA.0000000000000552.

Longley, R. L. *et al.* (1999) 'Control of morphology, cytoskeleton and migration by syndecan-4', *Journal of Cell Science*, 112(20).

Louis, D. N. *et al.* (2021) 'The 2021 WHO Classification of Tumors of the Central Nervous System: a summary', *Neuro-Oncology*. Oxford University Press, 23(8), p. 1231. doi: 10.1093/NEUONC/NOAB106.

Love, M. I., Huber, W. and Anders, S. (2014) 'Moderated estimation of fold change and dispersion for RNA-seq data with DESeq2', *Genome Biology*. BioMed Central Ltd., 15(12), pp. 1–21. doi: 10.1186/S13059-014-0550-8/FIGURES/9.

Lu, Y. *et al.* (2011) 'TGF-β1 promotes motility and invasiveness of glioma cells through activation of ADAM17', *Oncology reports*. NIH Public Access, 25(5), p. 1329. doi: 10.3892/OR.2011.1195.

Lyons, S. A. *et al.* (2007) 'Autocrine glutamate signaling promotes glioma cell invasion', *Cancer research*. Cancer Res, 67(19), pp. 9463–9471. doi: 10.1158/0008-5472.CAN-07-2034.

Major, T., Powers, A. and Tabar, V. (2017) 'Derivation of telencephalic oligodendrocyte progenitors from human pluripotent stem cells', *Current protocols in stem cell biology*. NIH Public Access, 39, p. 1H.10.1. doi: 10.1002/CPSC.17.

Makarov, A. *et al.* (2013) 'Ephrin-As, Eph receptors and integrin α3 interact and colocalise at membrane protrusions of U251MG glioblastoma cells', 37(10), pp. 1080–1088. doi: 10.1002/CBIN.10134.

Malric, L. *et al.* (2017) 'Interest of integrins targeting in glioblastoma according to tumor heterogeneity and cancer stem cell paradigm: An update', *Oncotarget*. Impact Journals LLC, 8(49), pp. 86947–86968. doi: 10.18632/oncotarget.20372.

Manini, I. *et al.* (2018) 'Role of microenvironment in glioma invasion: What we learned from in vitro models', *International Journal of Molecular Sciences*. MDPI AG. doi: 10.3390/ijms19010147.

Martin, S., Janouskova, H. and Dontenwill, M. (2012) 'Integrins and p53 pathways in glioblastoma resistance to temozolomide', *Frontiers in Oncology*. Frontiers Media SA, 2, p. 157. doi: 10.3389/fonc.2012.00157.

Massagué, J. (2012) 'TGF-β signaling in development and disease', *FEBS Letters*. John Wiley & Sons, Ltd, 586(14), pp. 1833–1833. doi: 10.1016/J.FEBSLET.2012.05.030.

Massaous, J. and Hata, A. (1997) 'TGF-β signalling through the Smad pathway', *Trends in Cell Biology*. Elsevier Ltd, 7(5), pp. 187–192. doi: 10.1016/S0962-8924(97)01036-2.

McLendon, R. *et al.* (2008) 'Comprehensive genomic characterization defines human glioblastoma genes and core pathways', *Nature 2008 455:7216*. Nature Publishing Group, 455(7216), pp. 1061–1068. doi: 10.1038/nature07385.

Mertsch, S. *et al.* (2008) 'Slit2 involvement in glioma cell migration is mediated by Robo1 receptor', *Journal of Neuro-Oncology*. Springer, 87(1), pp. 1–7. doi: 10.1007/s11060-007-9484-2.

Migliozzi, S. *et al.* (2023) 'Integrative multi-omics networks identify PKCδ and DNA-PK as master kinases of glioblastoma subtypes and guide targeted cancer therapy', *Nature Cancer 2023*. Nature Publishing Group, 9, pp. 1–22. doi: 10.1038/s43018-022-00510-x.

Mitra, S. K., Hanson, D. A. and Schlaepfer, D. D. (2005) 'Focal adhesion kinase: in command and control of cell motility', *Nature Reviews Molecular Cell Biology 2005 6:1*. Nature Publishing Group, 6(1), pp. 56–68. doi: 10.1038/nrm1549.

Mitra, S. K. and Schlaepfer, D. D. (2006) 'Integrin-regulated FAK-Src signaling in normal and cancer cells', *Current opinion in cell biology*. Curr Opin Cell Biol, 18(5), pp. 516–523. doi: 10.1016/J.CEB.2006.08.011.

Moradi, S. *et al.* (2019) 'Research and therapy with induced pluripotent stem cells (iPSCs): Social, legal, and ethical considerations', *Stem Cell Research and Therapy*, 10(1), pp. 1–13. doi: 10.1186/s13287-019-1455-y.

Neftel, C. *et al.* (2019) 'An Integrative Model of Cellular States, Plasticity, and Genetics for Glioblastoma', *Cell*. Elsevier BV, 178(4), pp. 835-849.e21. doi: 10.1016/j.cell.2019.06.024.

Ngo, M. T., Karvelis, E. and Harley, B. (2020) 'Multidimensional hydrogel models reveal endothelial network angiocrine signals increase glioblastoma proliferation, invasion, and temozolomide resistance', *bioRxiv Bioengineering*. Cold Spring Harbor Laboratory, (217), p. 2020.01.18.911396. doi: 10.1101/2020.01.18.911396.

Nishikawa, M. *et al.* (2018) 'Significance of glioma stem-like cells in the tumor periphery that express high levels of CD44 in tumor invasion, early progression, and poor prognosis in glioblastoma', *Stem Cells International*, 2018. doi: 10.1155/2018/5387041.

O'Duibhir, E., Carragher, N. O. and Pollard, S. M. (2017) 'Accelerating glioblastoma drug

discovery: Convergence of patient-derived models, genome editing and phenotypic screening', *Molecular and Cellular Neuroscience*. Academic Press, 80, pp. 198–207. doi: 10.1016/J.MCN.2016.11.001.

O'Neill, G. M. *et al.* (2010) 'Mesenchymal Migration as a Therapeutic Target in Glioblastoma', *Journal of Oncology*. Hindawi Publishing Corporation, 2010, p. 17. doi: 10.1155/2010/430142.

Ohgaki, H. and Kleihues, P. (2005) 'Epidemiology and etiology of gliomas', *Acta neuropathologica*. Acta Neuropathol, 109(1), pp. 93–108. doi: 10.1007/S00401-005-0991-Y.

Ostrom, Q. T. *et al.* (2013) 'CBTRUS Statistical Report: Primary Brain and Central Nervous System Tumors Diagnosed in the United States in 2006-2010', *Neuro-Oncology*. Oxford University Press, 15(Suppl 2), p. ii1. doi: 10.1093/NEUONC/NOT151.

Ostrom, Q. T. *et al.* (2014) 'Editor's choice: The epidemiology of glioma in adults: a "state of the science" review', *Neuro-Oncology*. Oxford University Press, 16(7), p. 896. doi: 10.1093/NEUONC/NOU087.

Ostrom, Q. T. *et al.* (2018) 'CBTRUS Statistical Report: Primary Brain and Other Central Nervous System Tumors Diagnosed in the United States in 2011–2015', *Neuro-Oncology*. Oxford University Press, 20(Suppl 4), p. iv1. doi: 10.1093/NEUONC/NOY131.

Ottone, C. *et al.* (2014) 'Direct cell-cell contact with the vascular niche maintains quiescent neural stem cells', *Nature cell biology*. Europe PMC Funders, 16(11), p. 1045. doi: 10.1038/NCB3045.

Ozawa, T. *et al.* (2014) 'Most human non-GCIMP glioblastoma subtypes evolve from a common proneural-like precursor glioma', *Cancer cell*. NIH Public Access, 26(2), p. 288. doi: 10.1016/J.CCR.2014.06.005.

Ozdemir-Kaynak, E., Qutub, A. A. and Yesil-Celiktas, O. (2018) 'Advances in glioblastoma multiforme treatment: New models for nanoparticle therapy', *Frontiers in Physiology*.

Frontiers Media S.A. doi: 10.3389/fphys.2018.00170.

Ozturk, M. S. *et al.* (2020) 'High-resolution tomographic analysis of in vitro 3D glioblastoma tumor model under long-term drug treatment', *Science advances*. NLM (Medline), 6(10), p. eaay7513. doi: 10.1126/sciadv.aay7513.

Paolillo, M., Comincini, S. and Schinelli, S. (2021) 'In vitro glioblastoma models: A journey into the third dimension', *Cancers*. Multidisciplinary Digital Publishing Institute (MDPI), 13(10), pp. 1–25. doi: 10.3390/cancers13102449.

Park, I. H. *et al.* (2008) 'Generation of human-induced pluripotent stem cells', *Nature Protocols*, 3(7), pp. 1180–1186. doi: 10.1038/nprot.2008.92.

Park, J. B., Kwak, H. J. and Lee, S. H. (2008) 'Role of hyaluronan in glioma invasion.', *Cell adhesion & migration*. Taylor & Francis, pp. 202–207. doi: 10.4161/cam.2.3.6320.

Parker, J. J. *et al.* (2013) 'Gefitinib selectively inhibits tumor cell migration in EGFR-amplified human glioblastoma', *Neuro-Oncology*. Oxford University Press, 15(8), p. 1048. doi: 10.1093/NEUONC/NOT053.

Patel, A. P. *et al.* (2014) 'Single-cell RNA-seq highlights intratumoral heterogeneity in primary glioblastoma', *Science*. American Association for the Advancement of Science, 344(6190), pp. 1396–1401. doi: 10.1126/science.1254257.

Phillips, H. S. *et al.* (2006) 'Molecular subclasses of high-grade glioma predict prognosis, delineate a pattern of disease progression, and resemble stages in neurogenesis', *Cancer Cell*. Cell Press, 9(3), pp. 157–173. doi: 10.1016/J.CCR.2006.02.019/ATTACHMENT/0B967CEF-1B18-4C7E-90C7-7AF2804EB01D/MMC7.XLS.

Pine, A. R. *et al.* (2020) 'Tumor Microenvironment Is Critical for the Maintenance of Cellular States Found in Primary Glioblastomas', *Cancer Discovery*. Author Manuscript Published OnlineFirst on, p. CD-20-0057. doi: 10.1158/2159-8290.cd-20-0057.

Pitz, M. W. *et al.* (2015) 'Phase II study of PX-866 in recurrent glioblastoma', *Neuro-Oncology*. Oxford University Press, 17(9), p. 1270. doi: 10.1093/NEUONC/NOU365.

Pollard, S. M. *et al.* (2009) 'Glioma Stem Cell Lines Expanded in Adherent Culture Have Tumor-Specific Phenotypes and Are Suitable for Chemical and Genetic Screens', *Cell Stem Cell*. Elsevier Ltd, 4(6), pp. 568–580. doi: 10.1016/j.stem.2009.03.014.

Pollen, A. A. *et al.* (2015) 'Molecular Identity of Human Outer Radial Glia during Cortical Development', *Cell*. Cell Press, 163(1), pp. 55–67. doi: 10.1016/j.cell.2015.09.004.

Polson, E. S. *et al.* (2018) 'KHS101 disrupts energy metabolism in human glioblastoma cells and reduces tumor growth in mice', *Science Translational Medicine*. American Association for the Advancement of Science, 10(454), p. 2718. Available at: https://www.science.org/doi/10.1126/scitranslmed.aar2718 (Accessed: 19 October 2022).

Prosniak, M. *et al.* (2013) 'Glioma grade is associated with the accumulation and activity of cells bearing M2 monocyte markers', *Clinical cancer research : an official journal of the American Association for Cancer Research*. Clin Cancer Res, 19(14), pp. 3776–3786. doi: 10.1158/1078-0432.CCR-12-1940.

Purschke, M. *et al.* (2010) 'Phototoxicity of Hoechst 33342 in time-lapse fluorescence microscopy', *Photochemical and Photobiological Sciences*. Royal Society of Chemistry, 9(12), pp. 1634–1639. doi: 10.1039/c0pp00234h.

Qin, E. Y. *et al.* (2017) 'Neural Precursor-Derived Pleiotrophin Mediates Subventricular Zone Invasion by Glioma', *Cell*. Cell, 170(5), pp. 845-859.e19. doi: 10.1016/J.CELL.2017.07.016.

Ramnarain, D. B. *et al.* (2006) 'Differential gene expression analysis reveals generation of an autocrine loop by a mutant epidermal growth factor receptor in glioma cells', *Cancer Research*. American Association for Cancer Research, 66(2), pp. 867–874. doi: 10.1158/0008-5472.CAN-05-2753.

Rao, S. S. *et al.* (2013) 'Mimicking white matter tract topography using core-shell electrospun nanofibers to examine migration of malignant brain tumors', *Biomaterials*. NIH Public Access, 34(21), pp. 5181–5190. doi: 10.1016/j.biomaterials.2013.03.069.

Rao, S. S. *et al.* (2014) 'Toward 3D biomimetic models to understand the behavior of glioblastoma multiforme cells', *Tissue Engineering - Part B: Reviews*. Mary Ann Liebert Inc., pp. 314–327. doi: 10.1089/ten.teb.2013.0227.

Renner, M. *et al.* (2017) 'Self-organized developmental patterning and differentiation in cerebral organoids', *The EMBO Journal*. EMBO, 36(10), pp. 1316–1329. doi: 10.15252/embj.201694700.

Ricklefs, F. L. *et al.* (2018) 'Immune evasion mediated by PD-L1 on glioblastoma-derived extracellular vesicles', *Science advances*. Sci Adv, 4(3). doi: 10.1126/SCIADV.AAR2766.

Robertson, F. L. *et al.* (2019) 'Experimental models and tools to tackle glioblastoma', *DMM Disease Models and Mechanisms*. Company of Biologists Ltd. doi: 10.1242/dmm.040386.

Romani, M., Pistillo, M. P. and Banelli, B. (2018) 'Epigenetic targeting of glioblastoma', *Frontiers in Oncology*. Frontiers Media S.A., 8(OCT), p. 448. doi: 10.3389/FONC.2018.00448/FULL.

Roy, S. *et al.* (2015) 'Recurrent Glioblastoma: Where we stand', *South Asian Journal of Cancer*. Thieme Medical Publishers, 4(4), p. 163. doi: 10.4103/2278-330X.175953.

Rybin, M. J. *et al.* (2021) 'Organoid Models of Glioblastoma and Their Role in Drug Discovery', *Frontiers in Cellular Neuroscience*, 15(February), pp. 1–11. doi: 10.3389/fncel.2021.605255.

Sachdeva, R. *et al.* (2019) 'BMP signaling mediates glioma stem cell quiescence and confers treatment resistance in glioblastoma', *Scientific Reports*. Nature Publishing Group, 9(1), pp. 1–14. doi: 10.1038/s41598-019-51270-1.

Sancho-Martinez, I. *et al.* (2016) 'Establishment of human iPSC-based models for the study and targeting of glioma initiating cells', *Nature Communications*, 7. doi: 10.1038/ncomms10743.

Serres, E. *et al.* (2014) 'Fibronectin expression in glioblastomas promotes cell cohesion, collective invasion of basement membrane in vitro and orthotopic tumor growth in mice', *British Dental Journal*. Nature Publishing Group, 217(1), pp. 3451–3462. doi: 10.1038/onc.2013.305.

Al Shboul, S. *et al.* (2021) 'Kinomics platform using GBM tissue identifies BTK as being associated with higher patient survival', *Life Science Alliance*. Life Science Alliance LLC, 4(12). doi: 10.26508/LSA.202101054.

Shi, Y., Kirwan, P. and Livesey, F. J. (2012) 'Directed differentiation of human pluripotent stem cells to cerebral cortex neurons and neural networks', *Nature Protocols*, 7(10), pp. 1836–1846. doi: 10.1038/nprot.2012.116.

da Silva, B. B. *et al.* (2018) 'Spontaneous Glioblastoma Spheroid Infiltration of Early-Stage Cerebral Organoids Models Brain Tumor Invasion', *SLAS Discovery*, 23(8), pp. 862–868. doi: 10.1177/2472555218764623.

da Silva, B. *et al.* (2019) 'Chemically induced neurite-like outgrowth reveals a multicellular network function in patient-derived glioblastoma cells', *Journal of cell science*. NLM (Medline), 132(19). doi: 10.1242/JCS.228452/VIDEO-6.

Singh, D. K. *et al.* (2017) 'Oncogenes Activate an Autonomous Transcriptional Regulatory Circuit That Drives Glioblastoma', *Cell Reports*. Elsevier B.V., 18(4), pp. 961–976. doi: 10.1016/j.celrep.2016.12.064.

Singh, J., Sharma, K. and Pillai, P. P. (2018) 'PDGFR inhibition mediated intracellular signalling in C6 glioma growth and migration: role of ERK and ROCK pathway', *Cytotechnology*. Springer, 70(1), p. 465. doi: 10.1007/S10616-017-0163-7.

Singh, S., Carpenter, A. E. and Genovesio, A. (2014) 'Increasing the Content of High-

Content Screening: An Overview', *Journal of Biomolecular Screening*. SAGE Publications, 19(5), p. 640. doi: 10.1177/1087057114528537.

Singh, S. K. *et al.* (2004) 'Identification of human brain tumour initiating cells', *Nature*. Nature, 432(7015), pp. 396–401. doi: 10.1038/nature03128.

Snijder, B. *et al.* (2017) 'Image-based ex-vivo drug screening for patients with aggressive haematological malignancies: interim results from a single-arm, open-label, pilot study', *The Lancet. Haematology*. Lancet Haematol, 4(12), pp. e595–e606. doi: 10.1016/S2352-3026(17)30208-9.

Ströbele, S. *et al.* (2015) 'A Potential Role for the Inhibition of PI3K Signaling in Glioblastoma Therapy', *PLOS ONE*. Public Library of Science, 10(6), p. e0131670. doi: 10.1371/JOURNAL.PONE.0131670.

Stupp, R. *et al.* (2005) 'Radiotherapy plus Concomitant and Adjuvant Temozolomide for Glioblastoma', *New England Journal of Medicine*. New England Journal of Medicine (NEJM/MMS), 352(10), pp. 987–996. doi: 10.1056/NEJMOA043330/SUPPL_FILE/987SA1.PDF.

Stupp, R. *et al.* (2009) 'Effects of radiotherapy with concomitant and adjuvant temozolomide versus radiotherapy alone on survival in glioblastoma in a randomised phase III study: 5-year analysis of the EORTC-NCIC trial', *The Lancet Oncology*. Lancet Publishing Group, 10(5), pp. 459–466. doi: 10.1016/S1470-2045(09)70025-7.

Stupp, R. *et al.* (2014) 'Cilengitide combined with standard treatment for patients with newly diagnosed glioblastoma with methylated MGMT promoter (CENTRIC EORTC 26071-22072 study): a multicentre, randomised, open-label, phase 3 trial', *The Lancet. Oncology*. Lancet Oncol, 15(10), pp. 1100–1108. doi: 10.1016/S1470-2045(14)70379-1.

Suvà, M. L. *et al.* (2014) 'Reconstructing and reprogramming the tumor propagating potential of glioblastoma stem-like cells', *Cell*. NIH Public Access, 157(3), p. 580. doi: 10.1016/J.CELL.2014.02.030.

Takahashi, K. *et al.* (2007) 'Induction of Pluripotent Stem Cells from Adult Human Fibroblasts by Defined Factors', *Cell*, 131(5), pp. 861–872. doi: 10.1016/j.cell.2007.11.019.

Tessier-Lavigne, M. and Goodman, C. S. (1996) 'The Molecular Biology of Axon Guidance', *Science*. American Association for the Advancement of Science , 274(5290), pp. 1123–1133. doi: 10.1126/SCIENCE.274.5290.1123.

Thakkar, J. P. *et al.* (2014) 'Epidemiologic and molecular prognostic review of glioblastoma', *Cancer epidemiology, biomarkers & prevention : a publication of the American Association for Cancer Research, cosponsored by the American Society of Preventive Oncology*. Cancer Epidemiol Biomarkers Prev, 23(10), pp. 1985–1996. doi: 10.1158/1055-9965.EPI-14-0275.

Tiek, D. M. *et al.* (2018) 'Alterations in Cell Motility, Proliferation, and Metabolism in Novel Models of Acquired Temozolomide Resistant Glioblastoma', *Scientific Reports*. Nature Publishing Group, 8(1), pp. 1–11. doi: 10.1038/s41598-018-25588-1.

Turner, K. M. *et al.* (2017) 'Extrachromosomal oncogene amplification drives tumour evolution and genetic heterogeneity', *Nature 2017 543:7643*. Nature Publishing Group, 543(7643), pp. 122–125. doi: 10.1038/nature21356.

Usaj, M. M. *et al.* (2020) 'Systematic genetics and single-cell imaging reveal widespread morphological pleiotropy and cell-to-cell variability', *Molecular Systems Biology*. John Wiley & Sons, Ltd, 16(2), p. e9243. doi: 10.15252/MSB.20199243.

Venkatesh, H. S. *et al.* (2015) 'Neuronal Activity Promotes Glioma Growth through Neuroligin-3 Secretion', *Cell*. Cell, 161(4), pp. 803–816. doi: 10.1016/J.CELL.2015.04.012.

Verhaak, R. G. W. *et al.* (2010) 'Integrated Genomic Analysis Identifies Clinically Relevant Subtypes of Glioblastoma Characterized by Abnormalities in PDGFRA, IDH1, EGFR, and NF1', *Cancer Cell*. NIH Public Access, 17(1), pp. 98–110. doi: 10.1016/j.ccr.2009.12.020.

Veschini, L. *et al.* (2021) 'High-content imaging to phenotype human primary and ipsc-

derived cells', *Methods in Molecular Biology*. Humana Press Inc., 2185, pp. 423–445. doi: 10.1007/978-1-0716-0810-4_27/COVER.

Wade, A. *et al.* (2013) 'Proteoglycans and their roles in brain cancer', *FEBS Journal*. NIH Public Access, pp. 2399–2417. doi: 10.1111/febs.12109.

Wang, C. *et al.* (2017) 'Scalable Production of iPSC-Derived Human Neurons to Identify Tau-Lowering Compounds by High-Content Screening', *Stem cell reports*. Stem Cell Reports, 9(4), pp. 1221–1233. doi: 10.1016/J.STEMCR.2017.08.019.

Wang, J. *et al.* (2017) 'Single-cell gene expression analysis reveals regulators of distinct cell subpopulations among developing human neurons', *Genome Research*. Cold Spring Harbor Laboratory Press, 27(11), pp. 1783–1794. doi: 10.1101/gr.223313.117.

Wang, Q. *et al.* (2017) 'Tumor Evolution of Glioma-Intrinsic Gene Expression Subtypes Associates with Immunological Changes in the Microenvironment', *Cancer Cell*. Cell Press, 32(1), pp. 42-56.e6. doi: 10.1016/j.ccell.2017.06.003.

Warburg, O. (1956) 'On the origin of cancer cells', *Science*. American Association for the Advancement of Science , 123(3191), pp. 309–314. doi: 10.1126/SCIENCE.123.3191.309/ASSET/A8D38B53-799F-4009-AAD3-E77CEF33D301/ASSETS/SCIENCE.123.3191.309.FP.PNG.

Wei, W., Wang, H. and Ji, S. (2017) 'Paradoxes of the EphB1 receptor in malignant brain tumors', *Cancer Cell International*. BioMed Central Ltd. doi: 10.1186/s12935-017-0384-z.

Wen, P. Y. *et al.* (2015) 'Phase I dose-escalation study of the PI3K/mTOR inhibitor voxtalisib (SAR245409, XL765) plus temozolomide with or without radiotherapy in patients with high-grade glioma', *Neuro-Oncology*. Oxford University Press, 17(9), p. 1275. doi: 10.1093/NEUONC/NOV083.

Wen, P. Y. *et al.* (2019) 'Buparlisib in Patients With Recurrent Glioblastoma Harboring Phosphatidylinositol 3-Kinase Pathway Activation: An Open-Label, Multicenter, Multi-

Arm, Phase II Trial', *Journal of Clinical Oncology*. American Society of Clinical Oncology, 37(9), p. 741. doi: 10.1200/JCO.18.01207.

Westphal, M., Maire, C. L. and Lamszus, K. (2017) 'EGFR as a Target for Glioblastoma Treatment: An Unfulfilled Promise', *CNS Drugs*. Springer, 31(9), p. 723. doi: 10.1007/S40263-017-0456-6.

Wick, A. *et al.* (2020) 'Phase 1b/2a study of galunisertib, a small molecule inhibitor of transforming growth factor-beta receptor I, in combination with standard temozolomide-based radiochemotherapy in patients with newly diagnosed malignant glioma', *Investigational New Drugs*. Springer, 38(5), p. 1570. doi: 10.1007/S10637-020-00910-9.

'World Health Organization Classification of Tumours of the Central Nervous System' (2021) *International Agency for Research on Cancer*, 5th editio(WHO Classification of Tumours Editorial Board).

Wu, A. *et al.* (2010) 'Glioma cancer stem cells induce immunosuppressive macrophages/microglia', *Neuro-oncology*. Neuro Oncol, 12(11), pp. 1113–1125. doi: 10.1093/NEUONC/NOQ082.

Wurdak, H. *et al.* (2010) 'An RNAi Screen Identifies TRRAP as a Regulator of Brain Tumor-Initiating Cell Differentiation', *Cell Stem Cell*. Elsevier, 6(1), pp. 37–47. doi: 10.1016/j.stem.2009.11.002.

Xi, G. *et al.* (2017) 'Therapeutic Potential for Bone Morphogenetic Protein 4 in Human Malignant Glioma', *Neoplasia (United States)*. Neoplasia Press, Inc., pp. 261–270. doi: 10.1016/j.neo.2017.01.006.

Xia, S. *et al.* (2016) 'Tumor microenvironment tenascin-C promotes glioblastoma invasion and negatively regulates tumor proliferation', *Neuro-Oncology*. Oxford University Press, 18(4), pp. 507–517. doi: 10.1093/neuonc/nov171.

Xiao, W., Sohrabi, A. and Seidlits, S. K. (2017) 'Integrating the glioblastoma

microenvironment into engineered experimental models', *Future Science OA*. Future Medicine Ltd. doi: 10.4155/fsoa-2016-0094.

Xie, Y. *et al.* (2015) 'The Human Glioblastoma Cell Culture Resource: Validated Cell Models Representing All Molecular Subtypes', *EBioMedicine*. Elsevier B.V., 2(10), pp. 1351–1363. doi: 10.1016/j.ebiom.2015.08.026.

Xu, Y. *et al.* (2010) 'Slit2/Robo1 signaling in glioma migration and invasion', *Neuroscience Bulletin*. Springer, 26(6), p. 474. doi: 10.1007/S12264-010-0730-9.

Yamanaka, S. (2007) 'Strategies and New Developments in the Generation of Patient-Specific Pluripotent Stem Cells', *Cell Stem Cell*, 1(1), pp. 39–49. doi: 10.1016/j.stem.2007.05.012.

Ylivinkka, I. *et al.* (2013) 'Netrin-1-induced activation of Notch signaling mediates glioblastoma cell invasion', *Journal of Cell Science*. The Company of Biologists, 126(11), pp. 2459–2469. doi: 10.1242/JCS.120022.

Yui, S. *et al.* (2014) 'Neutrophil cathepsin G, but not elastase, induces aggregation of MCF-7 mammary carcinoma cells by a protease activity-dependent cell-oriented mechanism', *Mediators of Inflammation*. Hindawi Limited, 2014. doi: 10.1155/2014/971409.

Zepecki, J. P. *et al.* (2019) 'Regulation of human glioma cell migration, tumor growth, and stemness gene expression using a Lck targeted inhibitor', *Oncogene*. Nature Publishing Group, 38(10), pp. 1734–1750. doi: 10.1038/s41388-018-0546-z.

Zhang, P. *et al.* (2020) 'Current Opinion on Molecular Characterization for GBM Classification in Guiding Clinical Diagnosis, Prognosis, and Therapy', *Frontiers in Molecular Biosciences*. Frontiers Media S.A., p. 241. doi: 10.3389/fmolb.2020.562798.

Zhang, Y. *et al.* (2013) 'Rapid Single-Step Induction of Functional Neurons from Human Pluripotent Stem Cells', *Neuron*. Cell Press, 78(5), pp. 785–798. doi: 10.1016/J.NEURON.2013.05.029.

Zhou, W. *et al.* (2019) 'Targeting CXCL12/CXCR4 Axis in Tumor Immunotherapy', *Current medicinal chemistry*. NIH Public Access, 26(17), p. 3026. doi: 10.2174/0929867324666170830111531.

Zhu, Y. *et al.* (2017) 'PDX1, Neurogenin-3, and MAFA: critical transcription regulators for beta cell development and regeneration', *Stem cell research & therapy*. Stem Cell Res Ther, 8(1). doi: 10.1186/S13287-017-0694-Z.